

AD-A039 617

UNITED TECHNOLOGIES CORP WINDSOR LOCKS CONN HAMILTON --ETC F/G 17/1  
SPEAR MODEL ACOUSTIC FEASIBILITY TESTS.(U)

JUN 62 L W SMITH

NONR-3350(00)

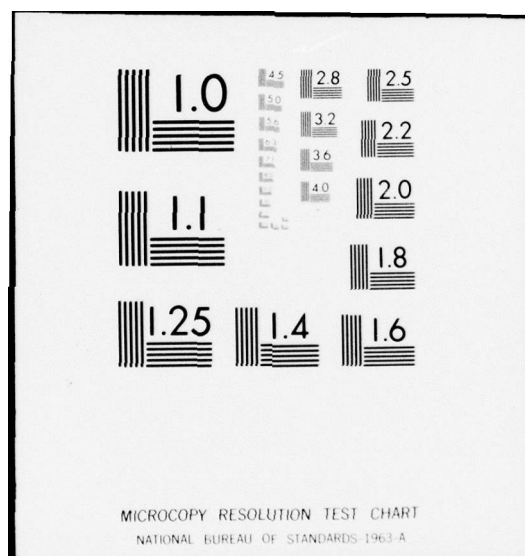
UNCLASSIFIED

HSER-2464

NL

1 of 2  
ADA039 617







MOST Project - 4

*Good*

Hamilton Standard

DIVISION OF UNITED AIRCRAFT CORPORATION  
U  
A

AD A 039617

*(P.S.)*

DDC  
RECEIVED  
MAR 7 1977  
C

AD No. \_\_\_\_\_  
DDC FILE COPY

# SPEAR MODEL

## Acoustic Feasibility Tests

GPI

DISTRIBUTION STATEMENT A  
Approved for public release;  
Distribution Unlimited

14 HSER-2464 ✓

REPRODUCTION IN WHOLE OR IN PART IS PERMITTED  
FOR ANY PURPOSE OF THE UNITED STATES GOVERNMENT

9 ENGINEERING REPORT

6 SPEAR MODEL  
ACOUSTIC FEASIBILITY TESTS.

11 30 JUN 62  
JUNE 30, 1962

10 Lester W. Smith



PREPARED BY :

Lester W. Smith

Senior Analytical Engineer

APPROVED BY :

Walter E. Amos

Chief of Advanced Analysis

Carl G. Steinhilber

Chief of Engineering Planning

12 139p.

161 400

15 N6NR-3350(00)

**Hamilton Standard**  
WINDSOR LOCKS • CONNECTICUT

DIVISION OF UNITED AIRCRAFT CORPORATION

U  
A

DISTRIBUTION STATEMENT A  
Approved for public release;  
Distribution Unlimited

6pg

SPEAR MODEL  
ACOUSTIC FEASIBILITY TESTS

TABLE OF CONTENTS

<u>Section</u>	<u>Page No.</u>
INTRODUCTION	1
CONCLUSIONS	2
DESCRIPTION OF TESTS	3
The General Approach	3
The One-Fifth Scale Tests - April and August	3
The January Tests	24
DISCUSSION OF TEST RESULTS	26
Background	26
Results of Air Tests	26
Frequency Studies	27
Results of the Pond Tests	28
SUPPORTING ANALYSES	33
The Impedance of a Non-Rigid Piston	33
The Effect of Bar Taper	33
The Effect of Rear Surface Motion on the Radiation Pattern	34
IMPLICATIONS FOR FUTURE WORK	35
APPENDIXES	
A. Figures	A-0
B. Tables	B-0
C. Test Data	C-0
D. Analyses	D-0

100-2464-1

1. NO. 100-2464-1

2. DATE 10/1/64

3. BY [Signature]

4. [Signature]

5. [Signature]

6. [Signature]

7. [Signature]

8. [Signature]

9. [Signature]

10. [Signature]

11. [Signature]

12. [Signature]

13. [Signature]

14. [Signature]

15. [Signature]

16. [Signature]

17. [Signature]

18. [Signature]

19. [Signature]

20. [Signature]

21. [Signature]

22. [Signature]

23. [Signature]

24. [Signature]

25. [Signature]

26. [Signature]

27. [Signature]

28. [Signature]

29. [Signature]

30. [Signature]

31. [Signature]

32. [Signature]

33. [Signature]

34. [Signature]

35. [Signature]

36. [Signature]

37. [Signature]

38. [Signature]

39. [Signature]

40. [Signature]

41. [Signature]

42. [Signature]

43. [Signature]

44. [Signature]

45. [Signature]

46. [Signature]

47. [Signature]

48. [Signature]

49. [Signature]

50. [Signature]

51. [Signature]

52. [Signature]

53. [Signature]

54. [Signature]

55. [Signature]

56. [Signature]

57. [Signature]

58. [Signature]

59. [Signature]

60. [Signature]

61. [Signature]

62. [Signature]

63. [Signature]

64. [Signature]

65. [Signature]

66. [Signature]

67. [Signature]

68. [Signature]

69. [Signature]

70. [Signature]

71. [Signature]

72. [Signature]

73. [Signature]

74. [Signature]

75. [Signature]

76. [Signature]

77. [Signature]

78. [Signature]

79. [Signature]

80. [Signature]

81. [Signature]

82. [Signature]

83. [Signature]

84. [Signature]

85. [Signature]

86. [Signature]

87. [Signature]

88. [Signature]

89. [Signature]

90. [Signature]

91. [Signature]

92. [Signature]

93. [Signature]

94. [Signature]

95. [Signature]

96. [Signature]

97. [Signature]

98. [Signature]

99. [Signature]

100. [Signature]

### LIST OF FIGURES

<u>Figure No.</u>	<u>Title</u>	<u>Page</u>
1	SPEAR Model - Bare Casting	5
2	SPEAR Model Casting	5a
3	Electromagnetic Exciter for SPEAR Model	7
4	Electromagnetic Exciter Installed on SPEAR Model	8
5	Air Shake Test of Electromagnetic Exciter	9
6	SPEAR Model With Piston Rim Removed (Configuration A11-0)	12
7	Hamilton Standard Instrumentation for Dodge Pond Test	13
8	Strain Gages on Piston Face	14
9	Air Shake Test of SPEAR Model	16
10	SPEAR Model Assembly at Dodge Pond (Configuration A6-4)	17
11	SPEAR Model Assembly (Configuration A4-0)	19
12	SPEAR Model With Piston Rim Removed and Celltite Covering (Configuration A11-6)	20
13	Exponential Projector for January Tests	21

### LIST OF TABLES

<u>Table No.</u>	<u>Title</u>	<u>Page</u>
Table I	Electromagnetic Exciter for SPEAR Model	10
Table II	Performance Comparisons	36



## ABSTRACT

A concept for a high-power, low frequency sonar projector proposed by Hamilton Standard to the Office of Naval Research resulted in a scale model feasibility study to verify certain acoustic assumptions of the design and to evaluate various other mechanical and acoustical parameters pertinent to a full scale design.

The proposed projector -- named SPEAR -- consists of two basic elements: the first is a resonant bar/piston which is used as an impedance matching device to couple the low force, high amplitude vibrations desired at the exciter to the high force, low amplitude vibrations required at the radiating face; the second basic element is the mechanical exciter which consists of banks of counter-rotating unbalanced weights supported on hydrodynamic journal bearings. The full scale projector output would be 1 megawatt of acoustic power at 400 cps with provision for both frequency modulation and amplitude control.

This report describes three series of tests conducted at the USN Underwater Sound Laboratory and presents the test results along with several supporting analyses. Several models were tested. Most of these were variations of a one-fifth scale model of the proposed full scale design and utilized an electro-magnetic exciter. The test ka was approximately 2 -- the same as the full scale configuration. The model test program concerned itself with four areas of investigation: the acoustic impedance presented by the water to the piston face, the transmitting directivity pattern, the transmitting response or tunability, and the vibratory structural action of the device.

The test results confirm that the basic assumptions of acoustic and mechanical performance made in the SPEAR design study are valid. The test results and supporting analyses also provide important design guidance for optimizing future configurations.

## INTRODUCTION

Hamilton Standard has proposed the development of a high-power, low-frequency, sonar projector which has been designated SPEAR -- Sonic Projector for Extended Acoustic Ranging. The configuration proposed will radiate one megawatt of acoustic power at 400 cps with the predicted advantages of high efficiency and relatively low weight and cost, along with moderate tunability and directivity. In this configuration, which is described in detail in Hamilton Standard Engineering Proposal EP-60806, "Engineering Proposal for a Sonic Projector for Extended Acoustic Ranging," June, 1960, the prime source of the acoustic power is an oscillator comprising a set of counter-rotating unbalanced masses driven by a pair of electric motors. These masses deliver vibratory energy to a radiating disk, or piston, through an axially flexible coupler which reduces the requirement for oscillator force in two ways. First, the oscillator needs to supply no force to accelerate the mass of the piston and its parasitic water mass back and forth, since at system resonance this force requirement is satisfied internally by the mass and stiffness of the vibratory system, i.e., the oscillator needs to supply no reactive force. Second, the remaining force required to radiate acoustic power into the water, the resistive force, is reduced by a kind of leverage effect, the motion at the oscillator end of the coupling bar being greater than the motion of the piston.

In the development of SPEAR, two technical areas appeared to warrant early attention: one involving the evaluation of acoustic impedances, the other involving the development of the rotating-weight oscillator assembly. The acoustic area was important because the analytical evaluation of the projector had depended in part on certain assumptions of acoustic impedance -- based on theoretical studies tempered with practical judgment -- and it was recognized that a degree of uncertainty existed in these assumptions. To facilitate the acoustic development of SPEAR, the Office of Naval Research authorized a model test program for investigating the acoustic impedance parameters of the proposed configuration and for formulating design recommendations for a full-scale acoustic projector. This effort was covered in Contract Nonr 3350 (00), dated November 1, 1960, and the current report is being submitted in fulfillment of this contract.

The model tests have been completed, as have certain supporting analytical studies. The results of this work are reported here in order to confirm the acoustic feasibility of the SPEAR concept and to record data which may be used to support the optimization of new designs.

## CONCLUSIONS

The basic acoustic assumptions made in the SPEAR design study are valid -- the acoustic impedance of the radiating piston, both resistive and reactive, found in the test were satisfactorily close to those assumed in the design.

Based on the measured acoustic parameters, an eight-foot diameter, one megawatt, 400 cps SPEAR projector may be built with a tunability indicated by a Quality Factor ( $Q = f/\Delta f_{-3\text{db}}$ ) of about five, a Directivity Index of about 6 1/2 db, a Front-to-Back Ratio of about 4 db, and acceptable vibratory stress levels. Special treatments to enhance directivity, such as a reflector or a rear coating of pressure release material, would raise the Front-to-Back Ratio to about 13 db; without such treatment directivity may be improved by beneficial configurations of the casting itself or by an increase in size.

The vibratory action of the SPEAR casting indicated by strain gages and accelerometers was approximately as predicted by the design analysis, but it would be desirable in further stages of development to extend the analytical work on secondary action of the bar and piston.

The test results and supporting analyses provide important design guidance for optimizing future configurations.

## DESCRIPTION OF TESTS

### THE GENERAL APPROACH

The information to be learned about the SPEAR configuration from this work consisted of the acoustic impedance presented by the water to the piston face, the transmitting directivity pattern, the transmitting frequency response, or tunability, and the vibratory structural action of the device. All of this information can be considered scalable according to basic acoustic laws, so for economy and convenience the tests were performed in model scale. For the main part of the program a one-fifth scale model of the proposed configuration was obtained; a series of tests were performed in air and water, covering several model modifications and a moderate frequency range; and the test results were summarized and interpreted.

During this program, in response to additional interest in directivity, several smaller models of a different configuration were prepared for test. (The original configuration had been designed primarily to optimize weight and tunability.) These models were tested to provide additional background in methods of reducing acoustic radiation to the rear.

Subsidiary to the program of model tests, three theoretical analyses were performed for their possible contributions to the SPEAR design. One, concerning the impedance of a non-rigid piston, was of interest because the piston of the one-fifth scale model was found to flex somewhat at the higher frequencies. The second, a study of the use of a tapered bar to couple the oscillator to the piston, was to explore an area that had been intentionally simplified out of the original design study, which assumed a constant-area bar. The third analysis considered the effect of rear surface vibration on the radiation pattern, with particular reference to the improvement of Front-to-Back Ratio.

All of these tests, their results, and the supporting analysis work, are reported in the sections that follow.

### THE ONE-FIFTH SCALE TESTS - APRIL AND AUGUST

The Model. A reduced scale model of the Spear casting was acquired during the study work leading up to Hamilton Standard's proposal. Except for size, this model is essentially the configuration that evolved from the proposal study, differing only in the detail design of the stiffening incorporated in the rear face of the piston. The model had a honeycomb pattern, whereas the proposed design had a system of radial ribs which would have given a somewhat improved stiffness-to-weight ratio. To avoid delay and additional expense, the model in hand was used for the test program.

The model is an aluminum casting consisting of a truncated hollow cone terminated with the honeycombed radiating piston. The shape may be seen in the photograph



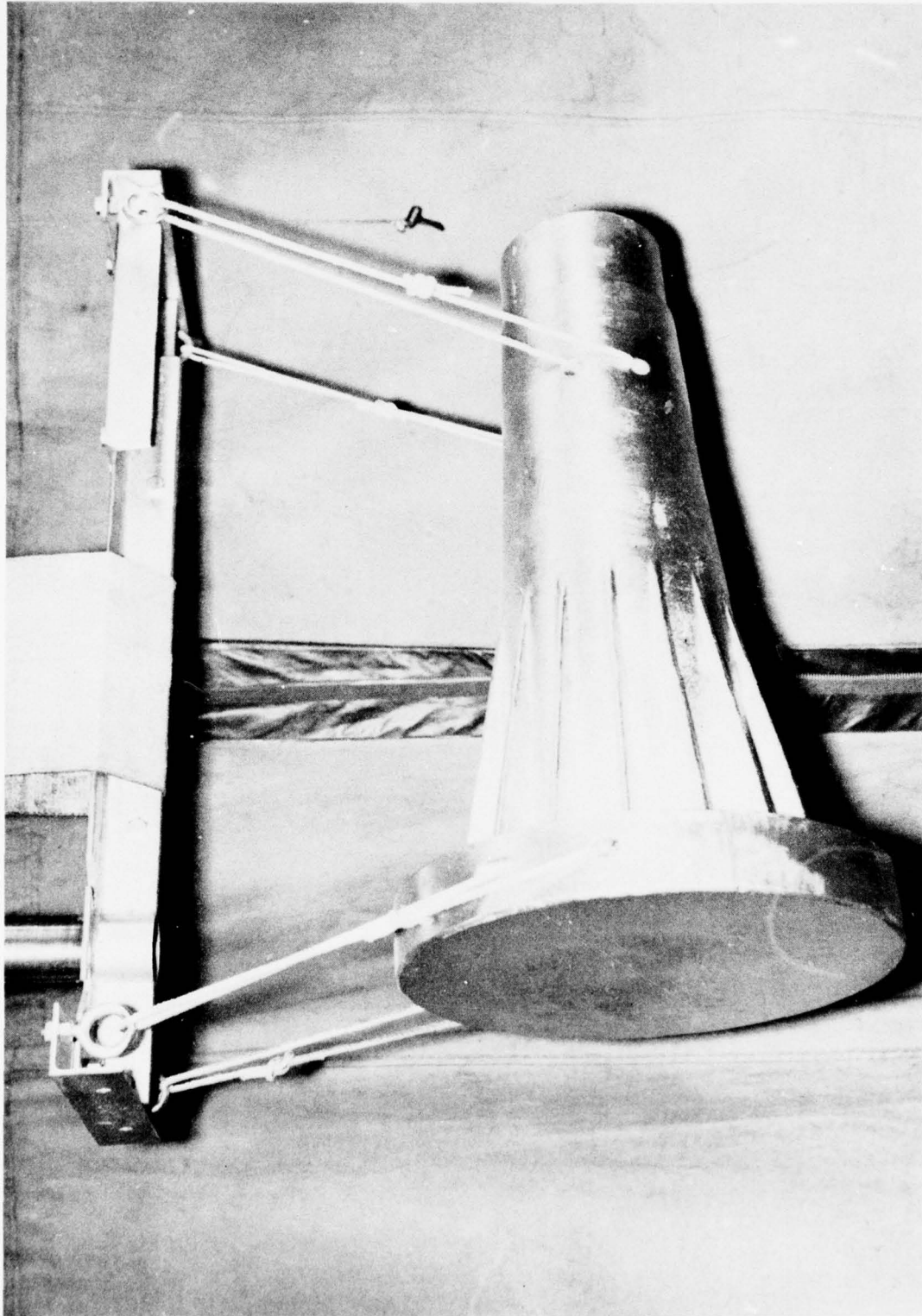
The Model. (Continued)

of Figure 1 and the drawing of Figure 2, which show the bare casting before it was trimmed to length for testing. In Table B-2 are summarized the major items of descriptive data. The basic piston diameter of 19.2 inches is just one fifth of the 8-foot diameter of the full-scale proposal. The length of the conical bar was first 25.5 inches and then 21.5 inches -- the change of length along with the addition of a heavy spacer at the end of the bar permitting a moderate adjustment of resonant frequency around the nominal test frequency of 2000 cps ( 5 times 400 cps).

For convenience in referring to the various model configurations tested, a system of nomenclature was established. This system is made clear in Table B-1, which shows schematically each of the assemblies tested, indicating by arrangement and notation the various "family relationships" among them. The basic model assemblies having different natural frequencies in air are differentiated by the designations A4, A5, A6, etc., as shown, where, for example, A5 identifies all test configurations incorporating the 25.5 inch bar length but not including the heavy spacer, and All identifies configurations with the 21.5 inch bar length, including the heavy spacer to shift frequency, and having the overhanging rim of the piston removed. A suffix, -0, -1, -2, etc., is added to the designation to indicate the particular acoustic modifications which were applied to some of the configurations, such as a tire inner tube or a ring of celltite foam rubber behind the piston rim ( to decouple this rear surface from the water), or a celltite rubber reflector positioned behind the piston.

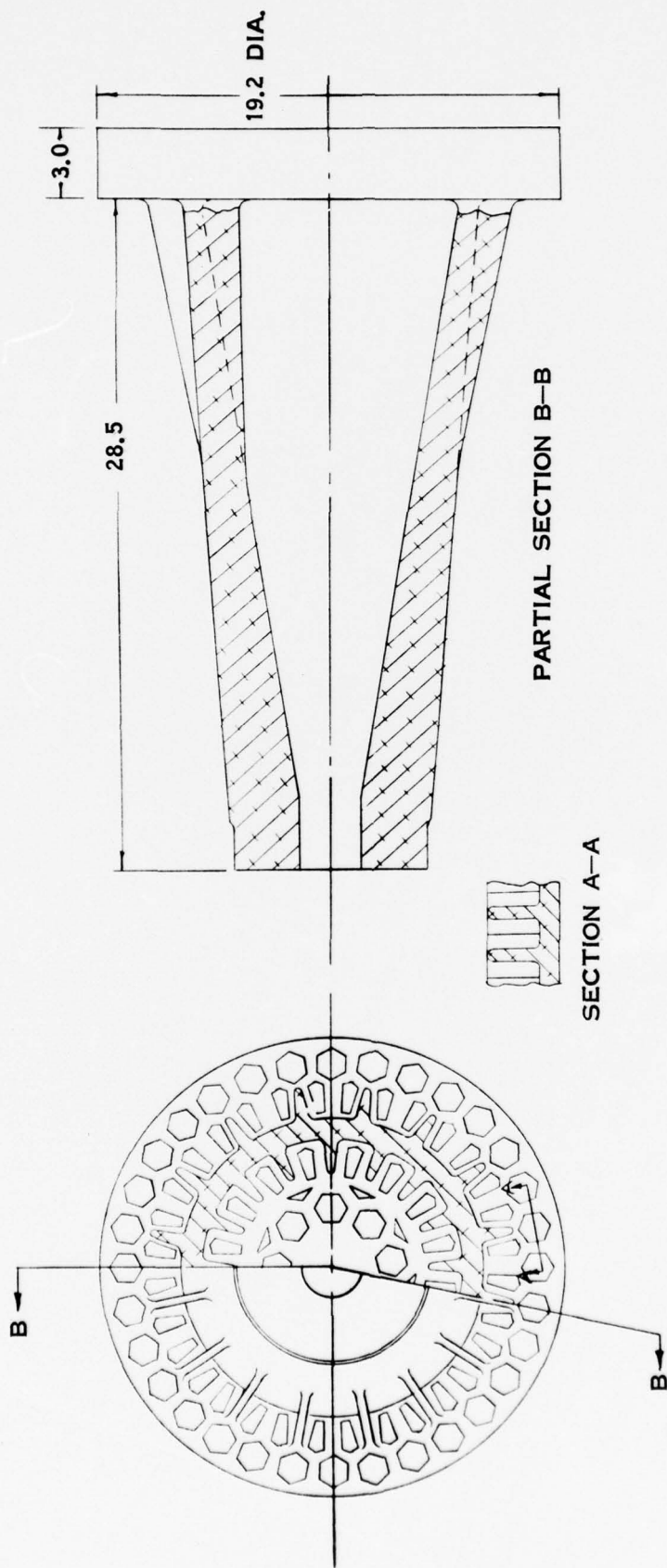
The Exciter. It was evident that the exciter for the model tests should not be a scaled version of the rotating-weight oscillator assembly, since the full-scale operating frequency scales to 2000 cps or 120,000 rpm on the model. The successful development of a 120,000 rpm unbalanced shaker seemed costly and unnecessary, because the acoustics of the model -- its vibratory mode shape, the impedance presented by the water, the acoustic directionality -- would be unaffected by the nature of the exciter. First efforts to obtain an exciter were then directed toward a barium titanate crystal device. Since a suitable "crystal" exciter was not available from existing Navy equipment, eight likely crystal suppliers were given a description of the approximate impedance of the Model SPEAR, as the crystal would see it, the desired power output (hopefully 100 watts), and the space envelope. None of those contacted would suggest anything more helpful than a several thousand dollar development program, after which they might be able to bid on the crystal. Learning of this, several representatives of the Navy suggested an electro-magnetic exciter. With some helpful advice from USNUSL and NRL this was designed and built.

The exciter takes the form of three electromagnets arranged symmetrically on a circular plate, each with an E core facing an I core across a small air gap.



G19880

SPEAR MODEL-BARE CASTING  
FIGURE 1



SPEAR MODEL CASTING  
FIGURE 2

### The Exciter. (Continued)

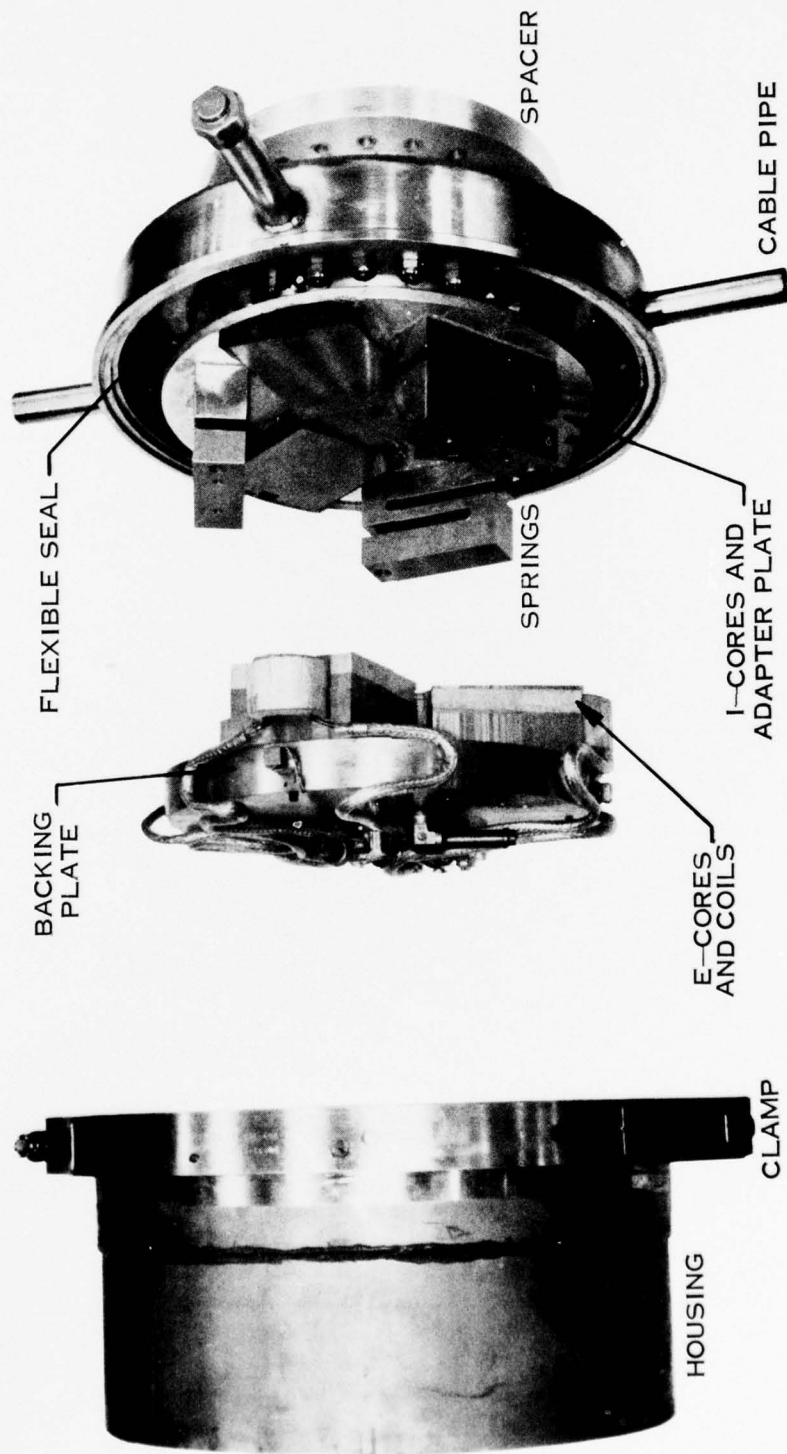
The E cores are bonded to a backing plate or ballast; the I cores, to an adapter which is attached to the SPEAR casting; the two sides of the exciter are held apart by three springs. An exploded view of the exciter is shown in Figure 3; Figure 4 shows the exciter attached to the casting. In operation, a DC biasing current establishes a bias flux and magnetic force, and an AC excitation superimposes an alternating force which is reacted on the one side by the inertia of the backing plate and on the other side by the driving-end impedance of the SPEAR casting. Component sizes were chosen so that the backing plate motion would be very much less than the casting motion at resonance, the oscillatory spring forces would be very much less than the magnetic forces, distortion and power loss would be as low as feasible, and local resonances of the exciter would be avoided. The core sizes were designed to provide as much total gap area, 17 sq. in., as could reasonably be squeezed into the 9-inch diameter space envelope desired. The operating flux density level of  $7440 \pm 3150$  gauss was calculated to produce  $\pm 426$  lbs. of alternating force, which would deliver 52 watts of power into the projector, whose impedance was then estimated at  $34 \times 10^6$  gm/sec. But since one of the unknowns to be determined from the SPEAR Model tests was this very impedance, all of the exciter design calculations were considered to be only nominal. A numerical description of the exciter geometry and a list of the nominal operating values is presented in Table I.

For the model tests the exciter was driven by an oscillator and 30 watt power amplifier supplied by the Navy. A special control console was prepared to facilitate the adjustment and measurement of input conditions, as well as to permit power factor correction by the installation of external capacitance. (A schematic diagram of the console is shown in Figure A-2. All of this equipment worked well during the tests, including a special test run with a larger amplifier during which the exciter power output was increased to 170 watts.

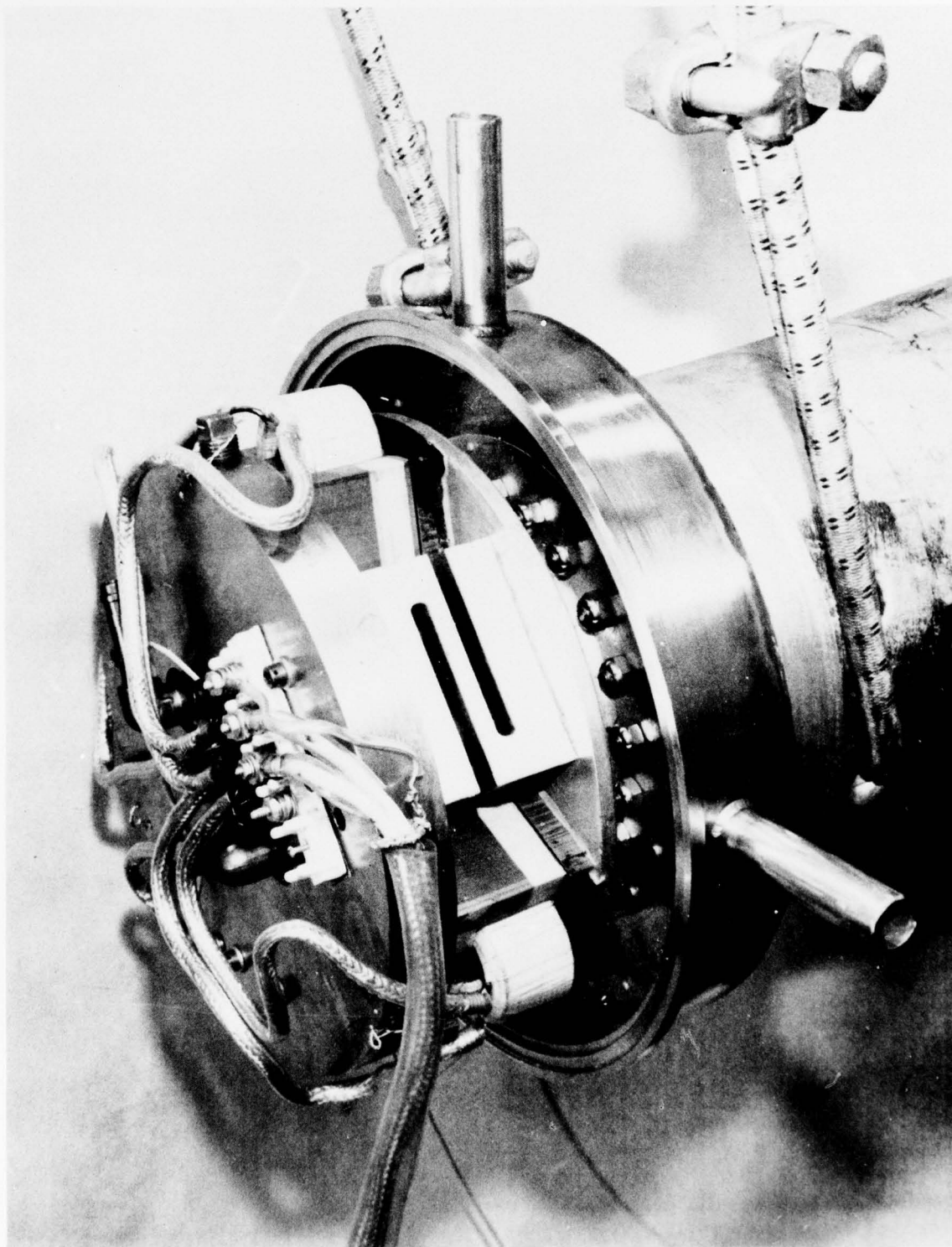
A crystal exciter was used for some early air shake tests of the SPEAR casting run at very low power. This exciter was a four-inch-square, half-inch-thick block of Glennite HT and was quite adequate to determine resonant frequencies of various test assemblies in air.

The Housing and Supporting Apparatus. Surrounding the electromagnetic exciter is a cylindrical housing to keep its work dry and to prevent motions in this area from radiating sound into the water. The housing is flexibly mounted on the exciter adapter with a sheet steel diaphragm which isolates the housing from the vibratory motions of the end of the SPEAR casting. Several stub tubes protrude from the housing allowing the passage of power and instrumentation lead wires and the attachment of an air hose. The housing was designed to be as compact as possible. It was not believed feasible to attempt a scale simulation of the proposed full-scale SPEAR accessory housing and motors, because no simple



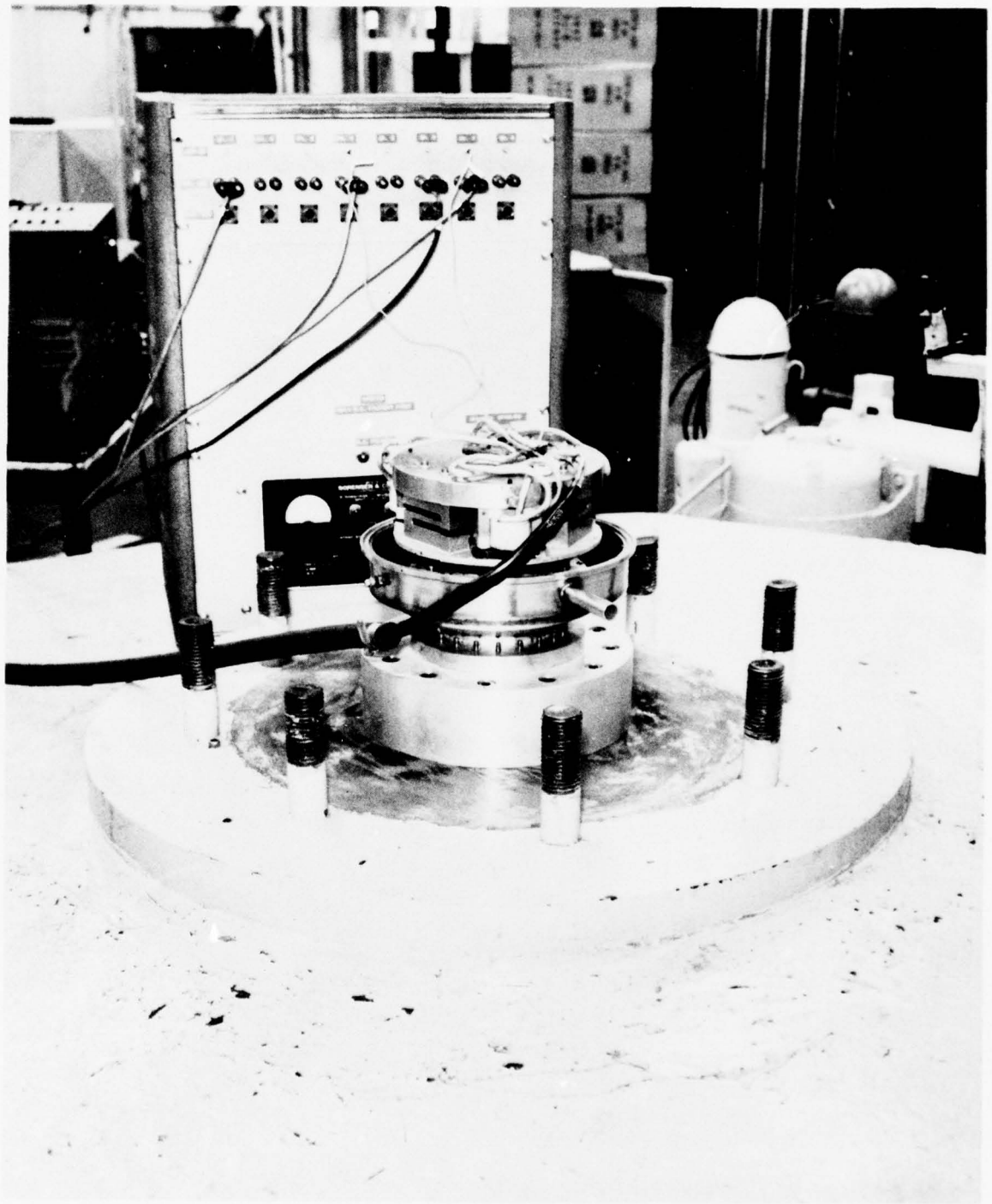


ELECTROMAGNETIC EXCITER FOR SPEAR MODEL  
FIGURE 3



G20390

ELECTROMAGNETIC EXCITER INSTALLED ON SPEAR MODEL  
FIGURE 4



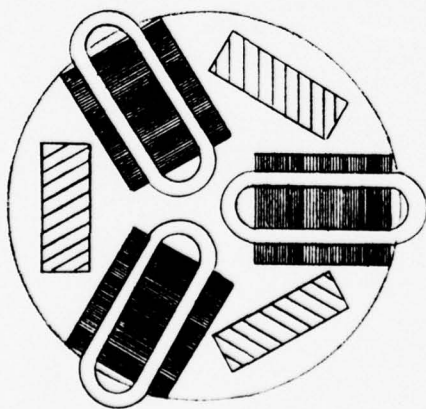
G21498

AIR SHAKE TEST OF ELECTROMAGNETIC EXCITER  
FIGURE 5

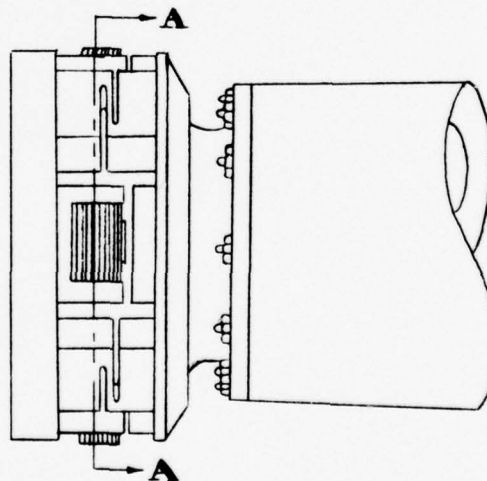
TABLE I

Electro-Magnetic Exciter for SPEAR Model

Outside Diameter:	9 in. (Coils overhang this a bit)
Total Gap Area:	17 sq. in. (not including windows for coils)
Gap - At Rest:	.019 in.
In Operation:	.015 $\pm$ .000170 in.
Gap at which exciter would become statically unstable:	Approx. .010 in.
Total Spring Rate:	125,000 lbs./in. (three springs in parallel)
Coils:	56 turns per magnet
Ballast Weight:	31.1 lbs. (E-Cores, backing plate, and spring ends)
Moving Weight:	25.7 lbs. (I-cores, adapter, and spring ends)
Ballast Motion:	$\pm$ .000033 in.



SECTION A-A



DC Bias Current:	24 amps.
DC Voltage:	30 V.
AC Exciting Current:	7.3 amps.
AC Voltage:	275 V.
Flux Density:	7440 $\pm$ 3150 gauss
Magnetic Force:	550 $\pm$ 426 lbs.
Acoustic Power Delivered:	52 watts
Estimated Power Loss:	350 watts

Total for three coils  
wired in parallel

All based on the estimated impedance of the SPEAR Model  
casting at resonance in water:  $34 \times 10^6$  gm/sec, resistive.



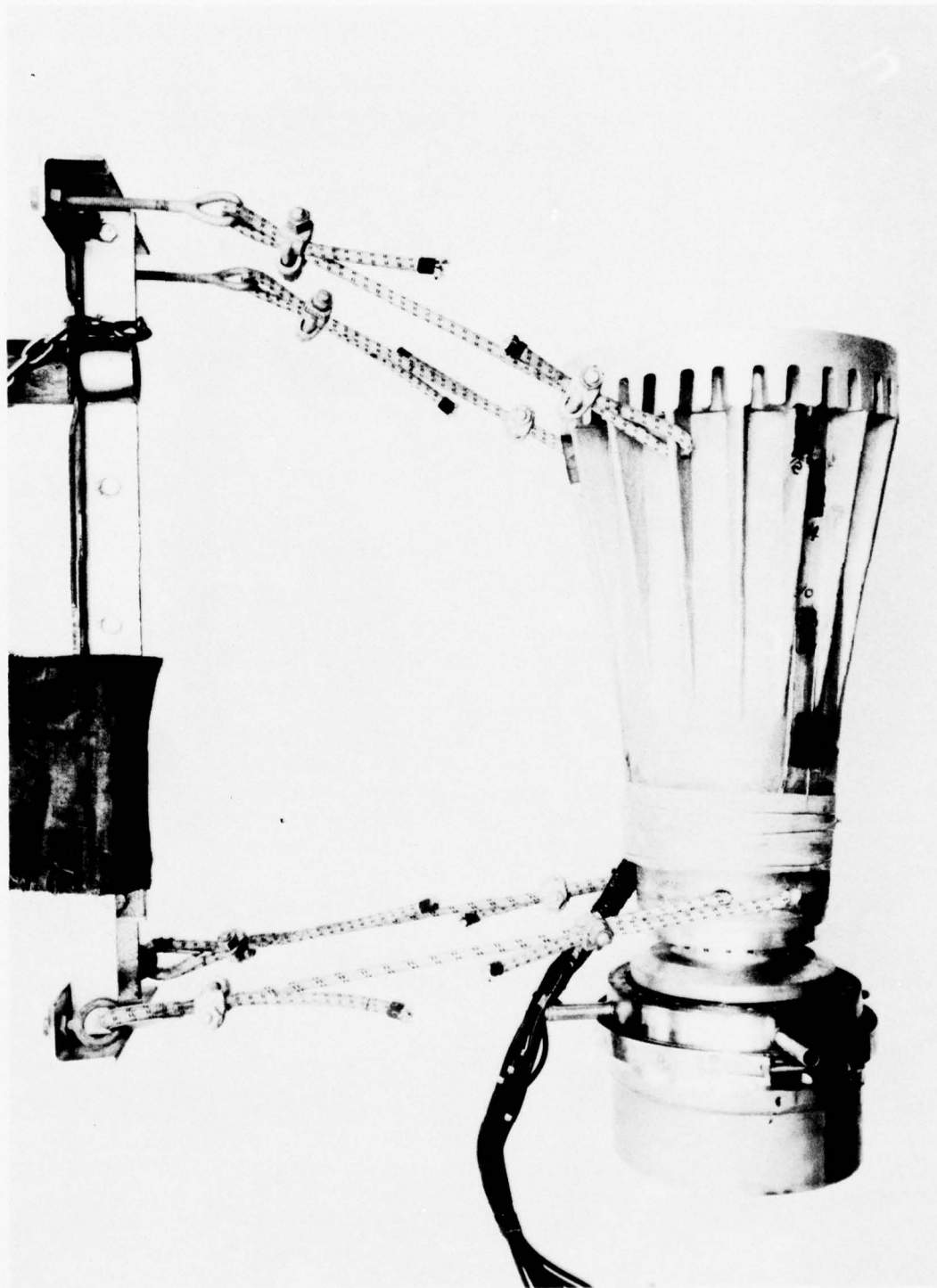
#### The Housing and Supporting Apparatus . (Continued)

scaling relationships would cover all the effects involved and, in addition, the full-scale design has not been sufficiently defined for this purpose. When the test assembly was submerged, air pressure in the housing was manually maintained slightly above the surrounding water pressure. The housing was found to be adequately airtight.

The SPEAR model was suspended in a horizontal attitude with rubber shock cords attached to a support frame which, in turn, was bolted to the lower end of the Navy's support shaft. For convenience in positioning, the face of the model projector was located on the centerline of the support shaft. The suspension configuration is shown in Figure 6.

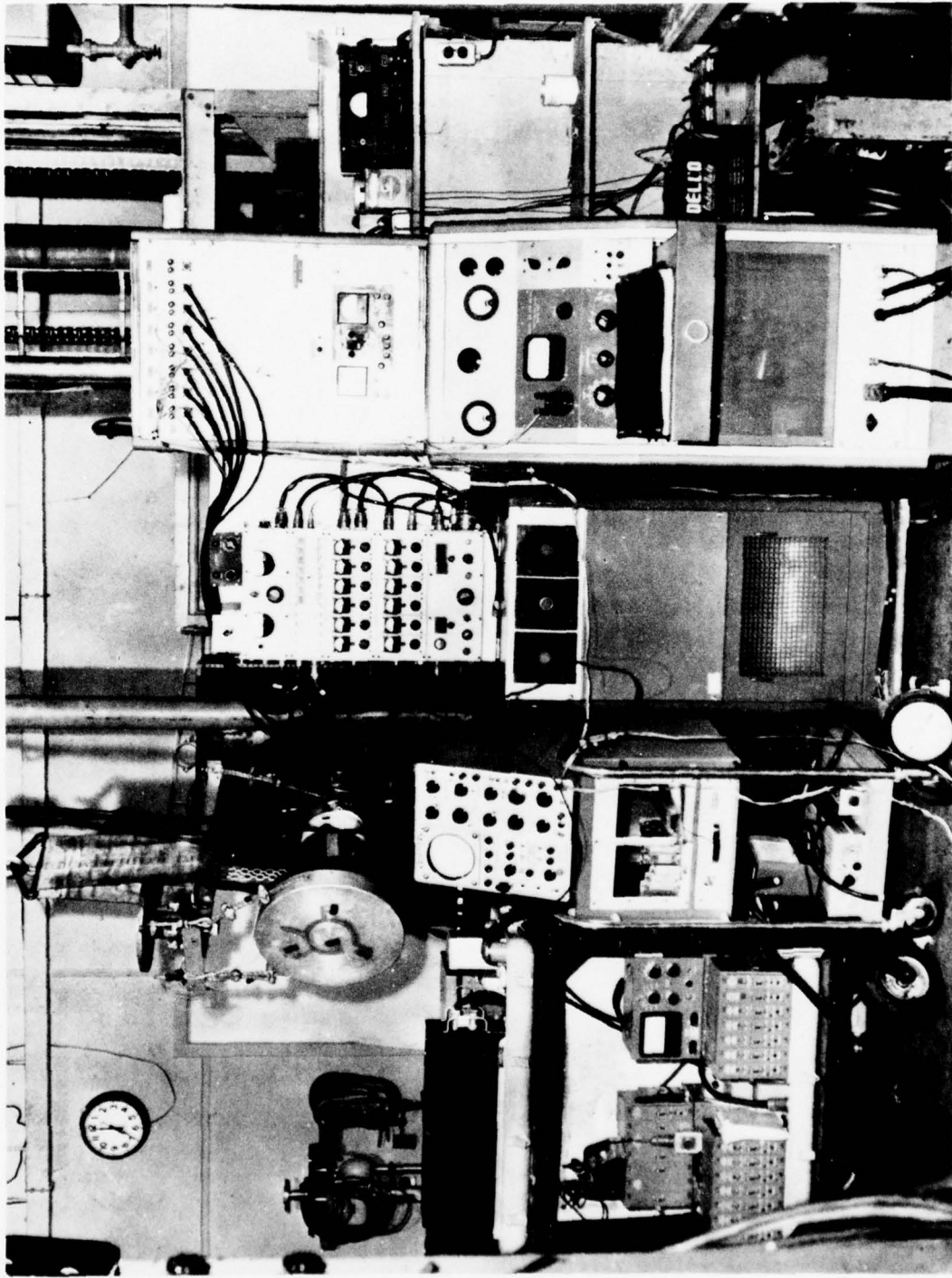
Instrumentation. The test instrumentation consisted of two main groups: one for making acoustic measurements in the water, the other to measure the vibratory behavior of the projector. The acoustic equipment was all supplied by the Navy, and constituted a conventional system for acoustic calibrations. The receiving hydrophone output was connected to a wide band receiver amplifier which had a variable gain of -20 to +80 db. The amplifier output was combined in the receiver modulator with the oscillator signal to produce a constant frequency signal. This frequency was amplified, filtered with a 20 cps band pass filter and used to drive the recording pen of a polar recorder (for directivity patterns) or a linear recorder (for frequency scans). This equipment was operated by Navy personnel. It is shown schematically at the right of Figure A-5. At the left of this Figure is shown the equipment supplied by Hamilton Standard to record accelerations and stresses on the test model. Signals from a number of accelerometers and strain gages were fed through preamplifiers and signal conditioners to an Ampex AR-800 magnetic tape recording system. A photograph of this measurement system is shown in Figure 7, which also includes, at the lower right, the exciter control console mentioned earlier.

The accelerometers (Endevco Model 2213M5) were installed at locations on the projector face and on the exciter assembly as shown in Figures A-3 and A-4. Lead wires were well shielded, and special checks were performed to ensure that the accelerometer outputs were unaffected by electromagnetic fields from the exciter or by acoustic pressure in the water. Strain gages were installed at locations on the resonant bar and on the projector face; these locations are also shown in Figures A-3 and A-4. The gages used were Kulite semi-conductor types (Model DB102) chosen because their high sensitivity was required to measure the extremely low vibratory stresses of the test. The waterproofing for these gages is shown in the photograph of Figure 8, which also shows some of the accelerometer mounting studs. All of the instrumentation on the test model was checked in a brief test run in a small tank at Hamilton Standard and found to operate satisfactorily. This test was also used to check air supply techniques and



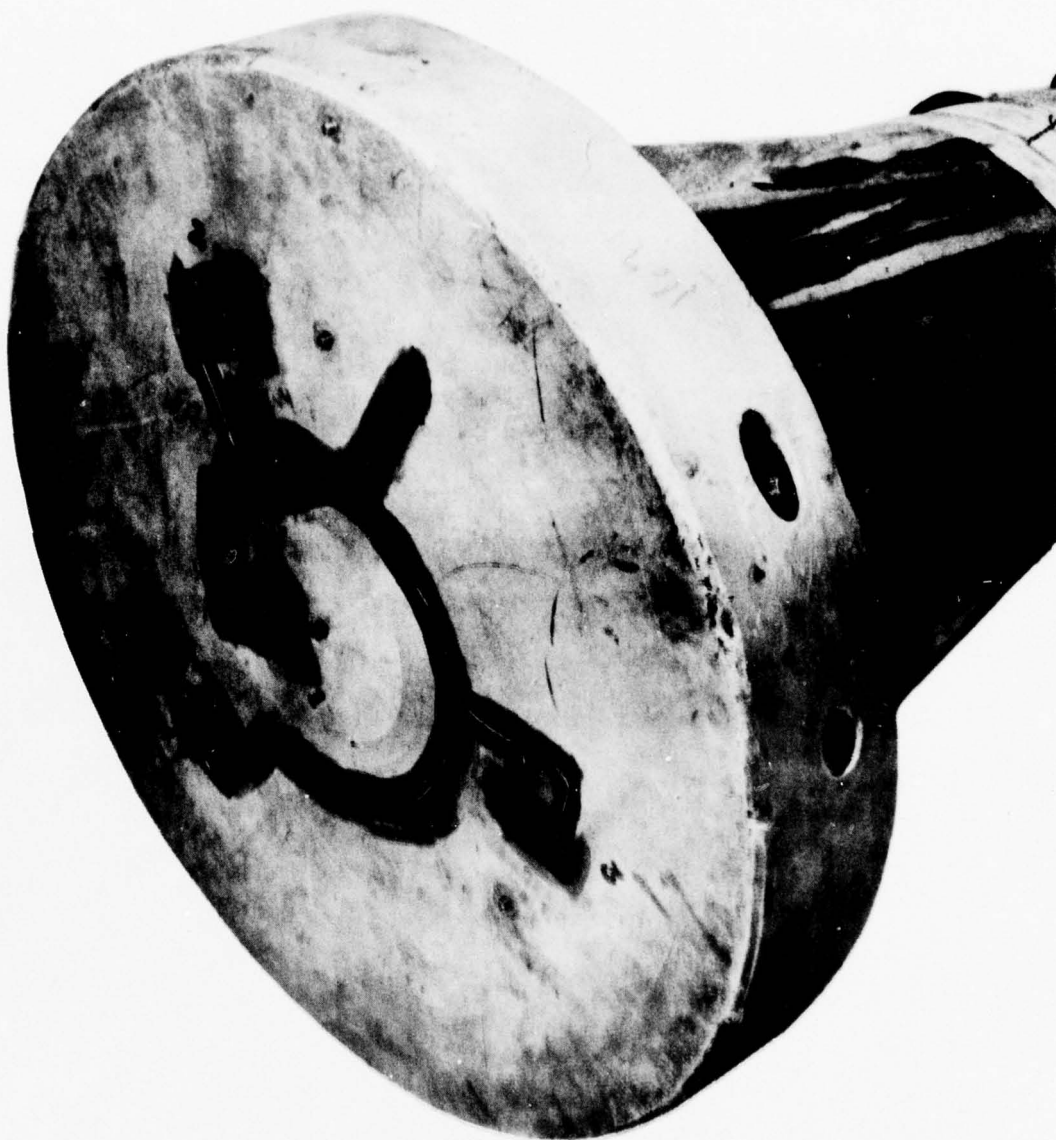
SPEAR MODEL WITH PISTON RIM REMOVED (CONFIGURATION A11-0)  
FIGURE 6

S 32637



S 33017

HAMILTON STANDARD INSTRUMENTATION FOR DODGE POND TEST  
FIGURE 7



G20672

STRAIN GAGES ON PISTON FACE  
FIGURE 8



#### Instrumentation. (Continued)

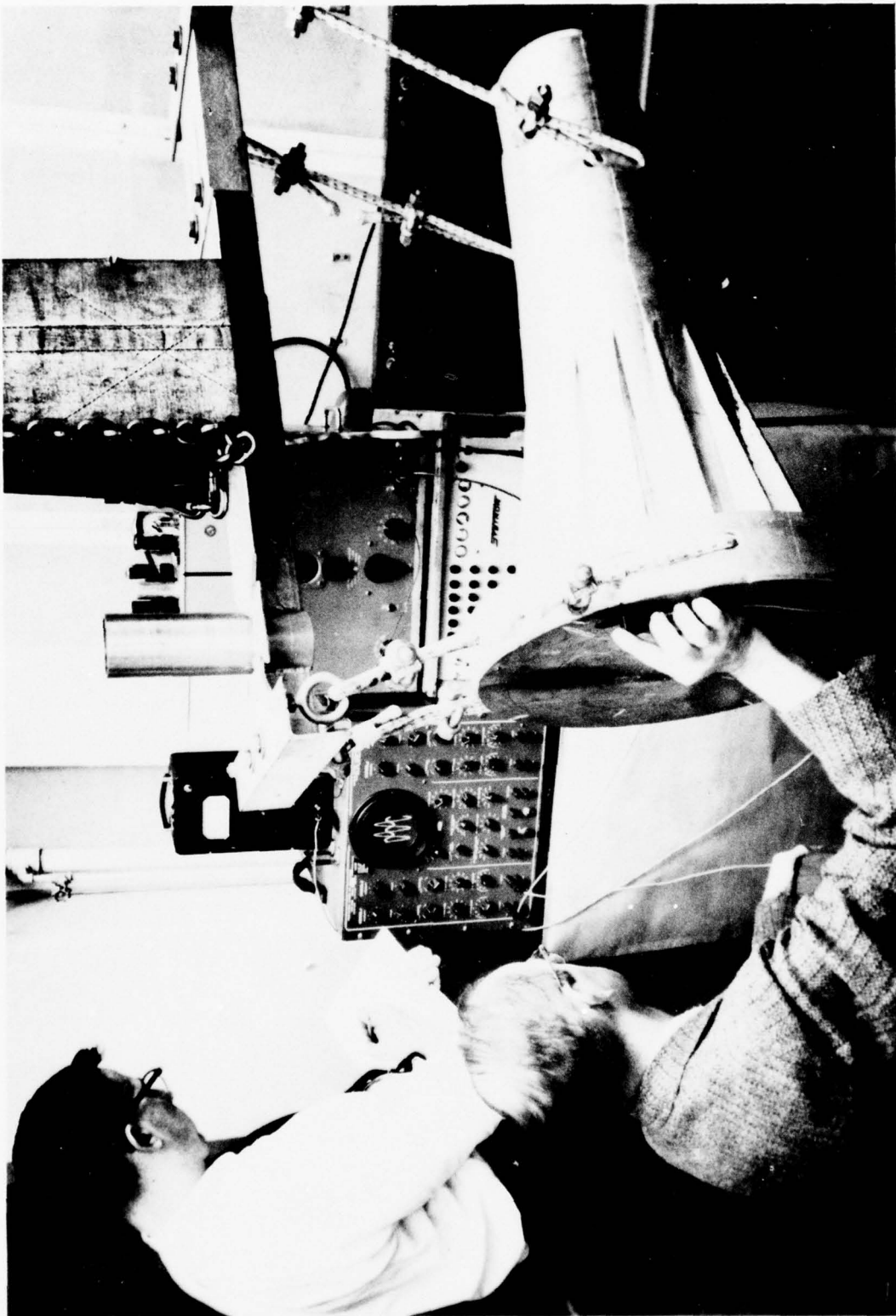
exciter operation (no acoustic data was obtained because of the small size of the tank).

In the preliminary air shake tests run with a crystal exciter, instrumentation was simply a hand-held crystal probe used for the gross determination of vibratory mode shapes. The photograph of Figure 9 and the schematic drawing of Figure A-1 show the test equipment used for this phase of the program.

The Test Facility. The major portion of the experimental work was performed at the Dodge Pond Field Test Station of Underwater Sound Laboratory. This Navy facility, located in Niantic, Connecticut, is well suited to acoustic work of this type. The pond averages 50 feet in depth and has a soft mud bottom which tends to reduce acoustic reflections. There are three test barges, each with an opening, or well, and handling equipment for positioning a projector and a hydrophone. A photograph of the test well used for these tests, showing the SPEAR model assembly being maneuvered into position on the support shaft, appears as Figure 10.

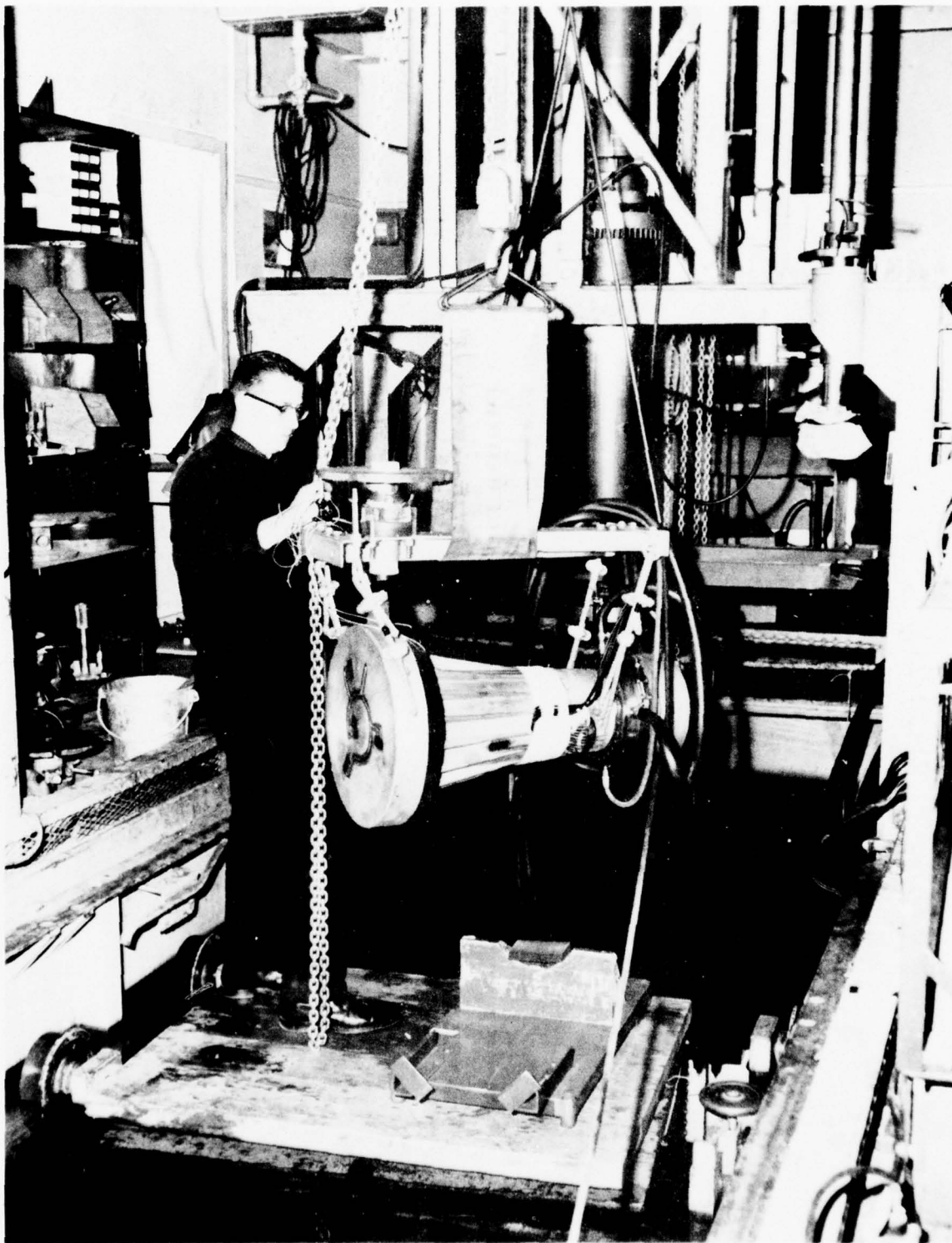
Preliminary Air Tests. The early shake tests of the SPEAR model in air were performed to check the resonant frequency of several test assemblies as well as to obtain some indications of vibratory mode shape. In these tests, run first with a low power crystal exciter and later with the electromagnetic exciter, frequency searches were made and resonances were detected by feel, by ear, and by the hand-held crystal probe. The exciter housing was installed and checked at this time. As desired, the flexible seal on which it was supported was soft enough to isolate the housing, even in air, while strong enough to carry the weight of the housing. At the maximum vibration amplitude tested, no housing motion could be detected.

Pond Test Procedures. For the pond test of each configuration the model was washed with detergent to facilitate wetting, and lowered into the water to soak for several hours before data was taken. Test depth for both projector and hydrophone was generally 17 feet, and test distances ranged generally from 10 to 15 feet. (These distances are considered adequate for the determination of far-field acoustic data). The tests were run at constant exciter current, manually adjusted, with the exciter control console used to adjust external capacitance so that the electrical resonance of the combination was near the mechanical resonance of the model. This adjustment was solely to ease the oscillator load and had no effect on the exciter conditions. Constant exciter current represents a condition of nearly constant exciter force output; over a limited frequency band this may be compared to the characteristics of the proposed full-scale exciter, in which the rotating unbalanced weights create exciter force which varies with the square of the frequency. Generally, the constant excitation used for the tests was 1 amp AC



G20220

AIR SHAKE TEST OF SPEAR MODEL  
FIGURE 9



S33016

SPEAR MODEL ASSEMBLY AT DODGE POND (CONFIGURATION A6-4)  
FIGURE 10

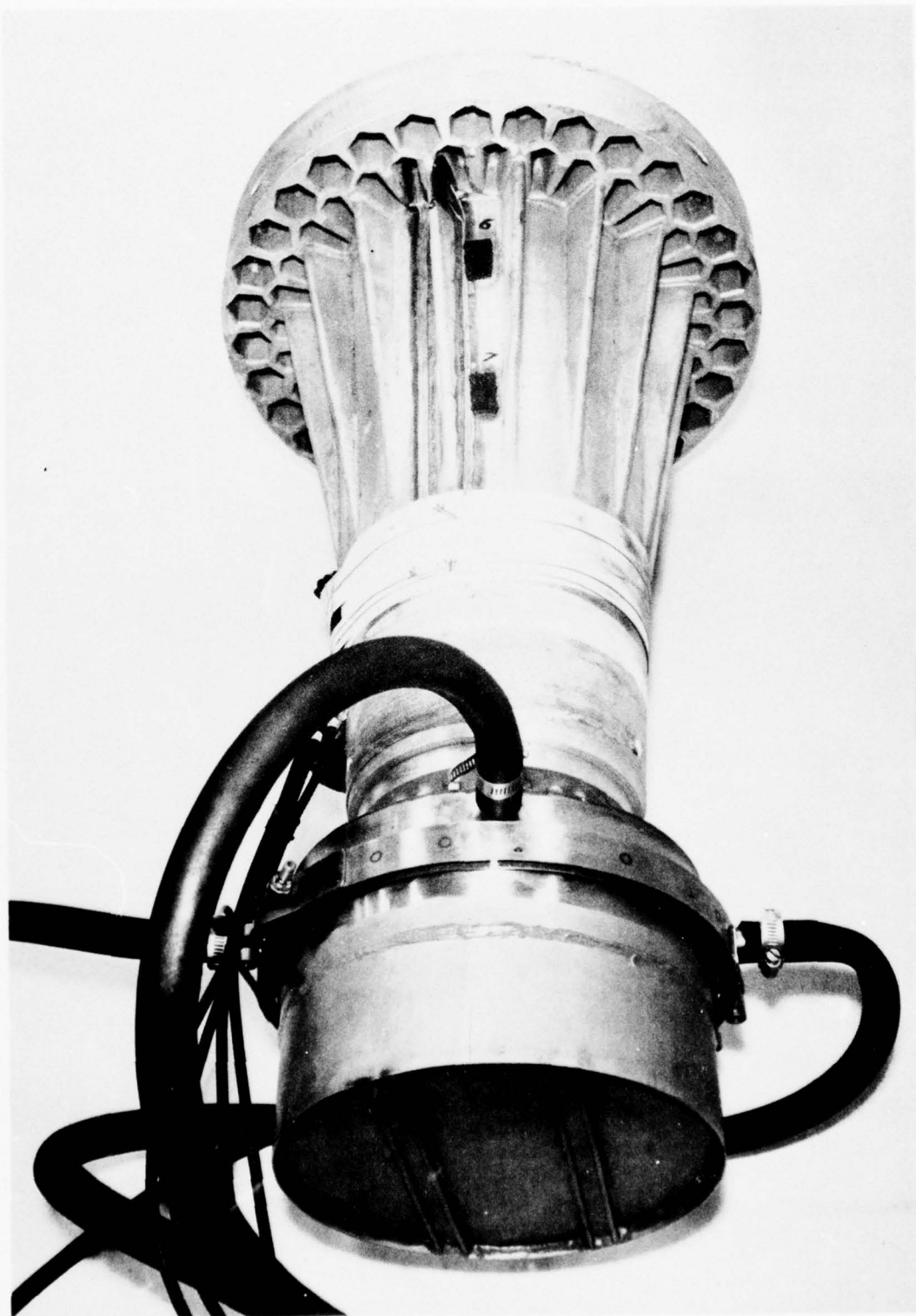
#### Pond Test Procedures. (Continued)

and 24 amp DC, which represented an acoustic output of about one-third of a watt, more or less, depending on the configuration. This was thoroughly adequate for the acoustic measurements, since it produced a source level ranging around 75db at resonance. Measurements of acceleration and stress on the model were also adequate for the purposes of the test at this excitation level. At the conclusion of one group of tests a series of runs were made with one test configuration up to an acoustic power output of 170 watts, using a special power amplifier to drive the exciter. All data showed good linearity in these runs. All of the tests were performed with continuous excitation; pinging was not utilized because it would have required extra equipment and would not have improved the data or added information applicable to the test purposes.

Transmitting directivity was recorded with polar plots of sound pressure level taken as the projector was rotated through 360° in azimuth. These plots were taken at or close to resonance for each configuration, and also at frequencies some five or ten percent above and below resonance for most configurations. Transmitting response was recorded at zero degrees azimuth as the frequency was automatically scanned past resonance with constant exciter amperage. A few frequency scans were recorded at 180° azimuth. All of the acoustic data was repeated at several distances in order to obtain enough information to compensate for the reflections which were present, producing significant local aberrations in individual data plots. For each of the configurations the results of a number of runs were adjusted by experienced Navy personnel to produce curves which are considered representative of what would have been recorded without reflections. Stress and acceleration data were recorded simultaneously with the acoustic data, with steady-state records taken during the directivity runs and continuous records during the frequency scans.

Summary of Pond Tests. The one-fifth scale model tests were run in two sessions, one from April 17 to May 2, 1961, (the April tests), the other from August 22 to September 5 (the August tests). The April tests were concerned most directly with the specific purpose of the program, that is, the evaluation of the basic projector design as originally proposed. The work commenced with a 25.5 inch bar length on the casting, and Configurations A4 and A5 were tested -- with and without the frequency-dropping spacer respectively. Both were tested bare (A4-0 and A5-0), and also with an inner tube around the exciter housing to simulate a more compliant enclosure (A4-1 and A5-1). A4-0 is shown in Figure 11, without the spacer, tests were also performed with an inner tube just behind the piston rim, to reduce rear radiation (A5-2 and A5-3). At this point it was found that the schedule would allow time to shorten the casting and test again at higher frequencies. After a quick machining operation, in which four inches were removed from the length, the tests were resumed and Configurations A6-0 and A7-0 were tested (bare, without and with the spacer, respectively) as well as





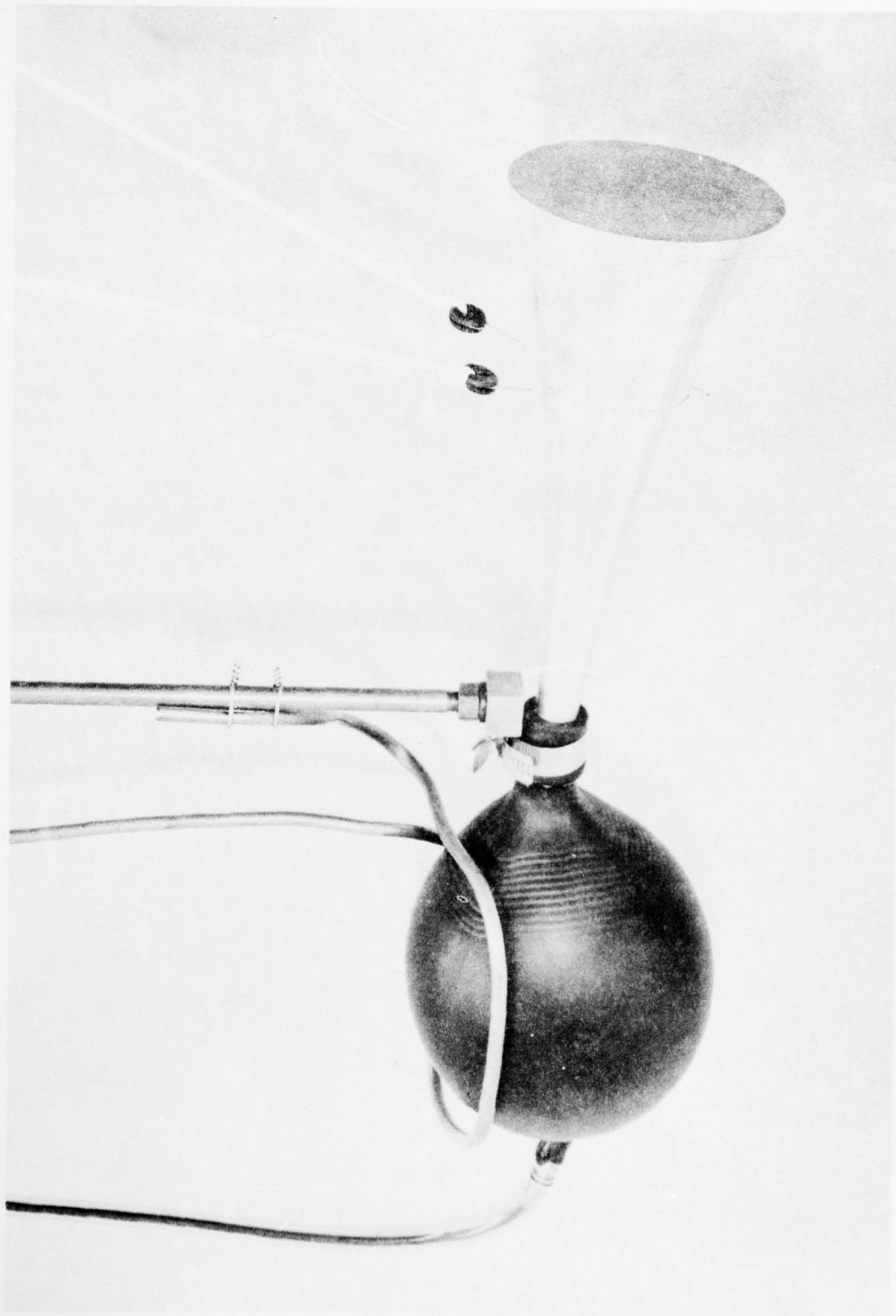
SPEAR MODEL ASSEMBLY (CONFIGURATION A4-0)  
FIGURE 11

G20671



S 32636

SPEAR MODEL WITH PISTON RIM REMOVED AND CELLTITE COVERING (CONFIGURATION A11-6)  
FIGURE 12



G21918

EXPONENTIAL PROJECTOR FOR JANUARY TESTS  
FIGURE 13

#### Summary of Pond Tests. (Continued)

several configurations involving the inner tubes or a ring of foam rubber behind the piston rim. The foam rubber ring may be seen in Figure 10. The April tests included twelve configurations as shown in Tables B-1 and B-4. These twelve, plus three similar configurations tested in August, have been designated "primary configurations" for this report, because they are a family of shapes representing most directly the original SPEAR design.

The August tests covered ten configurations, as shown in Tables B-1 and B-5. Except for the first three (A7-0, A7-4, and A7-6) these are designated "secondary configurations" and were selected with a purpose different from the primary group. Because the April tests had generally supported the original design assumptions (as will be shown) and because of an increased emphasis on directivity, it was felt that the second test series might be more useful if it covered several configurations which represented new experimentation rather than continued optimization of the early design. Accordingly, a newly-designed, re-proportioned, model was not manufactured, but instead, the existing model was tested with some additional modifications, all of which were intended to give information on the possibility of improving the front-to-back ratio of the projector. These modifications consisted of the following: For four models, (A7-6, A10-6, A11-6, and A12-6) the foam rubber behind the piston was augmented to the limit where all of the model assembly except the piston face was enclosed. For A7-7 a foam-rubber-faced reflector was located at several positions approximately a half wave-length behind the piston. In A10-0 and A10-6 the piston rim was ballasted with a ring of small masses to force a more severely curved piston face vibration, with the thought that this might also indicate by implication what rigidizing the piston would do. Finally, as another experiment in directivity, in Configurations A11-0, A11-6, A12-0, and A12-6, the model was tested with the piston diameter reduced to 14.7 inches, that is, the rim was machined off. This piston shape was tested with and without the spacer. The appearance of the casting after the diameter reduction is shown in Figures 6 and 12. Figure 6 also shows the frequency dropping spacer, and Figure 12 shows the celltite rubber used to cover all of the model except the piston face.

Test Data Reduction and Presentation. The data obtained in these tests and the various quantities calculated from the raw data are presented in Tables B-4 and B-5 and in Appendix C, Figures C-1 to C-49. Except for dimensionless data, all of the information has been normalized to an excitation level of 1 amp AC and 24 amp DC, the conditions at which most of the tests were run. The transmitting response curves and directivity patterns were prepared from data released for publication by the U. S. Navy Underwater Sound Laboratory.

The transmitting response curves for all configurations, Figures C-13 to C-21, have been summarized in the plots of Quality Factor versus normalized



#### Test Data Reduction and Presentation. (Continued)

frequency or  $ka$ , Figures C-1 and C-2, where Quality Factor was calculated from the relationship  $Q = f/\Delta f_{-3db}$ . The directivity patterns for each configuration are presented in Figures C-22 to C-43, one sheet per configuration, where the several patterns on each sheet represent the several frequencies at which each configuration was tested, the patterns being normalized to the forward sound level of the frequency nearest resonance. Directivity data is summarized in Figures C-3 to C-8 in three different ways: Beam Width, Front-to-Back Ratio, and Directivity Index. Beam Width is the total width of the main lobe to the half-power points; Front-to-Back Ratio is the ratio, in decibels, of the forward sound level to the maximum sound level within  $60^\circ$  of straight back (this choice of a rearward reference level, though somewhat arbitrary, was felt to be the best way to evaluate the particular shapes of pattern under study); Directivity Index is the ratio, in decibels, of the forward sound level to the average sound level.

The data obtained from the accelerometers and strain gages is listed in the data summaries, Tables B-4 and B-5, and shown in Figures C-47 to C-49, which present more detail on the vibratory action of the SPEAR model. The accelerometer data was converted to displacement for convenience in interpretation. This conversion could be simply done because the vibratory accelerations contained no measurable harmonics. The stresses presented were calculated from the uniaxial strain measurements by the relationship  $s = E \times e$ . A small amount of this data, covering the August repeat runs of Configurations A7-0 and A7-4, was lost because of instrumentation difficulties.

The acoustic impedances presented to the Spear piston face by the water were calculated from the test observations, and are presented in Tables B-4 and B-5. These impedances are also summarized graphically in Figures C-9 to C-12, where they are compared with the theoretical impedance of a free piston. Resistive impedance was calculated from the measurements of radiated acoustic power and the piston face motion. A calculation was made for all conditions at which a directivity pattern, a source level, and piston motion were recorded; therefore several resistive impedance points are available for each configuration. The computation procedure for obtaining these points is given in Appendix D-III, Page D-4. Reactive impedance is sensed by the projector as an accretion to the mass of the piston, which reduces the resonant frequency of the assembly from what it had been in air. The magnitude of the reactive impedance is calculated, then, from the frequency shift of each configuration upon immersion. This necessarily involves an accurate vibration analysis of the assembly; the techniques used for this part of the work are discussed in more detail subsequently, on Page 27, and in Appendix D-II, Page D-3.

### Test Data Reduction and Presentation. (Continued)

In analyzing the test observations, no attempt was made to interpret the electrical characteristics of the exciter because it was designed only as a device to permit testing the SPEAR acoustics and bore little similarity to the proposed rotating-mass exciter. It was felt that an analysis of the electrical input conditions would be unlikely to produce useful data.

### THE JANUARY TESTS

After the August tests were completed, it was decided to conduct an additional test program intended to give more information on directivity. In particular, it was hoped that by testing a projector design with a different shape and pattern of side wall action some insight would be gained into the possibility of obtaining greater front-to-back ratio without the use of pressure release materials. The configuration tested was a solid, exponentially-tapered, resonant bar, designed with no consideration to weight and tunability, since the purpose of the test was to study directivity. This limited purpose also permitted a reduction in scale and the use of a simple "crystal" exciter, which facilitated the performance of this additional program.

The three models tested are of approximately 3% scale, referred to the 400 cps full-scale frequency. All have a face diameter of 3.7 inches and a "throat" or narrow end diameter of 0.5 inches. The first is solid aluminum and 10.0 inches long; the second is solid magnesium and 9.02 inches long. A third model -- externally similar to the first, but hollow -- was also tested but gave no useful results because of local resonances and questionable structural action. The wall thickness of this model was quite thin, very much thinner proportionally than the one-fifth scale models previously tested. The exciters were 1/2 inch diameter rods of barium titanate, tuned to 15.5 K.C., and attached to the narrow end of each exponential bar by wax, which gave a sufficiently strong joint. Since only directional properties were of interest, the possible attenuation of the acoustic energy by the wax played no role. A rubber bag from a respirator was fitted over the ceramic and stretched over a rubber stopper on the small end of the bar, forming a watertight seal. A plastic tube was sealed to the opposite end of the bag, serving the dual purpose of carrying the wires to the transducer and supplying air to inflate the rubber bag. The ceramic was in effect enclosed in an air bubble and thereby prevented from radiating directly into the water. (A test was run with the bag deflated to determine whether or not the air bubble played an important role in the radiation pattern.) The test assembly is shown in Figure 13. For convenience, the models tested in January, and their nomenclature, are shown schematically in Table B-3.

The tests were carried out at Dodge Pond in the same location used for the earlier tests, again with the cooperation of U.S. Navy personnel. The models

#### THE JANUARY TESTS (Continued)

were suspended from the support shaft with a flexible cord at the node, a vertical rod clamped onto the rubber stopper at the small end of the bar, and a horizontal loop of rigid tubing holding down the inflated rubber bag. Test depth was 17 feet, and hydrophone distances were 6 and 9 feet. Test techniques and procedures were essentially the same as for the one-fifth scale model tests of April and August.

The test data obtained consisted of directivity patterns recorded at the frequency of peak amplitude and off the peak at the upper half-amplitude point. A minimum of adjustment for reflections was necessary, because the size and frequency of the models allowed close test distances where reflections were relatively unobtrusive. From the directivity patterns the Beam Width, Front-to-Back Ratio, and Directivity Index were determined; these are listed in Table B-6, the summary of test results for January, and appear in the Test Data graphs, Figures C-4, C-6, and C-8, along with the secondary configurations from the August test. The directivity patterns themselves are presented in Figures C-44 to C-46. These curves were prepared from USL Calibration Report No. 2355.

## DISCUSSION OF TEST RESULTS

### BACKGROUND

Prior to the tests, the characteristics of the SPEAR configuration which emerged from the optimization studies had been analyzed on the basis of a number of assumptions. Chief among these was the acoustic impedance of the radiating piston. In the optimization studies the impedance had been taken to be three-quarters of that for a free, un baffled, piston of the same size. Later, after additional consultation, it was felt that the impedance might be substantially lower, and an analysis was performed to predict how the model would operate if faced with one-quarter of the originally assumed resistive impedance and one-half of the assumed reactive impedance. In all of the early optimization studies, primary emphasis was given to tunability, and the size and proportions of the model were chosen to minimize Quality Factor and thereby maximize tunability, with due regard to weight, efficiency, cost, and size. With the original impedance assumptions, Quality Factor (from the energy definition,  $Q = 2 \pi \times \text{maximum potential energy} \div \text{energy dissipated per cycle}$ ) was calculated to be 6.7; the reduced impedance assumptions gave a value of  $Q = 15.5$ , substantially less desirable.

Directionality was not of itself a factor in the design optimization, since it was intended that the first SPEAR unit was to test the feasibility of the concept, and that attention would be given later to obtaining the most desirable pattern of acoustic radiation. However, during the model test program considerable additional emphasis was placed on directionality, and many of the configurations tested were chosen to study this factor.

### RESULTS OF AIR TESTS

The preliminary air shake tests were performed to determine the adequacy of the calculation procedure used to predict natural frequency and mode shape. A tap test of the raw casting before machining showed the axial natural frequency to be 2280 cps, just 4% lower than calculated, and a crystal-excited shake test of the casting after partial machining, but still retaining excess bar length left in manufacturing ( $L = 31 \frac{1}{2}$  inches), located the resonance at 2190 cps, or 3% lower than calculated. The calculations had been performed with the techniques described in EP-60806, "Engineering Proposal for a Sonic Projector for Extended Acoustic Ranging", which assumed a rigid piston. These optimistic results, which indicated that the calculation technique was generally correct, were moderated somewhat by subsequent tests with the additional mass of the frequency-changing spacer or the electromagnetic exciter attached to the driver end of the casting. The results of these and other air shake tests are covered in the next section.



## RESULTS OF AIR TESTS (Continued)

Natural frequencies of the system other than the fundamental axial mode were also identified in these air tests. Of these, the two most clearly seen were: one, the resonance of the exciter backing plate shaking axially on its springs with the casting as a ballast, at 198 cps; and, two, the lowest free-free bending mode of the system, found at 956 cps with the crystal exciter and the excess bar length. At frequencies substantially above the fundamental axial resonance, a number of indistinct higher order resonances were detected. In most cases these involved complex motions of the piston face.

## FREQUENCY STUDIES

The air shake tests indicated that, although the assumptions of the calculation procedure were generally correct and the frequency of the unshortened casting agreed well with predictions, the shifts in frequency produced by shortening the casting or by installing the electro-magnetic exciter and the spacer were less well predicted. Since shifts in frequency upon immersion were to be used to deduce reactive impedance, it was felt that a more comprehensive mathematical model would be desirable for the calculation.

The original calculation procedure was based on simple longitudinal vibration theory, with the piston acting as a rigid mass on the end of an elastic bar, the bar being unrestrained on its transverse boundaries. When the exciter and spacer were added to the other end of the bar, they also were regarded as rigid masses. However, the observed resonant frequency for the system with the exciter and spacer, and with the bar length shortened to 25 1/2 inches, was 14% lower than the prediction based on these assumptions. It seemed evident that the effective mass of the components attached to the bar was greater than their actual mass; that is, the attachments were not rigid, but were elastically deforming in such a way as to appear more massive. The new mathematical model chosen represented these attachments, as well as the piston, as simple spring-mass systems whose frequency ( $\sqrt{K/M}$ ) was above the total system resonance. The quantitative description of these spring-mass systems was achieved by a kind of "boot-strap" method in which the magnitudes of the springs and masses were chosen to be in general agreement with the geometry of the parts and to produce frequency predictions which most consistently agreed with the actual resonant frequencies of a large number of different configurations. Since the purpose of this representation was to permit a more effective calculation of reactive impedance in the water, this empirical method was felt to be preferable to a rigorous analysis of the exact geometry involved. The expressions utilized in establishing the mathematical model are included in Appendix D. With this approach, the agreement achieved between observation and prediction was generally within 1% and at the worst about 2%.

## FREQUENCY STUDIES (Continued)

The next analytical step was to proceed from the establishment of a system description consistent with all of the axial resonant frequencies observed in air to the calculation of the reactive impedance from the downward shift in frequency observed when the model was operated in water. The reactance of the water is sensed by the piston as an increase in effective mass, thereby lowering the axial natural frequency. The amount of mass necessary to lower the frequency by the observed amount could be calculated directly and then translated into a value of dimensionless reactive impedance, using appropriate factors. This step is also covered in Appendix D.

## RESULTS OF THE POND TESTS

(During the following discussion, cumbersome and repetitious reference to specific tables and figures will be avoided. Generally, the arrangement of the figures follows the order of discussion of the various topics. The layout of test data in the tables and figures is summarized on Page 22 under Test Data, Reduction and Presentation.)

The April Tests. The tunability of the model SPEAR assembly, as demonstrated in the April test series, was indicated by a Quality Factor of about  $5 \frac{1}{2}$  for the frequency where the relative piston size, or  $ka$ , was 2.0; at lower frequencies the  $Q$  was higher, up to about 8 at a  $ka$  of 1.6. There was no substantial effect on tunability from the addition of pressure release material anywhere on the model.

To describe the directivity of the model, three factors must be used, each identifying a different aspect of the radiation pattern: Beam Width is important to Source Level and to the operational system; Front-to-Back Ratio is significant to Source Level up to a point, however, improvements over about 6 db no longer enhance the Source Level yet are still very important in an operational system; Directivity Index is the specific indication of what Source Level can be expected from any given power level.

For the configurations tested in April without pressure release material behind the piston rim the Beam Width at a  $ka$  of 2.0 was about  $65^\circ$ . At lower frequencies the beam was a bit broader. The installation of the inner tube or foam rubber behind the rim broadened the beam considerably, up to  $110^\circ$  at a  $ka$  of 1.74. At 2.0 the Beam Width with pressure release was about  $75^\circ$ , and at higher frequencies the trend of all configurations seemed to level out at about  $60^\circ$ . The Front-to-Back Ratio of the "bare" configurations was generally about 3 or 4 db, with extremes of 0.7 and 5 db, and no noticeable trend with  $ka$ . Adding the pressure release material had a dramatic effect on this parameter, raising the ratio to

The April Tests. (Continued)

about 14 db at a  $ka$  of 2.0, with a definite trend of increasing Front-to-Back Ratio with increasing  $ka$ . (Two stray points, A5-2 and A5-3, with intermediate values of this ratio are unexplained.) Directivity Index was about 7 db at 2.0, with a general upward trend as  $ka$  increased, up to 9.5 db at  $ka$  of 2.59. Configurations with the pressure release materials had about the same D.I. as the "bare" configurations; apparently the narrower Beam Width of the "bare" configurations was balanced by their lower Front-to-Back Ratio. In all of the data it appeared that the addition of the inner tube on the exciter housing had an insignificant effect on the radiation pattern. In summary, the directivity of the "bare" configurations was generally like that of a free piston; the addition of pressure release material behind the piston rim reduced the rear lobe and broadened the forward beam, tending toward the pattern of a piston in the end of a long cylinder.

The impedance of the test model -- the acoustic load imposed by the water on the model piston -- was found to be generally similar to the theoretical impedance of a free piston. For the "bare" configurations the trend of the resistive impedance followed closely the free piston curve, running generally slightly higher. When pressure release material was applied, the resistance lowered a bit, moving closer to the theoretical impedance of a piston in a cylinder. Considering the limitations on accuracy inherent in this kind of test, and the somewhat indirect method used to compute resistance (which is covered in Appendix D), the scatter of the test data is surprisingly small. The more extreme strays are less meaningful because they occur at the upper edge of the frequencies covered, where the radiating piston is beginning to flex, as will be discussed subsequently. Reactive impedance, also, followed generally the same trend. The reactance of the "bare" configurations was clustered near the theoretical reactance of a free piston, whereas for the configurations with pressure release the reactance was somewhat lower.

From the accelerometer data it was found that the piston vibrated in a kind of "cupping" mode, in which the edges moved more than the middle. This action was trivial at the lower frequencies -- for configuration A4-0 at 1535 cps the edges moved only about 7% more than the average face motion -- but at 2160 cps configuration A6-0 showed edge motion about 35% more than the average. Figure C-49 best illustrates this trend; it shows the change in piston action of configuration A5-0 as frequency is changed. In this case the frequency scan was carried to 2500 cps, where the piston deformation became severe enough that the center and edges, which were previously in phase, were  $180^\circ$  out of phase. (The data for 1700 cps, which is not in agreement with the trend, is not explainable, except as a possible error in measurement.) The stress measurements, although they were of such a low level that their magnitudes were less



#### The April Tests. (Continued)

accurate than other data of the test, showed that the nodal stress in the bar was generally in agreement with the observed vibratory motions. Because of the cupping action of the piston, the stress in the fillet between the piston and the bar exceeded the nodal stress by about half. This area will need careful attention in a full-scale design. All of the stress and accelerometer data was examined for evidence of unsymmetrical bending action as an element of the axial mode. There was no indication of such action (nor was any consistent dissymmetry evident in the directivity patterns).

The accelerometer data also indicated deformations of the electro-magnetic exciter adapter. Although deformation here has no acoustic significance and is unrelated to the full-scale SPEAR design, it did affect the resonant frequency of the model assembly, as noted under FREQUENCY STUDIES. This deformation also made unfeasible a proposed redundant method of computing the acoustic power level, which would have required an accurate knowledge of exciter displacements.

In summary, the results of the April test series generally confirmed the design assumptions and the acoustic feasibility of the SPEAR concept. They also provided a basis for further design work. The directivity and radiation impedances of the "bare" model configurations were found to be similar to a free, unbaffled piston; when an inner tube or foam rubber was placed behind the piston rim the acoustic characteristics shifted toward those of a piston in the end of a long tube. Changes in exciter housing compliance (effected by mounting an inner tube on the housing) did not produce significant acoustic changes. None of these conclusions were altered by subsequent work.

The August Tests. For convenience in discussion, the configurations tested in August may best be divided into two categories: primary and secondary. The primary configurations were those in the same "family", so to speak, as in the April tests; the others differ substantially in various ways. Of the primary configurations tested in August, A7-0 was a direct repetition of one of the April configurations to establish repeatability. The repeat data at best was an almost exact duplication of the earlier information, in the case of the resistive impedance, and at the worst differed from the earlier runs only by an amount consistent with the general scatter expected. The only item whose repetition was not good was the resonant frequency in water, which in August was inexplicably 2% lower than in April. The other primary configurations tested in August had foam rubber behind the piston rim or around the entire rear of the assembly. On the latter configuration the effect of the additional pressure release material was not significant except for Front-to-Back Ratio, which was enhanced about 3 db compared to configurations with the material located only behind the rim.



The August Tests. (Continued)

The first of the secondary configurations tested was A7-7, which consisted of a "bare" model (A7-0) with a large pressure-release reflector approximately a half wave-length behind the piston. This modification had a dramatic effect on most of the acoustic parameters. Q was raised about 2 units above the trend of other data. Directivity was substantially affected: Beam Width was reduced to 50°, narrower than any of the one-fifth scale configurations; Front-to-Back Ratio was up a bit (although this is difficult to interpret because the shape of the radiation pattern was generally different from other configurations -- see Figure C-37); Directivity Index was raised to 10 1/2 db, higher than anything else tested. Resistive impedance was not much affected but reactive impedance was increased by about a third. (The shift in reactance was also indicated in the Q increase).

Next tested were A10-0 and A10-6, which consisted of the same assembly as A6-0 with the addition of a set of small masses on the rear side of the piston rim, to force a more severely curved piston face vibration. The weights in fact did aggravate the cupping, as shown in Figure C-48, and raised the Quality Factor 3 1/2 units. Directivity was not much affected -- data taken both "bare" and with pressure release material covering the rear fell in with similar points for other configurations. Acoustic impedance was computed to be somewhat less than other configurations, but this result is felt to be less certain than other parameters because the severe piston flexing undoubtedly compromised the accuracy of the computation. The vibratory stress in the fillet behind the piston was relatively greater than before. By implication, this modification indicated the desirability of minimizing piston flexing.

The remaining configurations tested in August were modified by the complete removal of the overhanging piston rim in order to experiment with a possible improvement in directivity. The data on these rimless configurations was obtained at about the same ka as most of the other data, since the diameter reduction was compensated by the frequency increase. It was found that the piston deformation shape changed from concave to convex, as might be expected, and the rim fillet stress dropped drastically, since there was no rim. Surprisingly, none of the acoustic parameters was much affected by this radical change. The implications of this outcome on the detailed mechanism of acoustic radiation from the SPEAR shape are not fully understood, but it would appear, at least, that some radiation originates at the sidewalls of the bar as well as the rear rim of the piston.

From the August series of tests four salient points resulted:

1. Completely covering the rear portions of the model with foam rubber gave a small increase in Front-to-Back Ratio over that

The August Tests. (Continued)

observed with the rubber located only behind the piston rim, but otherwise made little change.

2. A reflector can significantly improve directivity at the expense of tunability.
3. Piston flexing should be minimized.
4. Without foam rubber, the side walls of the conical bar participate in the radiation of sound.

The January Tests. The primary result of the tests run on the small, solid, exponentially-tapered models is the greater Front-to-Back Ratio obtained without the use of reflectors or pressure release material. The Beam Width and Directivity Index were generally better than was achieved with the one-fifth scale models, but no more so than might expected from the higher  $ka$  of the January models. (The data centered around a  $ka$  of 2.7 rather than 2.0 as before.) The Front-to-Back Ratio, on the other hand, was in the region of 10 or 11 db -- much greater than might have been extrapolated from the earlier data on "bare" configurations. The large air bag enclosing the crystal exciter is not thought to have contributed significantly to the acoustic performance, since it was two and a half wave lengths behind the front face; a test run with the bag partially deflated showed little change, and previous tests on the larger models had shown the effect of a similarly-located inner tube to be small.

Useful quantitative data on tunability was not obtained in the January tests, but it was observed that the models were sharply tuned -- much more so than the one-fifth scale models. The nature of the test also precluded the determination of acoustic impedances or structural action.

From the January tests it was inferred that the radiation pattern can be improved by some favorable pattern of structural action, without recourse to pressure release material. The shape tested lacks the assets of low Quality Factor and low weight, but the opportunity for effective improvements in external shape or internal structure does seem to exist.

## SUPPORTING ANALYSES

### THE IMPEDANCE OF A NON-RIGID PISTON

In addition to its effect on the radiation pattern, the structural action of the SPEAR projector has a bearing on acoustic impedance and on Quality Factor. The manner in which the non-rigid component of piston motion can affect these parameters has been considered in a short analytical study, which suggests that by judicious control of the mass and stiffness of the radiating piston the Quality Factor of the system may be reduced, with a corresponding improvement in tunability. This study is included in Appendix D. The scope of the analysis undertaken, which was intended to be only exploratory, did not include the determination of the particular design configurations which would best accomplish this improvement, but it is felt that the approach to be followed in a more comprehensive analysis of this technical area was usefully identified.

### THE EFFECT OF BAR TAPER

During the early design studies from which the one-fifth scale SPEAR model emerged it was recognized that the choice of a constant cross-section area for the conical bar portion was an arbitrary decision, and might be modified by subsequent analysis. An analysis of bar taper has now been completed, and the results may be applied to the optimization of improved SPEAR designs. Since the details of the analysis are presented in Appendix D, only the conclusions will be discussed here.

In comparison to a constant area bar, it was found that a desirable reduction in Quality Factor could be obtained by a diverging taper, that is, the area increasing with increasing distance aft of the node. In compensation, this improvement in tunability is accompanied by a small increase in total weight and an undesirable decrease in exciter amplitude, which would then require more exciter force and ultimately result in reduced system efficiency. A converging taper produces the opposite effect. The proper choice for a particular design would be dependent on the relative importance of the various design parameters.

For simplicity, the analysis was limited to bar taper aft of the node, with a constant bar area from the node to the radiating piston, in order to hold bar nodal stress constant. By allowing stress to vary, as well as  $Q$ , weight, and exciter amplitude the effects of taper in the remainder of the bar could be

#### THE EFFECT OF BAR TAPER (Continued)

studied. It would appear by interpretation of the present analysis that an increasing bar area from the node to the piston could improve the exciter amplitude ratio and provide a broader support to the piston, at the expense of an increase in nodal stress. Again, the premises of a particular design optimization would dictate the choice of taper.

#### THE EFFECT OF REAR SURFACE MOTION ON THE DIRECTIVITY PATTERN

As a result of the desire to improve directivity without the use of pressure release material, and in view of the results of the January tests (which showed that the exponential projectors had a better Front-to-Back Ratio than the primary configurations), an analysis was undertaken to gain some insight into what contribution the rear surfaces of the projector gave to the overall radiation pattern. This analysis is included in Appendix D-VI. For three selected configurations, the far-field acoustic pressure radiated by the rear rim of the piston and the sidewalls of the flexible coupling bar was computed analytically. The computations indicated that the contributions of these surfaces to the rearward radiation are of such a magnitude that they can modify the overall directivity pattern to a moderate extent. For Configuration A4-0, for instance, the rear surfaces could contribute from plus three to minus six decibels to the rearward radiation from the front surface. The scope of the analysis did not include determining the relative phase of the rear surface contribution, so specific overall patterns were not computed. Nevertheless, it is felt that an extension of this work, coupled with good descriptions of the vibratory mode shape of the structure, would be helpful in the design of new projector configurations with improved directivity.



### IMPLICATIONS FOR FUTURE WORK

If the one-fifth scale model were enlarged to the full eight-foot diameter and driven at one megawatt, its operating characteristics, as predicted by the model tests, would be as shown in Table II. These figures are taken from the data of Configuration A5-O, which most closely approximated the nominal design originally proposed, but they reflect the trends of all similar configurations as well. For comparison, the characteristics predicted in the proposal are also tabulated. Since the models performed generally as predicted, the assumptions of the design were shown to be essentially correct. The specific results of the tests provide important design guidance for optimizing future configurations. It should be recognized, nevertheless, that this design work is by nature inexact and that scale model tests should be regarded as a vital step in the definition of a new configuration.

A considerably more advantageous SPEAR configuration would result from a reoptimization of the design, using the results obtained in this program and a renewed set of design goals or "trade-off" assumptions. Since most of the acoustic parameters would improve substantially with an increase in  $ka$ , a larger piston diameter might be justified, even at the expense of an increase in weight. This would also permit more power capacity for the same nodal stress. Considerable attention should be given to piston rigidity and to local areas of higher stress, such as the fillets near the piston. In a new design analysis, variation in cross section area of the bar should be utilized as much as possible to obtain the best combination of piston support, tunability, and other factors.

The use of a reflector or coatings of pressure release material would depend on factors not covered in this work, but such modifications are potentially capable of greatly reducing the rearward radiation. Additional analysis work might give better directivity without pressure release by ingenious design to produce beneficial vibratory action of the rear surfaces of the projector. The use of arrays to obtain directivity was beyond the scope of this work, and would very much expand the analysis of a SPEAR projector, but it might nevertheless be a factor in the design of a Sonar system utilizing SPEAR.

Another implication of the acoustic feasibility tests, which has resulted in effective progress in one of the two technical areas that appeared to warrant early attention in the development of SPEAR, is that effort should now be directed toward the second area; the development of the rotating weight oscillator assembly. The requirements for this oscillator -- the vital component in the high-efficiency generation of underwater sound with SPEAR -- can now be more accurately defined. These requirements should be translated into concrete design configurations for experimental verification.

TABLE II  
PERFORMANCE COMPARISONS

<u>Description</u>			Original Analysis (from Proposal EP-60806)	Data Scaled from Model Test Results on Configuration A5-0
Frequency	f		400 cps	375 cps
Piston Diameter	2a		8 ft.	8 ft.
Dimensionless Size	ka		2.01	1.97
Piston Weight	Mp		8450 lbs.	8130 lbs.
Bar Area	A		1120 sq. in.	1125 sq. in.
<u>Operation</u>				
Piston Impedance:	Resistance	Ri	1.525	1.6
	Reactance	Xi	1.448	1.8
Quality Factor	Q		6.71 (Energy Definition)	5.1 (f/Δf Definition)
Directivity:	Beam Width	B. W.	Not Specified	65°
	Front-to- Back Ratio	F/B	Not Specified	2-1/2 db.
	Directivity Index	D. I.	Not Specified	6.5 db.
Power	W		1,000,000 watts	1,000,000 watts
Piston Amplitude	U <sub>L</sub>		.0067 in.	.0065 in.
Oscillator Amplitude	U <sub>O</sub>		.0165 in.	.0197 in.
Oscillator Force	F <sub>O</sub>		429,000 lbs.	360,000 lbs.
Node Stress	σ <sub>n</sub>		2100 psi	1600 psi

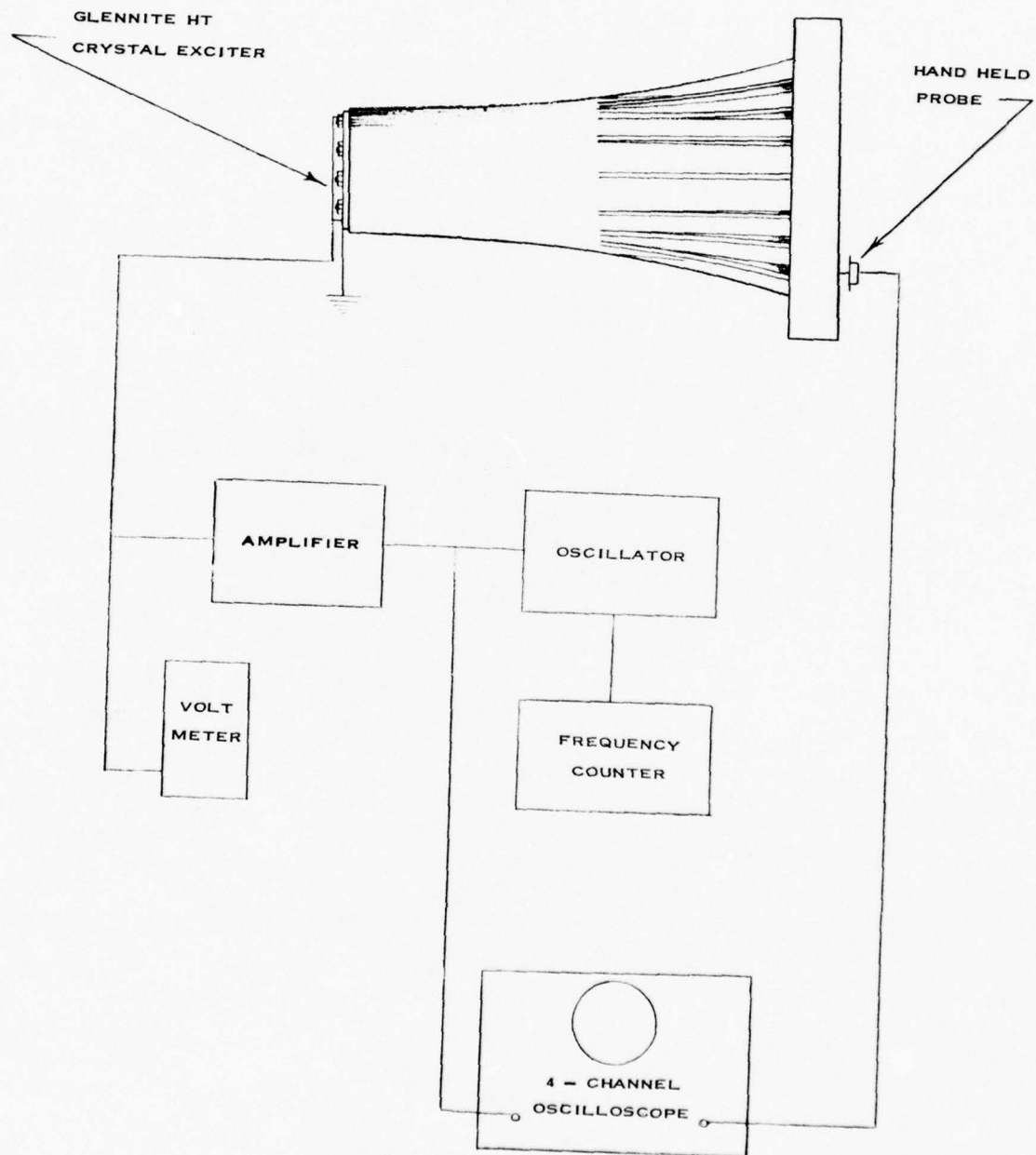
## APPENDIX A

### INSTRUMENTATION AND CIRCUITRY

#### Figure

- A-1 Instrumentation for Air Shake Test
- A-2 Schematic of SPEAR Model Test Control Console
- A-3 Strain Gage and Accelerometer Locations for April Test
- A-4 Strain Gage and Accelerometer Locations for August Test
- A-5 Instrumentation for Dodge Pond Tests

# SPEAR MODEL TEST

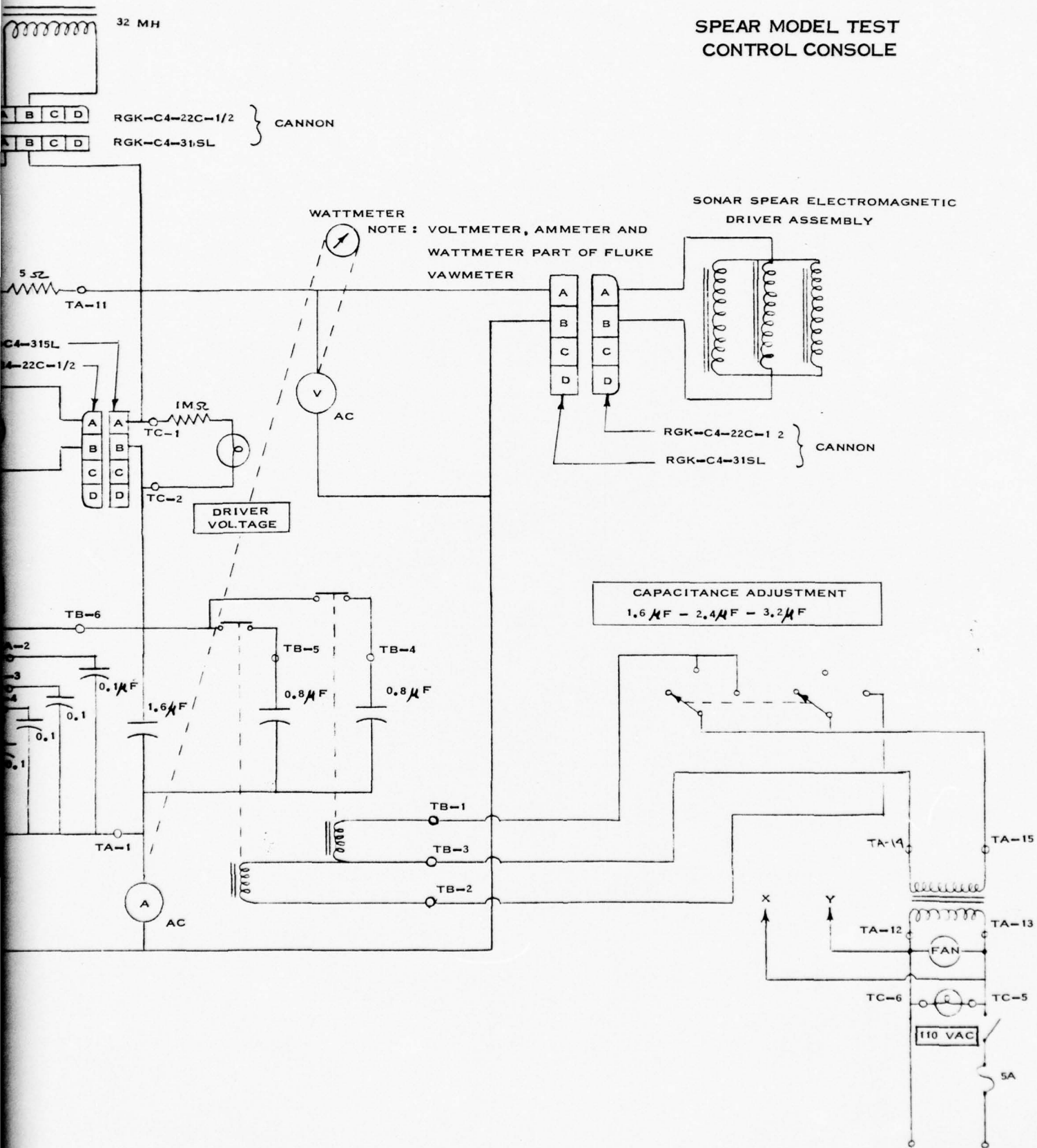


INSTRUMENTATION FOR AIR SHAKE TEST  
FIGURE A-1

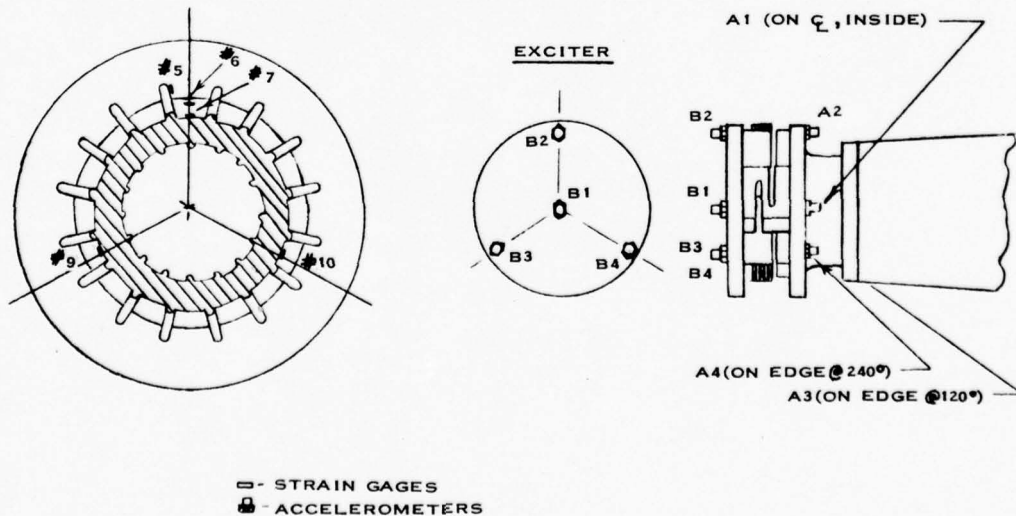
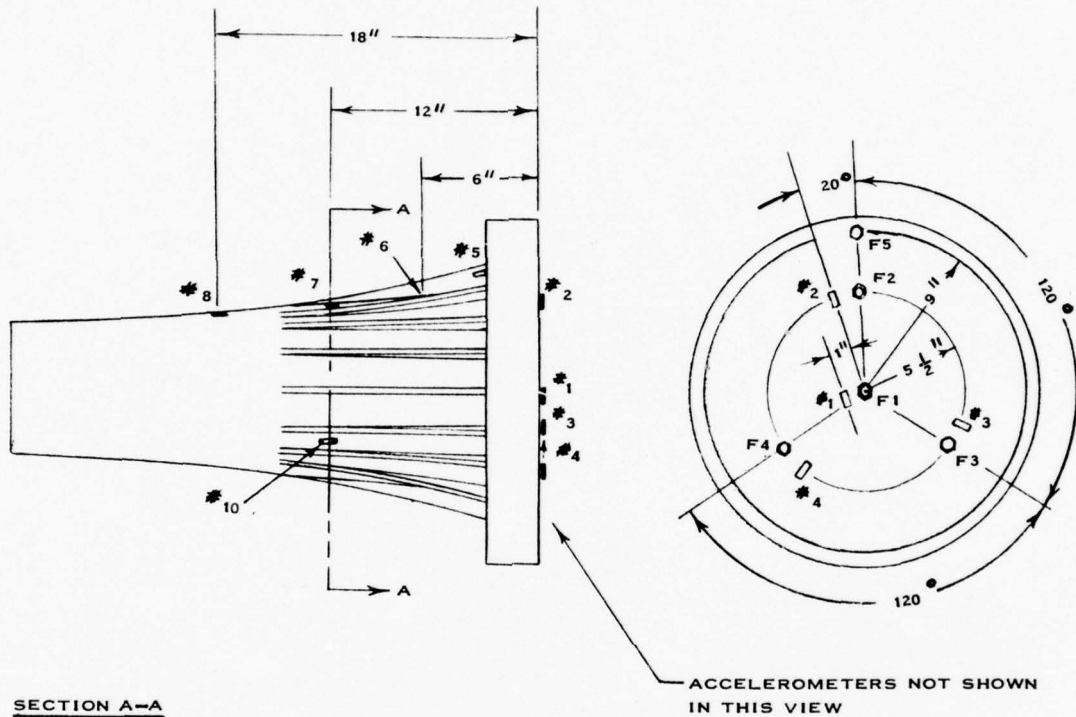




# SPEAR MODEL TEST CONTROL CONSOLE

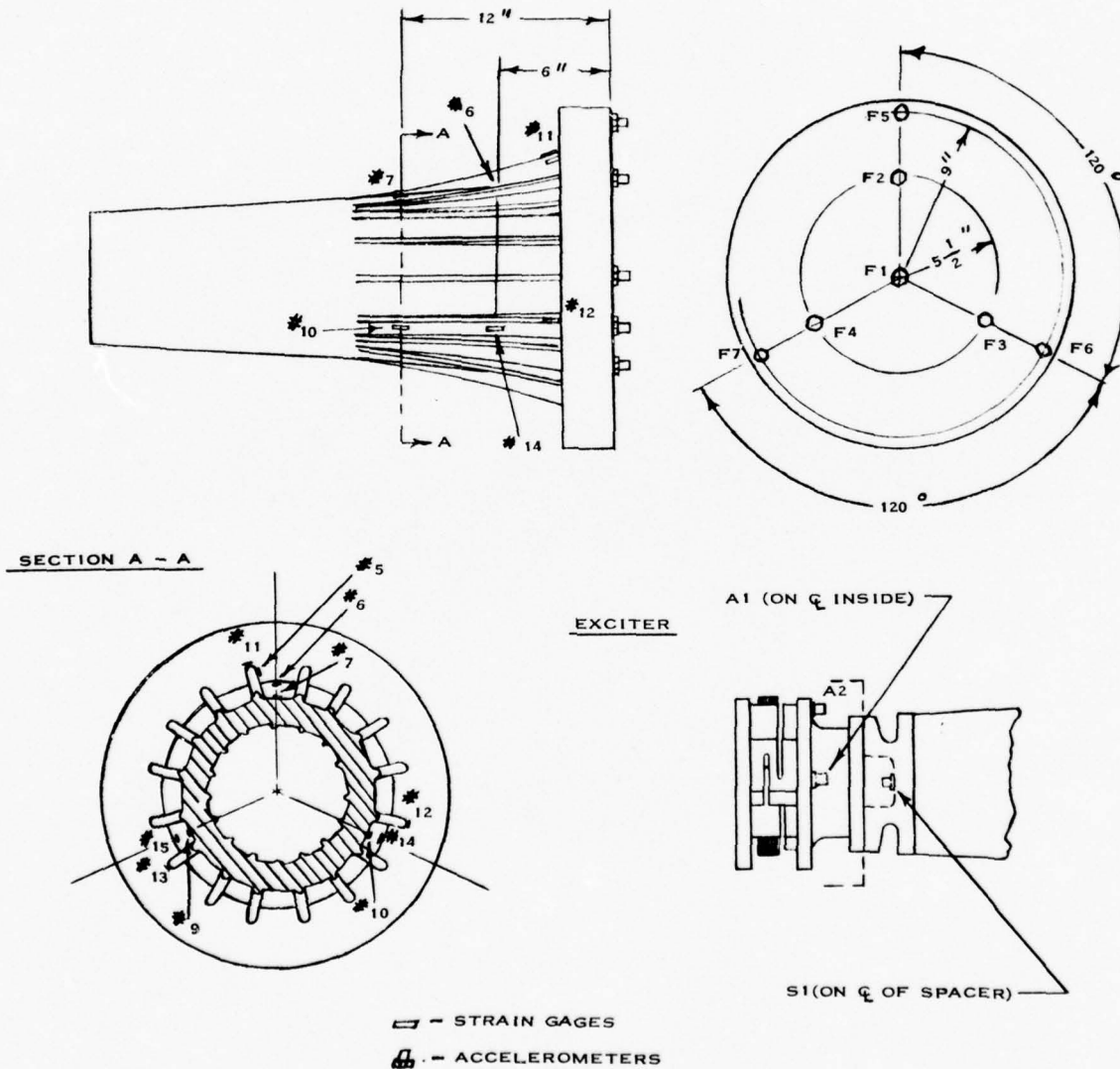


# SPEAR MODEL TEST



STRAIN GAGE AND ACCELEROMETER LOCATIONS FOR APRIL TEST  
FIGURE A-3

# SPEAR MODEL TEST

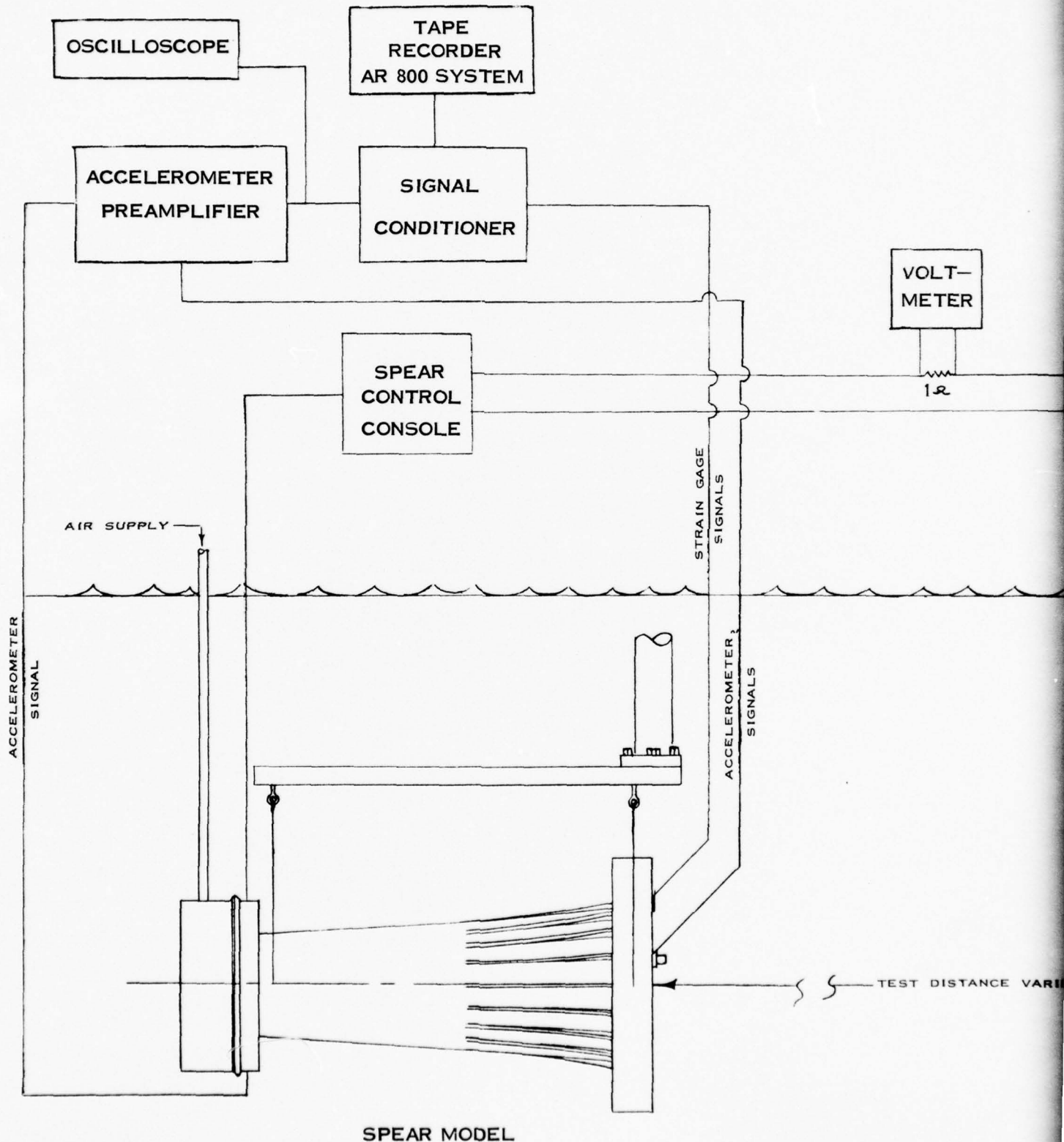


STRAIN GAGE AND ACCELEROMETER LOCATIONS FOR AUGUST TEST

FIGURE A-4

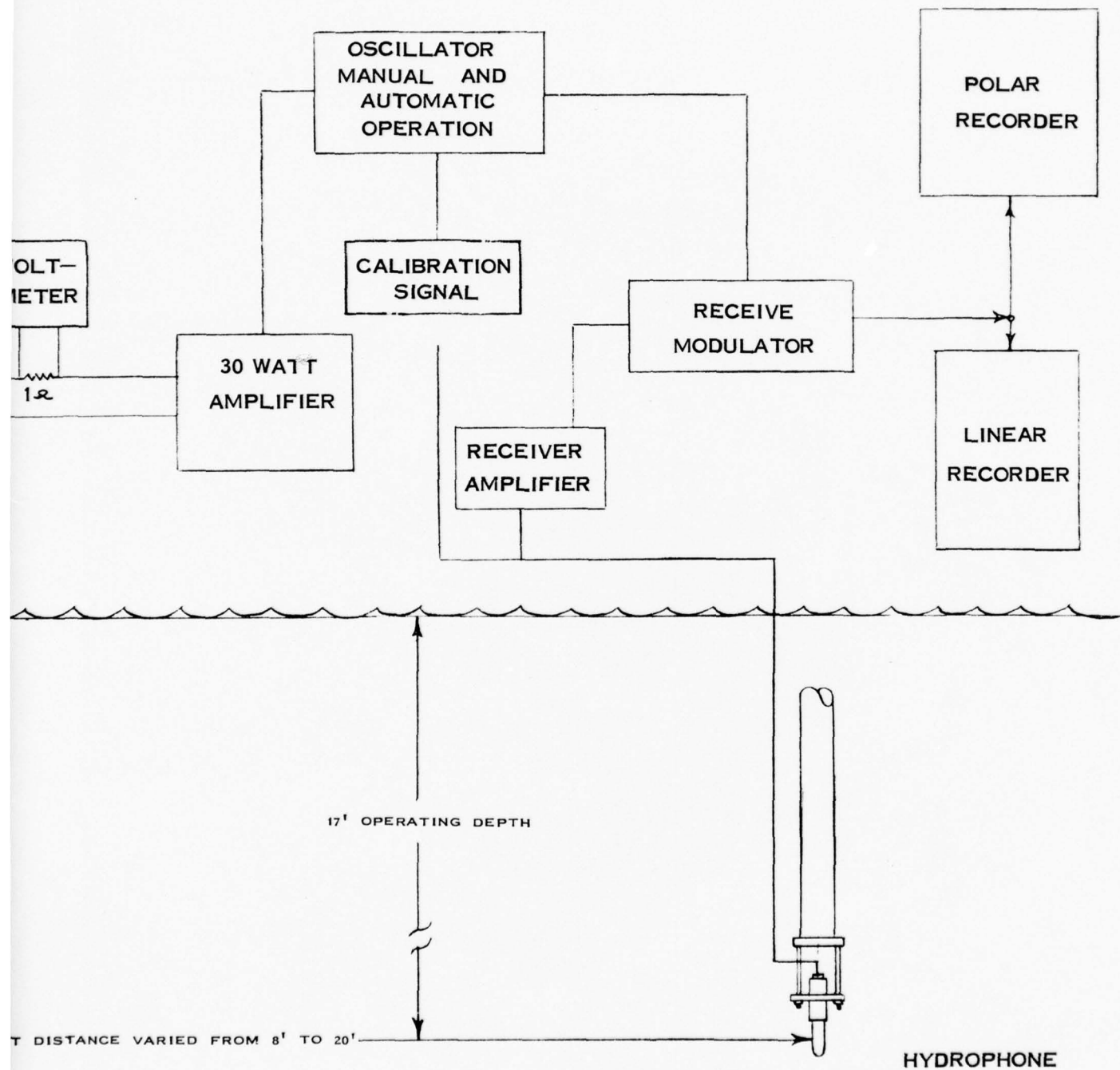


INSTRUMENTATION SUPPLIED BY HAMILTON STANDARD



INSTRUMENTATION SUPPLIED BY USNUSL

2



INSTRUMENTATION FOR DODGE POND TESTS  
FIGURE A-5

## APPENDIX B

### TABLES

#### DODGE POND TEST CONFIGURATIONS

##### Table

B-1	Pictorial Summary	} April and August
B-2	Descriptive Data	
B-3	January Test	

#### SUMMARY OF TEST RESULTS

##### Table

B-4	April Test
B-5	August Test
B-6	January Tests

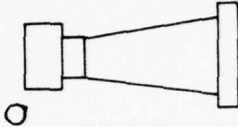
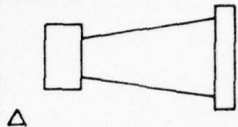
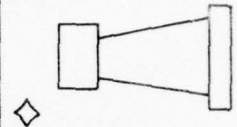
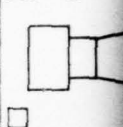
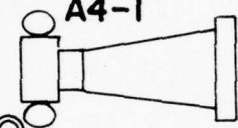
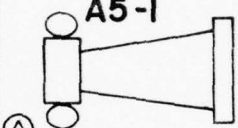
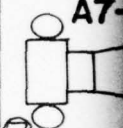
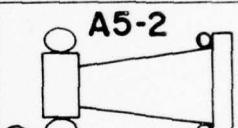
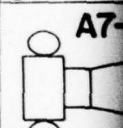
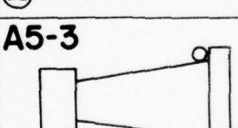
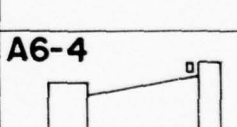

APRIL POND TEST				
	A4 LONG CASTING WITH SPACER	A5 LONG CASTING WITHOUT SPACER	A6 SHORT CASTING WITHOUT SPACER	A7 SHORT WITH S
-0 BARE	A4-0 	A5-0 	A6-0 	A7-0 
-1 INNER TUBE ON HOUSING	A4-1 	A5-1 		A7-1 
-2 TWO INNER TUBES		A5-2 		A7-2 
-3 INNER TUBE ON REAR FACE		A5-3 		
-4 CELLTITE ON REAR FACE			A6-4 	
-5 CELLTITE PLUS INNER TUBE				A7-5 
-6 CELLTITE REAR ENCLOSURE				
-7 REFLECTOR BEHIND PISTON				



TABLE B-1  
DODGE POND TEST CONFIGURATIONS

2


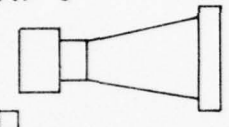
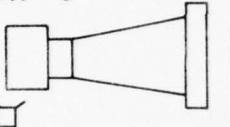
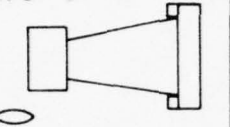
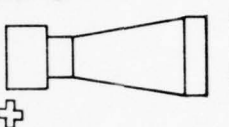
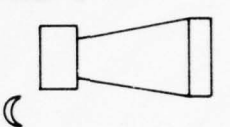

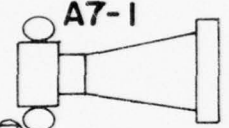

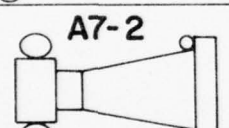

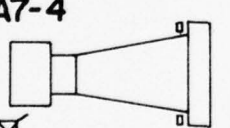

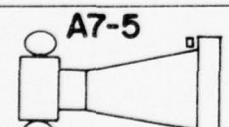
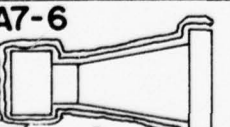
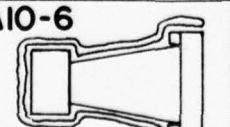
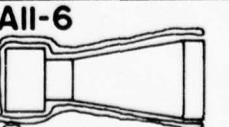
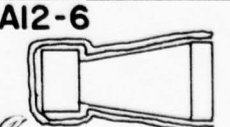

		AUGUST POND TEST			
TING ACER	A7 SHORT CASTING WITH SPACER	A7 SHORT CASTING WITH SPACER	A10 SHORT CASTING WITHOUT SPACER, WITH RIM WEIGHTS	A11 SHORT CASTING WITH SPACER, RIM REMOVED	A12 SHORT CASTING WITHOUT SPACER, RIM REMOVED
	A7-0 	A7-0 	A10-0 	A11-0 	A12-0 
	A7-1 				
	A7-2 				
	A7-4 				
	A7-5 				
		A7-6 	A10-6 	A11-6 	A12-6 
		A7-7 			

TABLE B-2

DODGE POND TEST CONFIGURATIONSDESCRIPTIVE DATAThe Test Model

Bar Length:	A4 and A5	25.5 in.
	A6 thru A12	21.5 in.
Piston Diameter:	A4 thru A10	19.2 in.
	A11 and A12	14.7 in.
Area of Bar Portion:		48 sq. in.
Weight of Bar:	A4 and A5	118 lb.
	A6 thru A12	102 lb.
Weight of Piston:	A4 thru A10	66 lb.
	A11 thru A12	39.5 lb.
Rim Weights:	A10 only	16 weights, 0.94 lb. each
Spacer:	A4, A7 and A11	33 lb.
Exciter Adapter:	All configurations	25.7 lb.
Exciter Housing:	All configurations	11.0 in. dia., 7.6 in. long

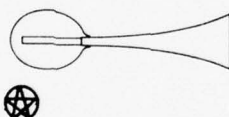
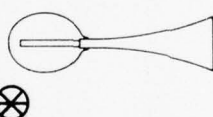
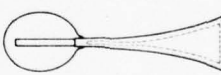
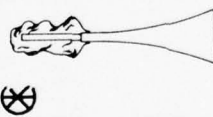
The Pressure Release Material

Inner tube on Exciter Housing:	11 in. I. D. x 4 in. dia. cross section
Inner Tube Behind Piston Face:	15 in. I. D. x 1.5 in. dia. cross section
Celltite rubber sheets:	0.37 in. thick - April tests 0.25 in. thick - August tests

The Reflector

Diameter:	4 feet
Construction:	0.25 in. aluminum plate faced with 0.25 in. of Celltite rubber.

**TABLE B-3**  
**JANUARY POND TEST CONFIGURATIONS**

	<b>B1 ALUMINUM</b>	<b>B2 MAGNESIUM</b>	<b>B3 HOLLOW ALUMINUM</b>
<b>-1 AIRBAG INFLATED</b>	<b>B1-1</b> 	<b>B2-1</b> 	<b>B3-1</b> 
<b>-2 AIRBAG DEFLATED</b>		<b>B2-2</b> 	

BAR LENGTH

B1 & B3  
B2


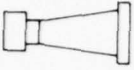



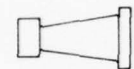


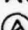
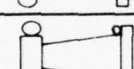
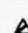







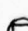

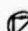


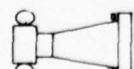
10.00 in.  
9.02 in.

FACE DIAMETER

3.70 in.

THROAT DIAMETER

.50 in.

		RESONANT FREQUENCY: cps		TUNEABILITY $Q = \frac{f}{\Delta f} - 3db$	TEST FREQUENCY cps	ALL REFERRED TO 1 AMPERE EXCITATION					RELATIVE PISTON SIZE: TEST kg	BEA (-3)
		AIR	WATER			SOURCE LEVEL db/1μb, 1yd.	ACOUSTIC POWER WATTS	AVERAGE PISTON DISPLACEMENT ± μ IN.	STRESS AT GAGE #5 ± psi			
A4-0 		1838	1530	8.3	1435 1535 1660	68.6 73.3 70.1	.137 .371 .222	4.7 7.5 4.4	5 10 6	1.51 1.62 1.75		
A4-1 		1838	1540	7.7	1550	73.9	.408	—	—	1.63		
A5-0 		2195	1870	5.1	1675 1875 1975	69.0 73.4 71.8	.131 .352 .262	3.6 4.3 3.3	6 6 8	1.76 1.97 2.08		
A5-1 		2195	~1870	~5.1	1875	~73.9	.388	—	—	1.97		
A5-2 		2195	2000	5.6	1870	72.5	.198	3.8	6	1.97		
A5-3 		2195	~2000	~5.6	1870	~72.5	.194	—	—	1.97		
A6-0 		2374	~2160	~5.4	2001 2157 2299	~73.0 ~75.0 ~73.6	.256 .435 .252	3.4 3.7 2.8	— — —	2.10 2.27 2.41		
A6-4 		2374	2220	5.4	2030 2250 2460	73.1 75.8 72.1	.250 .353 .131	3.5 3.7 3.4	— — —	2.14 2.37 2.59		
A7-0 		1961	1680	5.6	1575 1650 1825	70.1 73.0 71.5	.182 .331 .214	6.0 6.3 3.4	— 5 —	1.66 1.74 1.92		
A7-1 		1961	1670	7.1	1575 1650 1825	70.3 73.5 70.5	.185 .354 .165	5.2 6.0 3.4	— — —	1.66 1.74 1.92		
A7-2 		1961	1730	5.8	1694 1786	74.8 74.5	.405 .345	6.3 6.2	— —	1.78 1.88		
A7-5 		1961	1800	6.4	1650 1764 1837 1925	71.3 74.0 73.7 71.5	.250 .396 .316 .190	4.8 5.8 4.7 4.9	— — — —	1.74 1.86 1.93 2.03		



2

TABLE B-4  
SPEAR MODEL TEST  
SUMMARY OF TEST RESULTS—APRIL

ESS PAGE #5 1	RELATIVE PISTON SIZE: TEST ka	DIRECTIVITY			NORMALIZED IMPEDANCE	
		BEAM WIDTH (-3db)	FRONT/BACK db*	D.I. db	Ri	Xi
5	1.51	80°	2.5	5.8	0.86	1.66 at ka=1.61
0	1.62	80°	3.8	6.2	0.79	
6	1.75	80°	2.0	5.2	1.16	
—	1.63	74°	4.0	6.4	—	1.54 at ka=1.62
6	1.76	67°	3.0	6.4	1.03	1.62 at ka=1.97
6	1.97	58°	2.5	6.5	1.55	
8	2.08	62°	0.7	6.2	2.04	
—	1.97	58°	3.6	6.6	—	1.62 at ka=1.97
6	1.97	62°	7.2	8.1	1.10	.85 at ka=2.10
—	1.97	62°	7.5	8.2	—	.85 at ka=2.10
—	2.10	58°	3.5	7.5	1.83	.92 at ka=2.27
—	2.27	60°	2.7	7.3	1.85	
—	2.41	64°	5.0	8.2	1.73	
—	2.14	78°	13.0	7.7	1.36	.74 at ka=2.34
—	2.37	62°	13.0	8.9	.88	
—	2.59	60°	16.2	9.5	.52	
—	1.66	64°	4.0	6.2	.57	1.40 at ka=1.77
8	1.74	72°	4.0	6.4	.85	
—	1.92	78°	4.0	6.8	1.36	
—	1.66	60°	3.7	6.2	1.05	1.55 at ka=1.76
—	1.74	70°	4.5	6.6	1.05	
—	1.92	72°	4.0	6.9	1.19	
—	1.78	88°	12.0	7.3	.99	1.15 at ka=1.82
—	1.88	78°	13.0	7.7	.81	
—	1.74	110°	9.8	5.9	1.11	.685 at ka=1.89
—	1.86	96°	11.0	6.6	1.03	
—	1.93	96°	11.0	6.6	.93	
—	2.03	86°	13.4	7.3	.77	

**NOTES:**

~ EXTRAPOLATED OR ESTIMATED  
FROM CLOSELY RELATED DATA.

— DATA NOT AVAILABLE.

\* FRONT TO BACK RATIO IS REFERRED  
TO MAX INTENSITY WITHIN 60° OF  
STRAIGHT BACK.

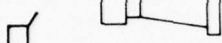
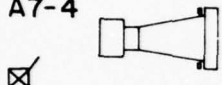

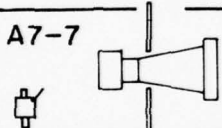
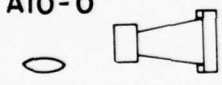
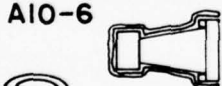
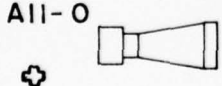
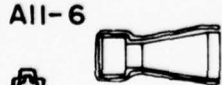
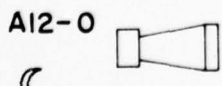
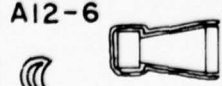
		RESONANT FREQUENCY: cps		TUNEABILITY $Q = \frac{f}{\Delta f - 3db}$	TEST FREQUENCY cps	ALL REFERRED TO 1 AMPERE EXCITATION				RELATIVE PISTON SIZE: TEST kg	BEAR (-3db)
						SOURCE LEVEL db/μab, lyd.	ACOUSTIC POWER WATTS	AVERAGE PISTON DISPLACEMENT ± μ IN.	STRESS ** AT GAGE #5 ± psi		
		AIR	WATER								
A7-0 		1934	1645	7.1	1535 1634 1780	70.8 73.5 70.0	.219 .363 .167	— — —	— — —	1.60 1.71 1.86	
A7-4 		1934	1750	5.5	1609 1753 1911	70.8 73.2 70.2	.252 .316 .109	— — —	— — —	1.68 1.83 2.00	
A7-6 		1934	1750	5.3	1647 1755 1935	71.2 73.3 70.6	.225 .313 .127	5.7 7.4 6.4	6 9 5	1.72 1.83 2.02	
A7-7 		1934	1585	9.6	1529 1592 1689	75.2 77.8 75.0	.179 .408 .200	5.6 6.9 5.0	— 11 —	1.60 1.66 1.76	
A10-0 		2237	2120	8.5	1987 2103 2238	71.7 74.4 70.7	.252 .408 .130	4.5 5.2 3.1	7 12 9	2.07 2.20 2.34	
A10-6 		2237	2155	9.4	2027 2167 2242	72.3 75.6 72.9	.263 .425 .220	4.7 6.6 4.6	15 21 8	2.12 2.26 2.34	
A11-0 		2109	1920	7.4	1779 1932 2062	68.2 71.8 68.8	.122 .408 .187	8.7 12.4 7.1	6 7 5	1.42 1.54 1.64	
A11-6 		2109	1950	12.2	1860 1958 2048	70.7 75.1 71.5	.171 .692 .289	11.8 18.2 10.6	5 10 6	1.48 1.56 1.63	
A12-0 		2565	2360	5.2	2189 2363 2629	71.2 74.3 71.5	.258 .380 .215	7.0 7.6 4.6	5 5 3	1.74 1.88 2.09	
A12-6 		2565	2375	6.8	2261 2386 2593	73.6 75.5 72.5	.417 .457 .220	8.6 10.3 5.6	7 7 4	1.80 1.90 2.07	

TABLE B-5  
SPEAR MODEL TEST  
SUMMARY OF TEST RESULTS—AUGUST

2

CITATION	STRESS ** AT GAGE #5 ± psi	RELATIVE PISTON SIZE: TEST ka	DIRECTIVITY			NORMALIZED IMPEDANCE	
			BEAM WIDTH (-3db)	FRONT/BACK db *	DI. db	R <sub>i</sub>	X <sub>i</sub>
	—	1.60	78°	1.0	6.0	~0.49	1.76 at ka=1.72
	—	1.71	78°	3.5	6.5	~0.72	
	—	1.86	84°	3.0	6.4	~1.15	
	—	1.68	86°	9.0	5.4	~1.10	1.00 at ka=1.83
	—	1.83	86°	10.5	6.8	~0.96	
	—	2.00	92°	12.5	7.1	~0.74	
6	1.72	92°	11.5	6.3	0.72	1.00 at ka=1.83	
9	1.83	88°	14.0	7.6	0.52		
5	2.02	76°	15.0	7.0	0.71		
—	1.60	50°	14.0	10.6	0.70	2.20 at ka=1.66	
11	1.66	50°	13.0	10.3	0.97		
—	1.76	58°	15.0	10.6	0.80		
7	2.07	84°	2.5	6.3	0.89	.71 at ka=2.22	
12	2.20	58°	1.5	6.9	0.97		
9	2.34	50°	2.5	8.2	0.79		
15	2.12	86°	12.0	6.7	0.81	.54 at ka=2.25	
21	2.26	68°	16.5	7.9	0.58		
8	2.34	74°	19.0	8.1	0.60		
6	1.42	102°	3.0	4.7	0.25	1.34 at ka=1.53	
7	1.54	124°	4.0	4.3	0.35		
5	1.64	112°	2.0	4.7	0.43		
5	1.48	90°	10.5	6.2	0.17	1.10 at ka=1.55	
10	1.56	104°	9.5	5.3	0.27		
6	1.63	108°	11.5	5.5	0.30		
5	1.74	94°	5.0	5.7	0.53	2.22 at ka=1.88	
5	1.88	66°	5.5	7.1	0.58		
3	2.09	64°	5.5	6.8	0.73		
7	1.80	100°	12.5	6.0	0.54	2.03 at ka=1.89	
7	1.90	74°	16.0	7.5	0.36		
4	2.07	72°	16.5	7.7	0.51		

**NOTES:**








~ EXTRAPOLATED OR ESTIMATED  
FROM CLOSELY RELATED DATA.

— DATA NOT AVAILABLE.

\* FRONT TO BACK RATIO IS REFERRED  
TO MAX INTENSITY WITHIN 60° OF  
STRAIGHT BACK.

\*\*FOR CONFIGURATIONS A11 AND  
A12 (RIM REMOVED) THE GAGE  
REPORTED IS\*9.

TABLE B-6  
SPEAR MODEL TEST  
SUMMARY OF TEST RESULTS—JANUARY

	RESONANT FREQUENCY: cps		TEST FREQUENCY cps	RELATIVE PISTON SIZE: TEST ka	DIRECTIVITY		
	AIR	WATER			BEAM WIDTH (-3db)	FRONT/BACK db*	D.I. db
B1-1 	13,090	12,945	12,945	2.51	51°	10.0	8.9
			13,607	2.64	54°	8.5	8.9
B2-1 	14,042	13,860	13,860	2.69	60°	10.5	8.4
			15,275	2.96	46°	11.5	10.2
B2-2 	14,042	13,858	13,858	2.69	57°	12.5	9.6
							
B3-1 	—	—	—	—	—	—	—

NOTES:

— DATA NOT AVAILABLE

\* FRONT TO BACK RATIO IS  
REFERRED TO MAX. INTENSITY  
WITHIN 60° OF STRAIGHT  
BACK

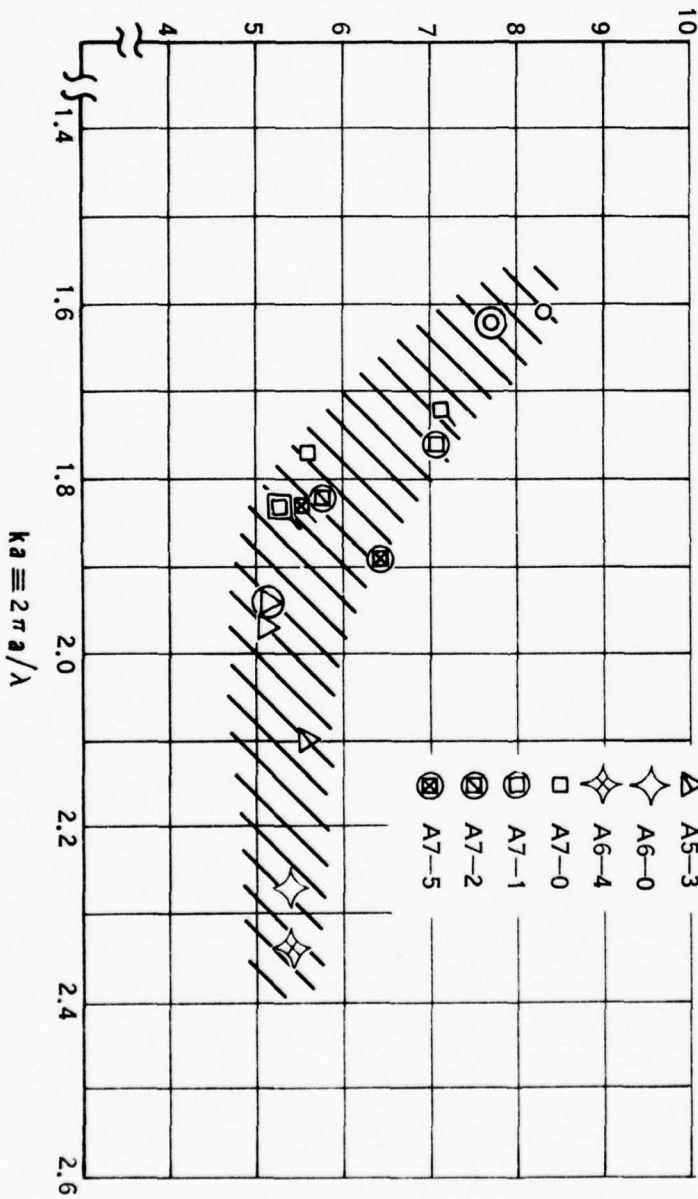


## APPENDIX C

### Test Data

<u>Figure</u>	<u>Title</u>
C-1	Quality Factor Summary, Primary Configurations
C-2	Quality Factor Summary, Secondary Configurations
C-3	Beam Width Summary, Primary Configurations
C-4	Beam Width Summary, Secondary Configurations
C-5	Front-to-Back Ratio Summary, Primary Configurations
C-6	Front-to-Back Ratio Summary, Secondary Configurations
C-7	Directivity Index Summary, Primary Configurations
C-8	Directivity Index Summary, Secondary Configurations
C-9	Resistive Impedances, Primary Configurations
C-10	Resistive Impedances, Secondary Configurations
C-11	Reactive Impedances, Primary Configurations
C-12	Reactive Impedances, Secondary Configurations
C-13 to C-21	SPEAR Model Test Transmitting Response
C-22 to C-46	SPEAR Model Test Directivity Patterns
C-47	Displacements and Stresses, Primary Configurations
C-48	Displacements and Stresses, Secondary Configurations
C-49	Piston Displacements vs. Frequency, Configuration A5-O Only

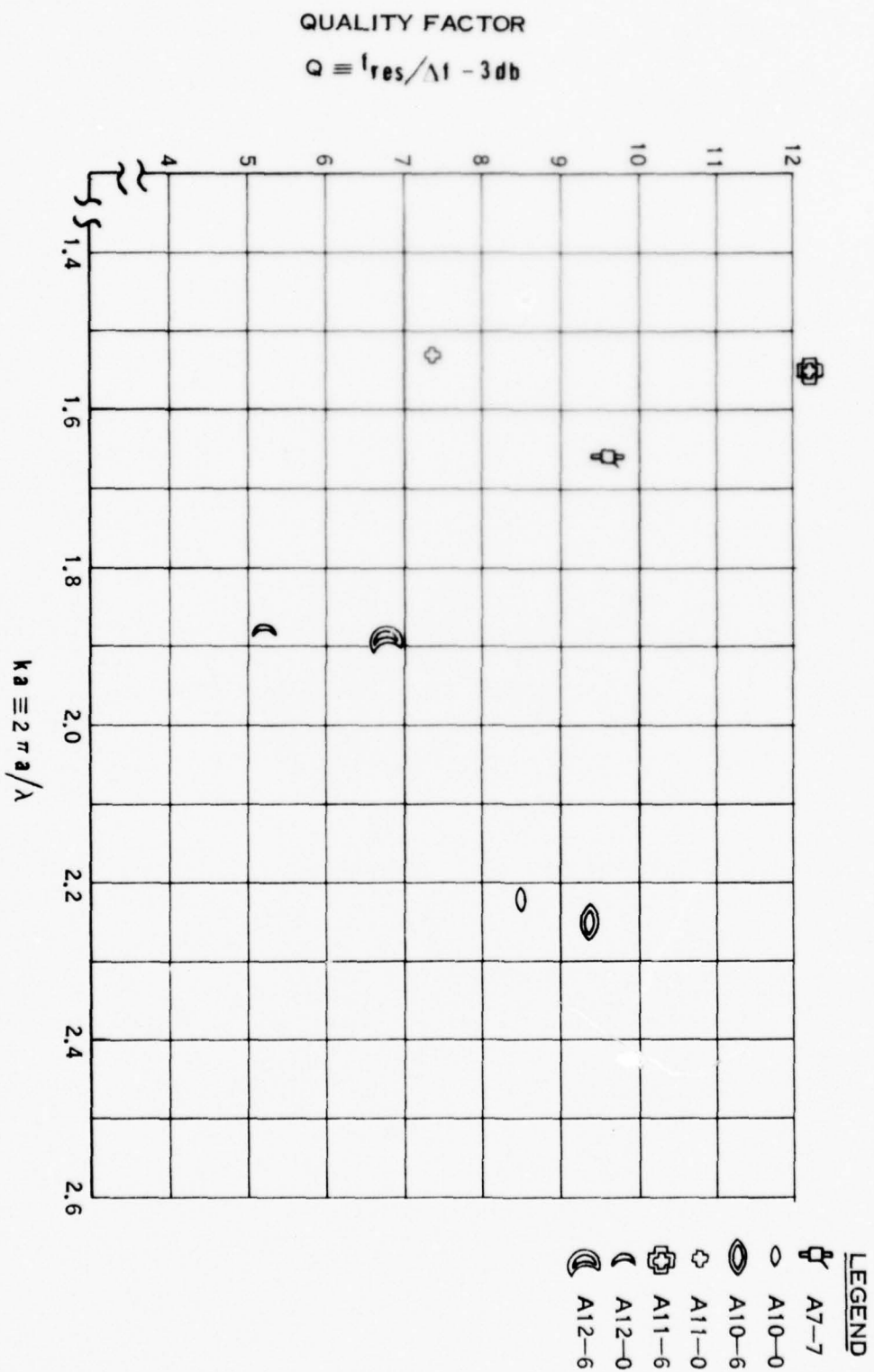
QUALITY FACTOR  
 $Q \equiv f_{res} / \Delta f - 3db$



LEGEND

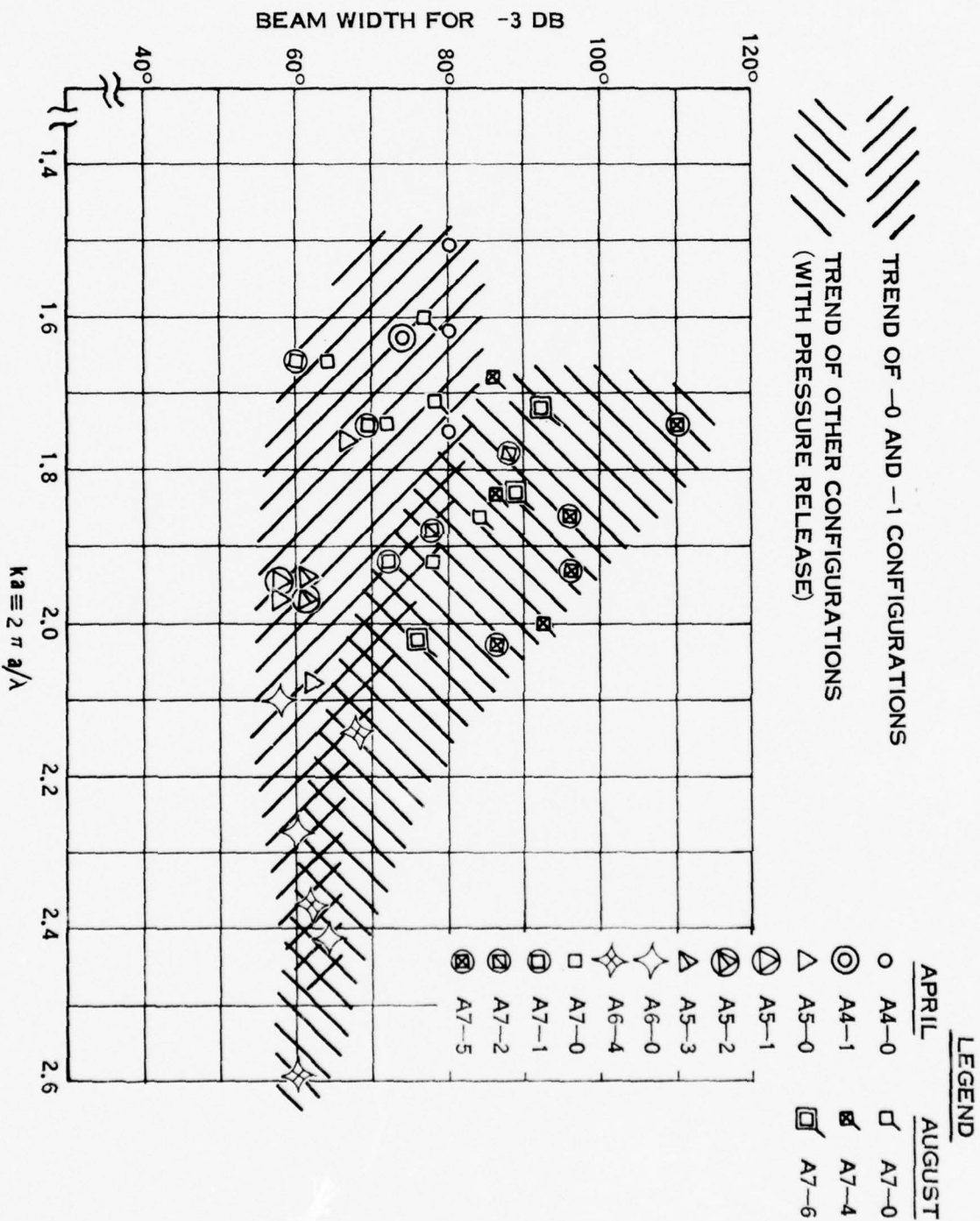
APRIL	AUGUST
○ A4-0	◻ A7-0
⊙ A4-1	◻ A7-4
△ A5-0	◻ A7-6
◻ A5-1	
◻ A5-2	
◻ A5-3	
◻ A6-0	
◻ A6-4	
◻ A7-0	
◻ A7-1	
◻ A7-2	
◻ A7-5	

SPEAR MODEL TEST  
 QUALITY FACTOR SUMMARY FOR PRIMARY CONFIGURATIONS  
 FIGURE C-1



SPEAR MODEL TEST  
 QUALITY FACTOR SUMMARY FOR SECONDARY CONFIGURATIONS

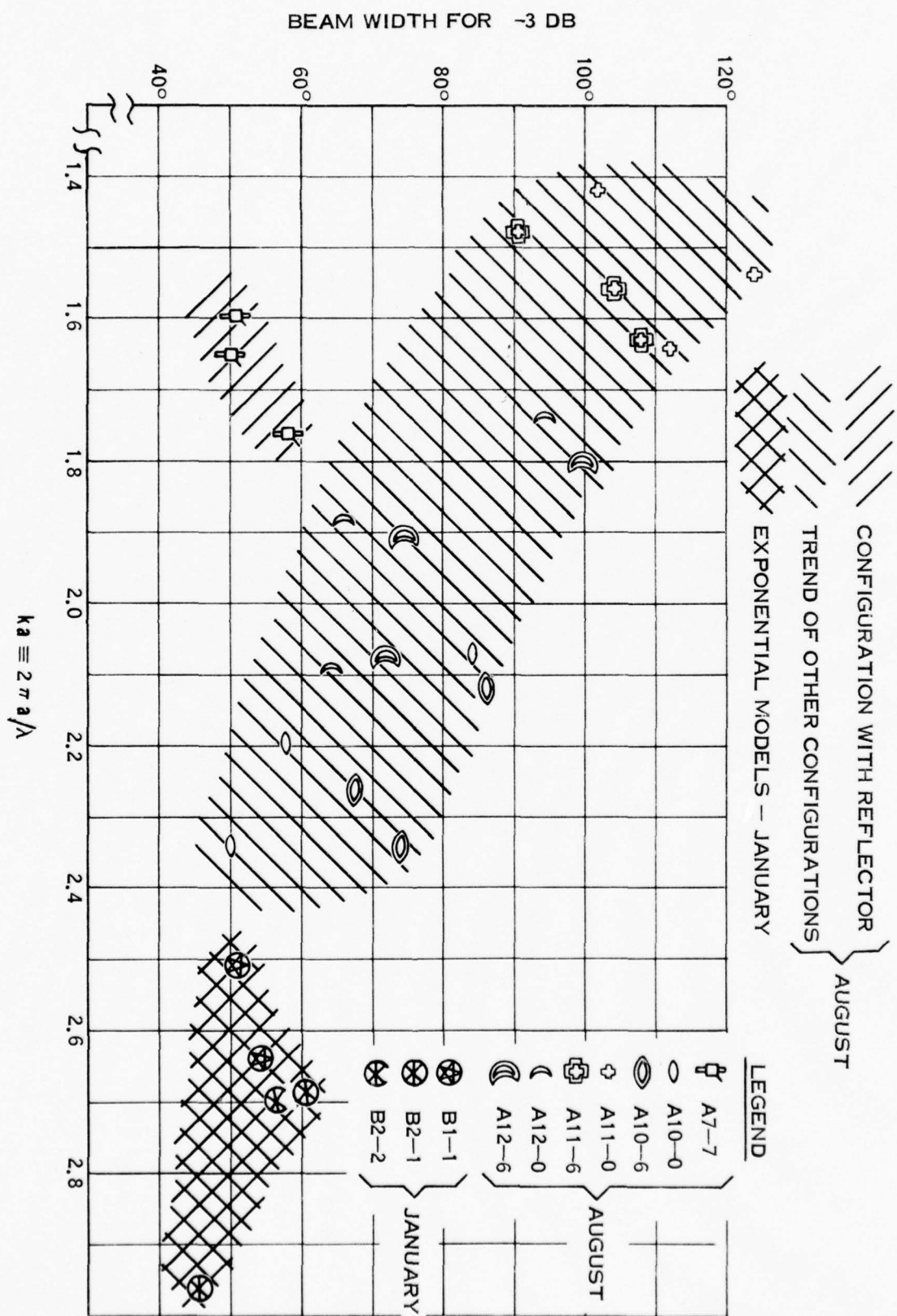
FIGURE C-2



SPEAR MODEL TEST  
BEAM WIDTH SUMMARY FOR PRIMARY CONFIGURATIONS

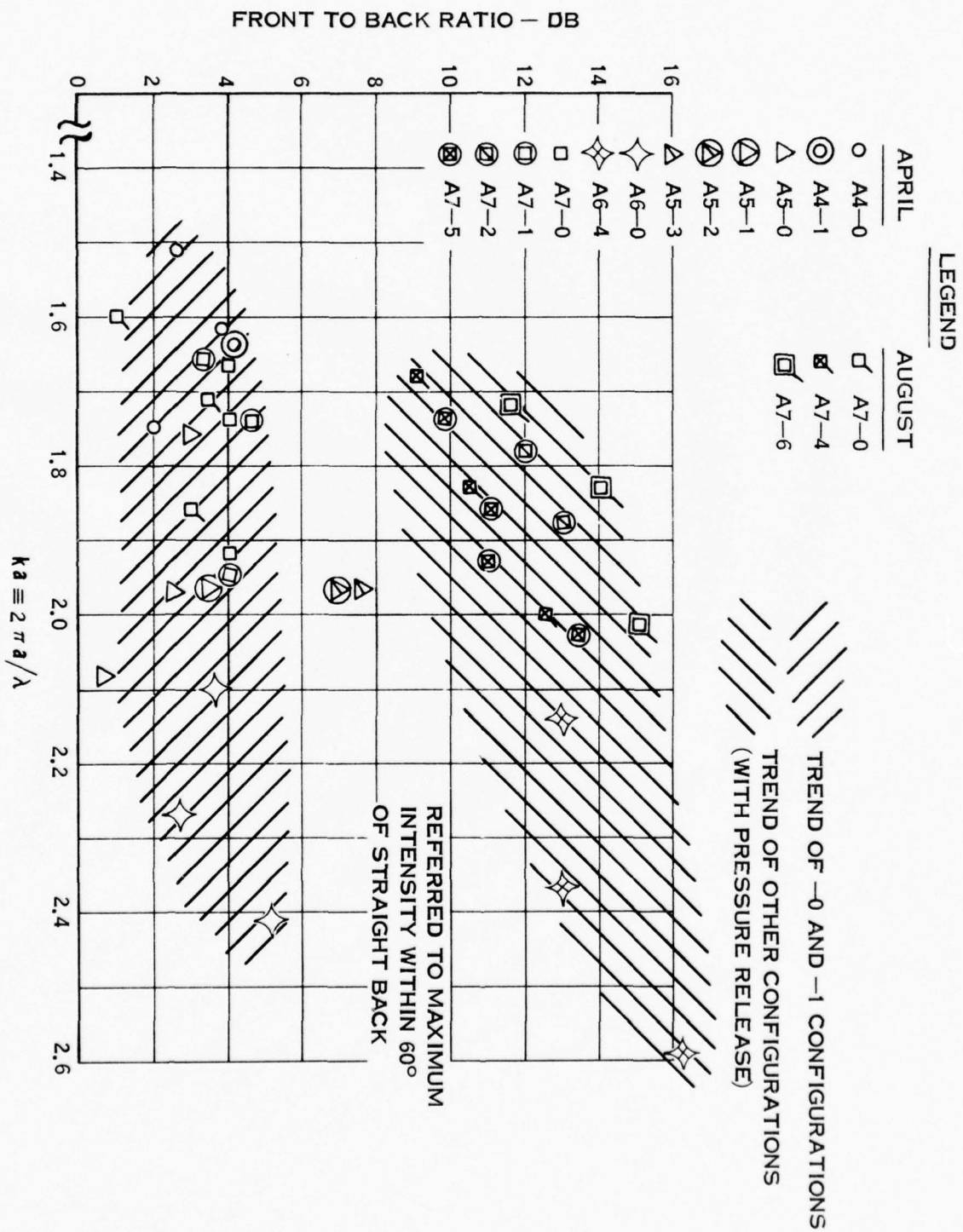
FIGURE C-3



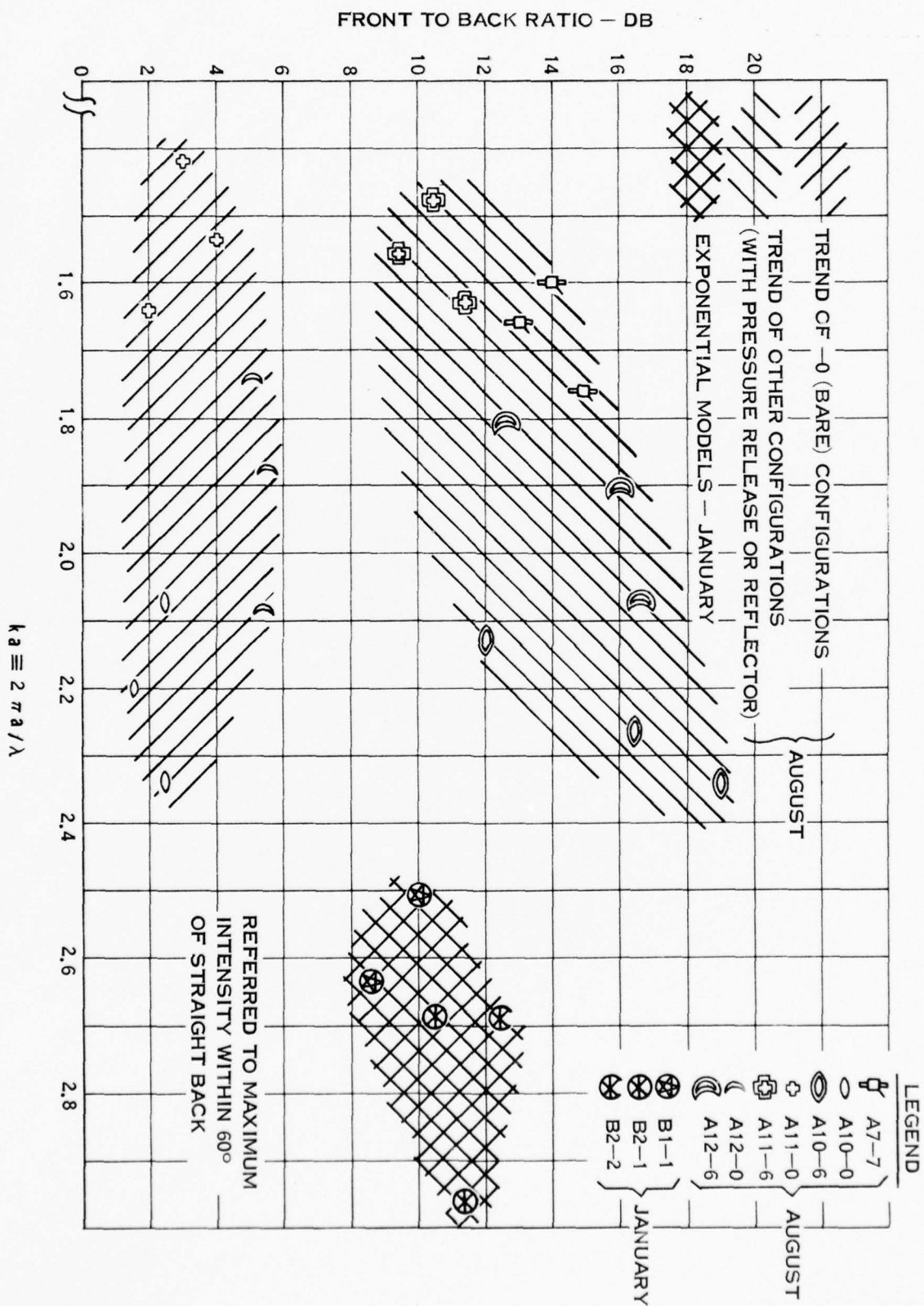


BEAM WIDTH SUMMARY SPEAR MODEL TEST FOR SECONDARY CONFIGURATIONS

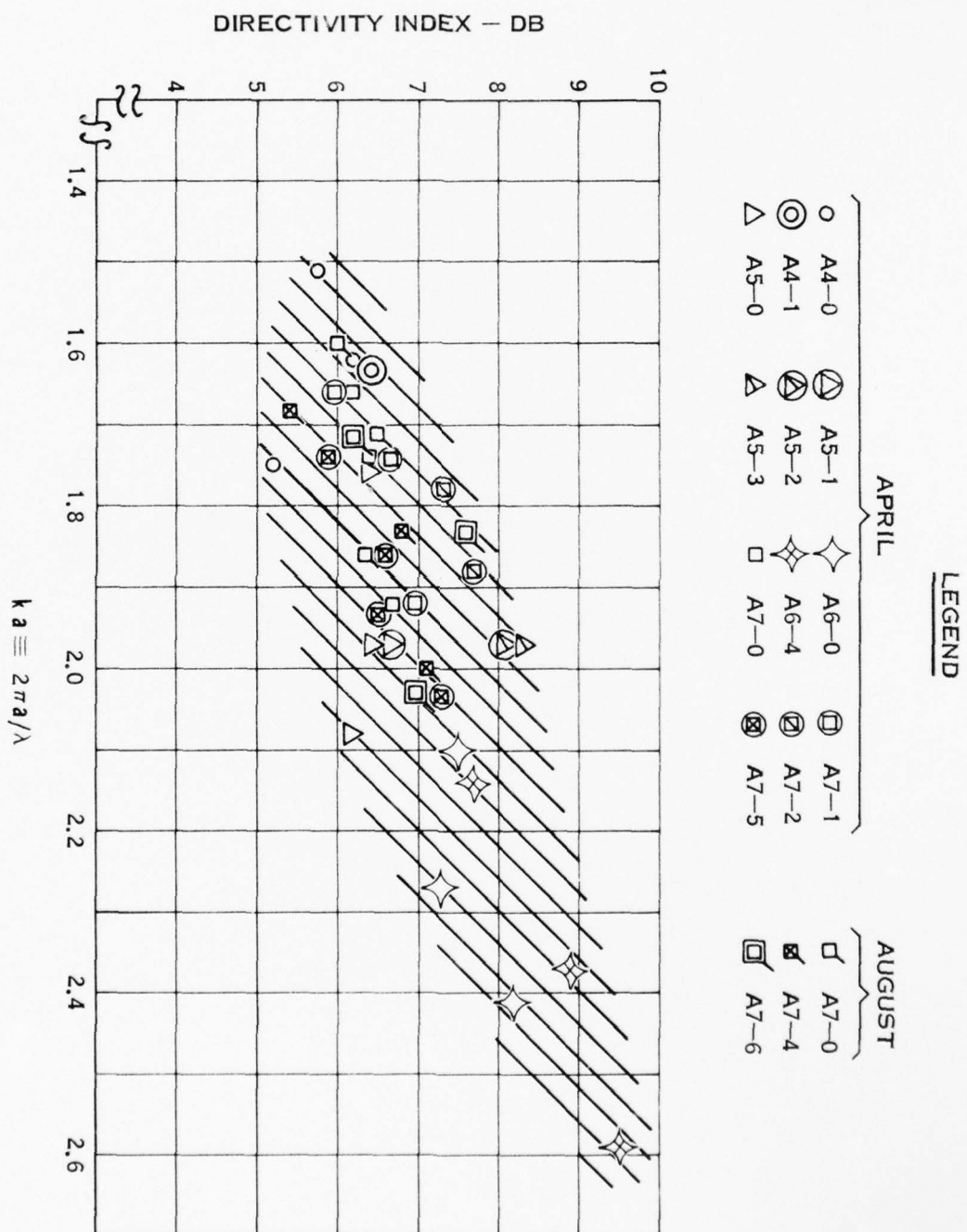
FIGURE C-4



SPEAR MODEL TEST  
FRONT TO BACK RATIO SUMMARY FOR PRIMARY CONFIGURATIONS  
FIGURE C-5

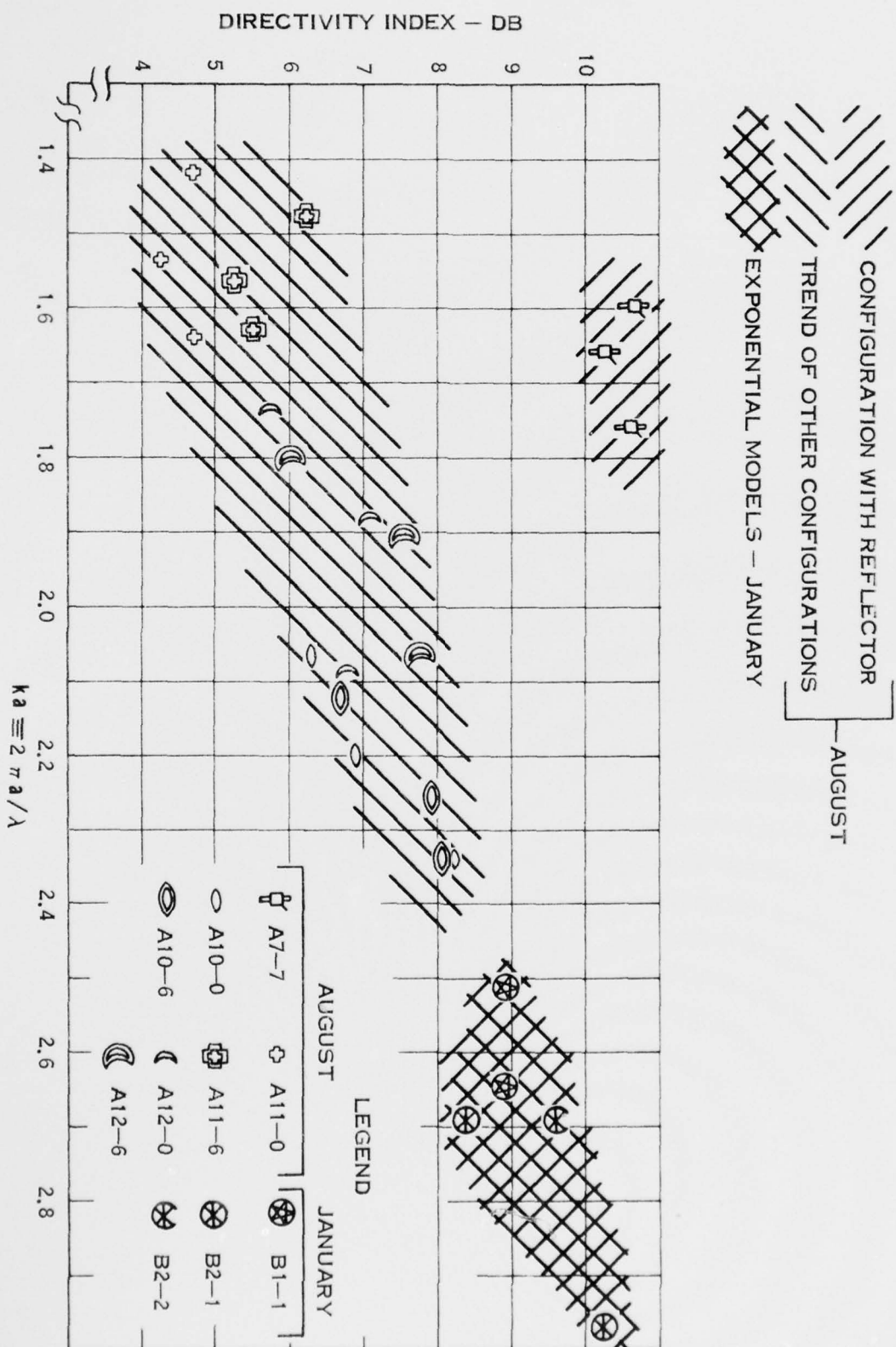


SPEAR MODEL TEST  
FRONT TO BACK RATIO SUMMARY FOR SECONDARY CONFIGURATIONS  
FIGURE C-6



SPEAR MODEL TEST  
DIRECTIVITY INDEX SUMMARY FOR PRIMARY CONFIGURATIONS  
FIGURE C-7

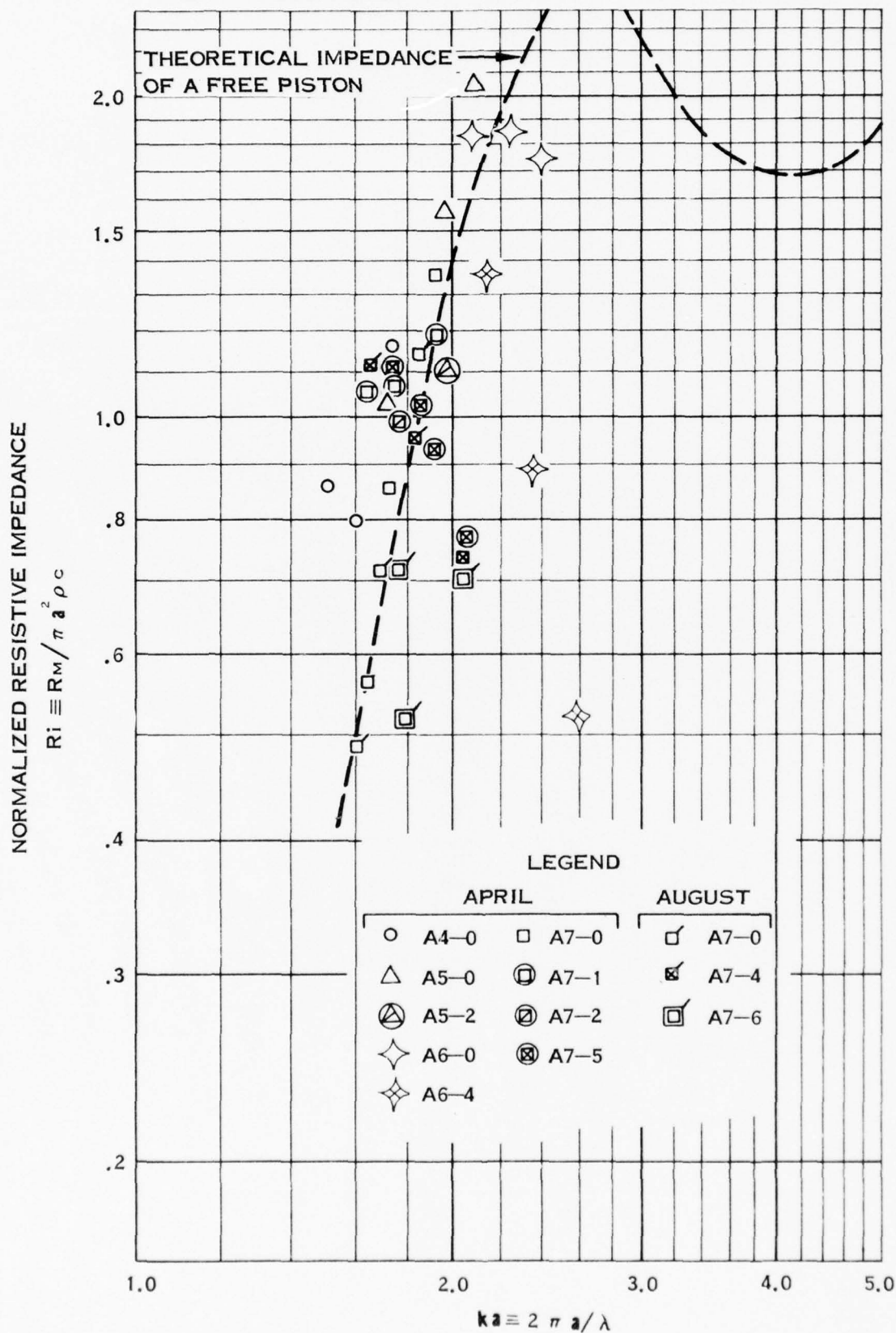




SPEAR MODEL TEST  
DIRECTIVITY INDEX SUMMARY FOR SECONDARY CONFIGURATIONS

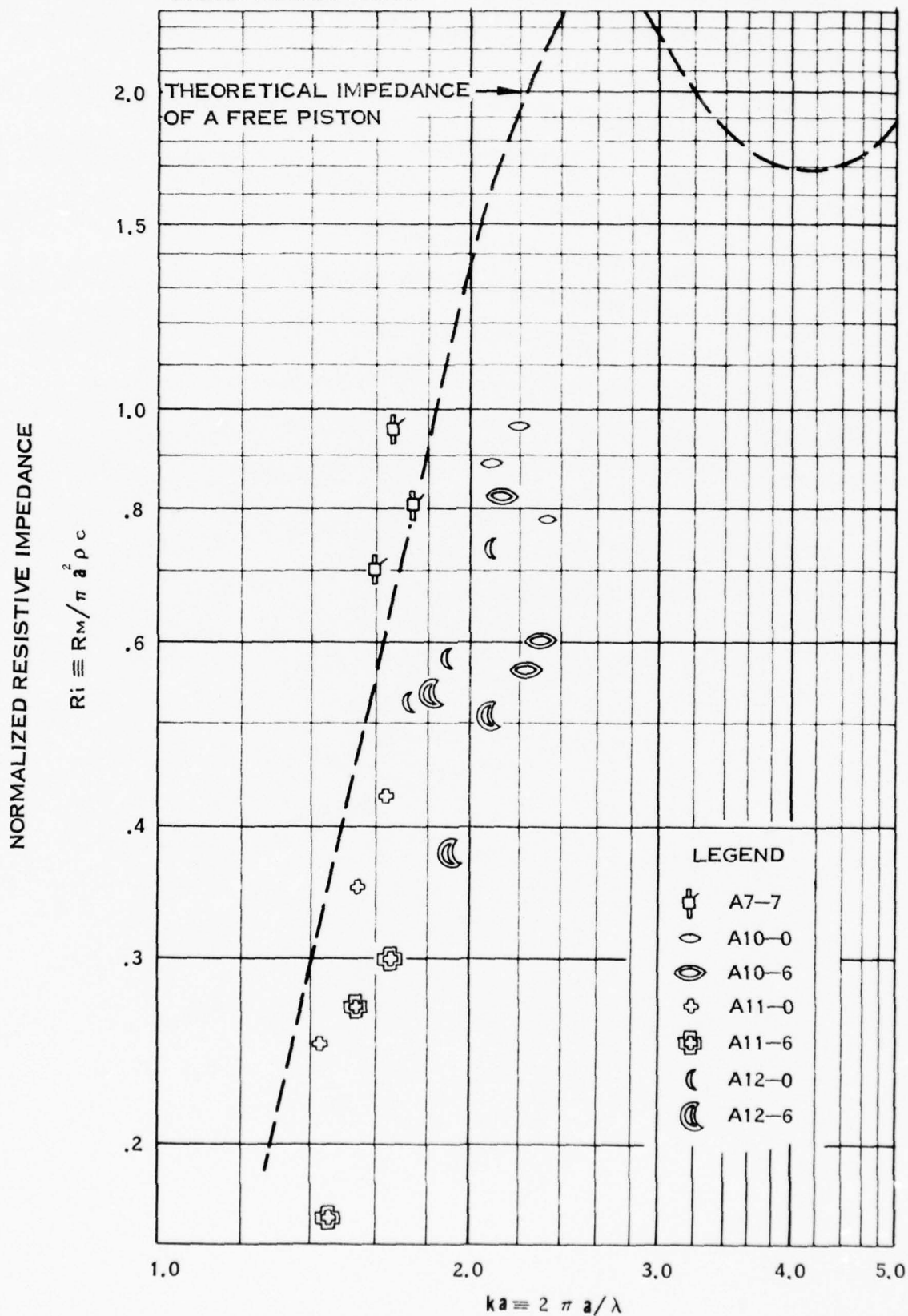
FIGURE C-8

# SPEAR MODEL TESTS



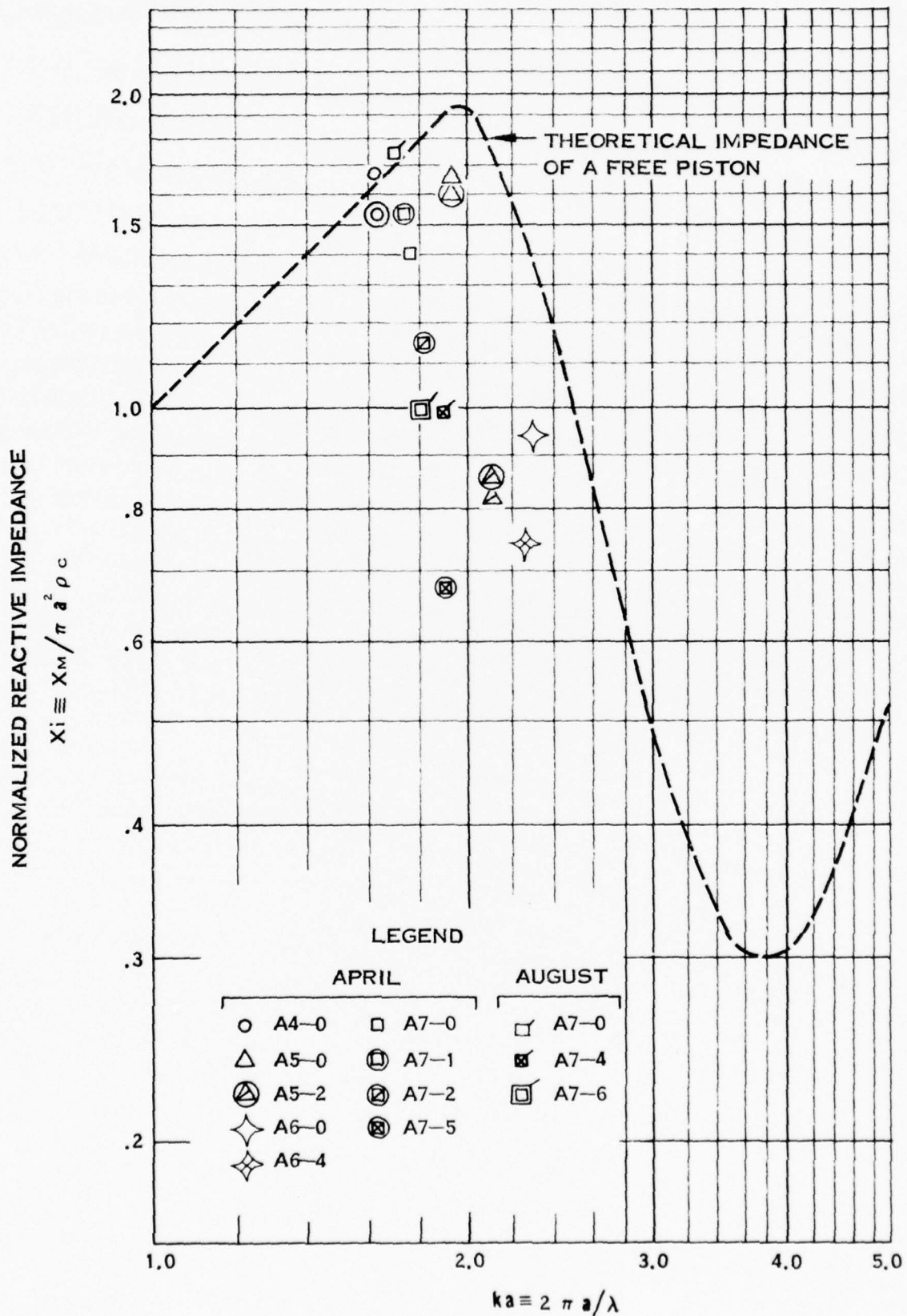
RESISTIVE IMPEDANCES  
 FOR PRIMARY CONFIGURATIONS  
 FIGURE C-9

# SPEAR MODEL TESTS



RESISTIVE IMPEDANCES  
FOR SECONDARY CONFIGURATIONS  
FIGURE C-10

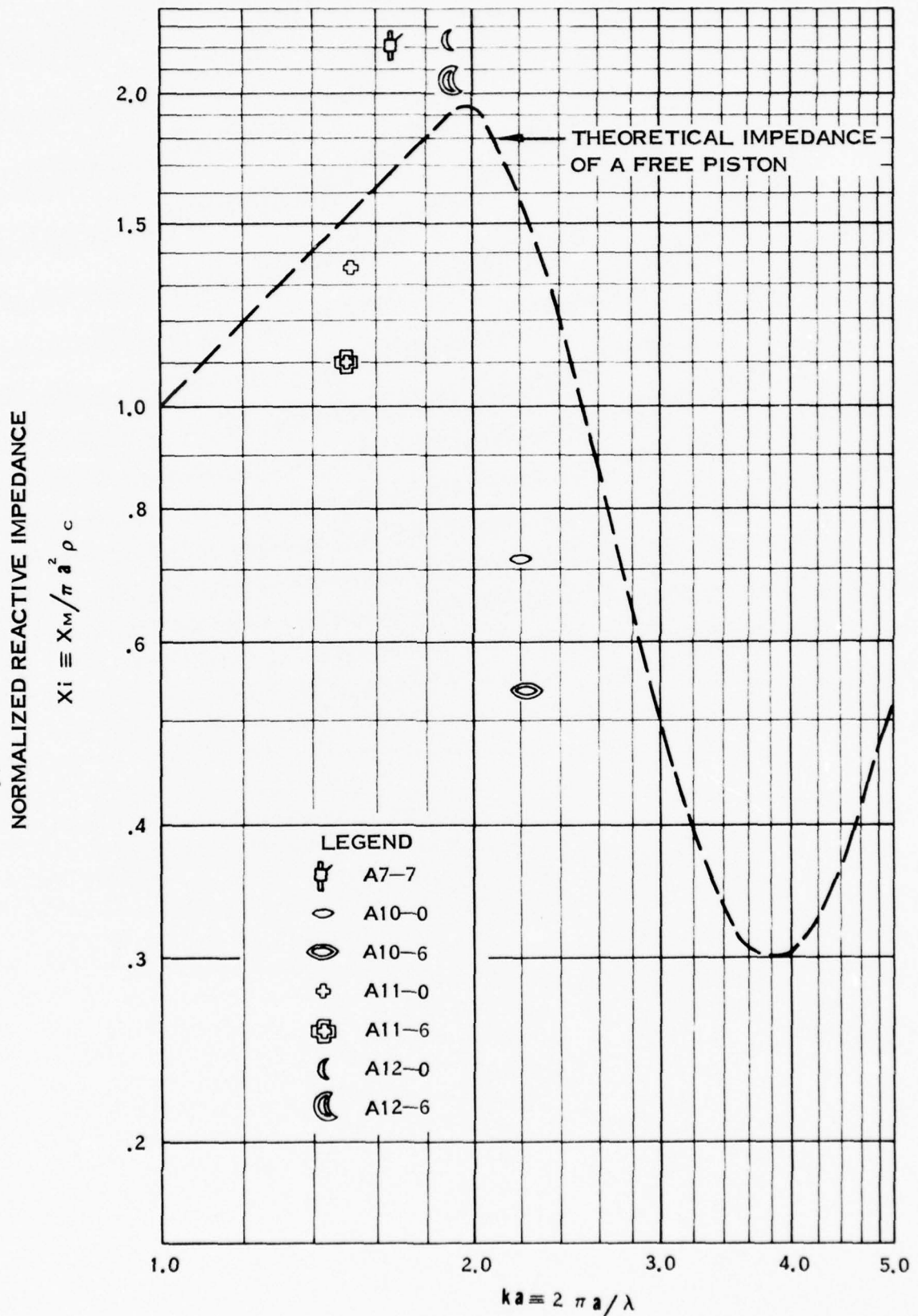
# SPEAR MODEL TESTS



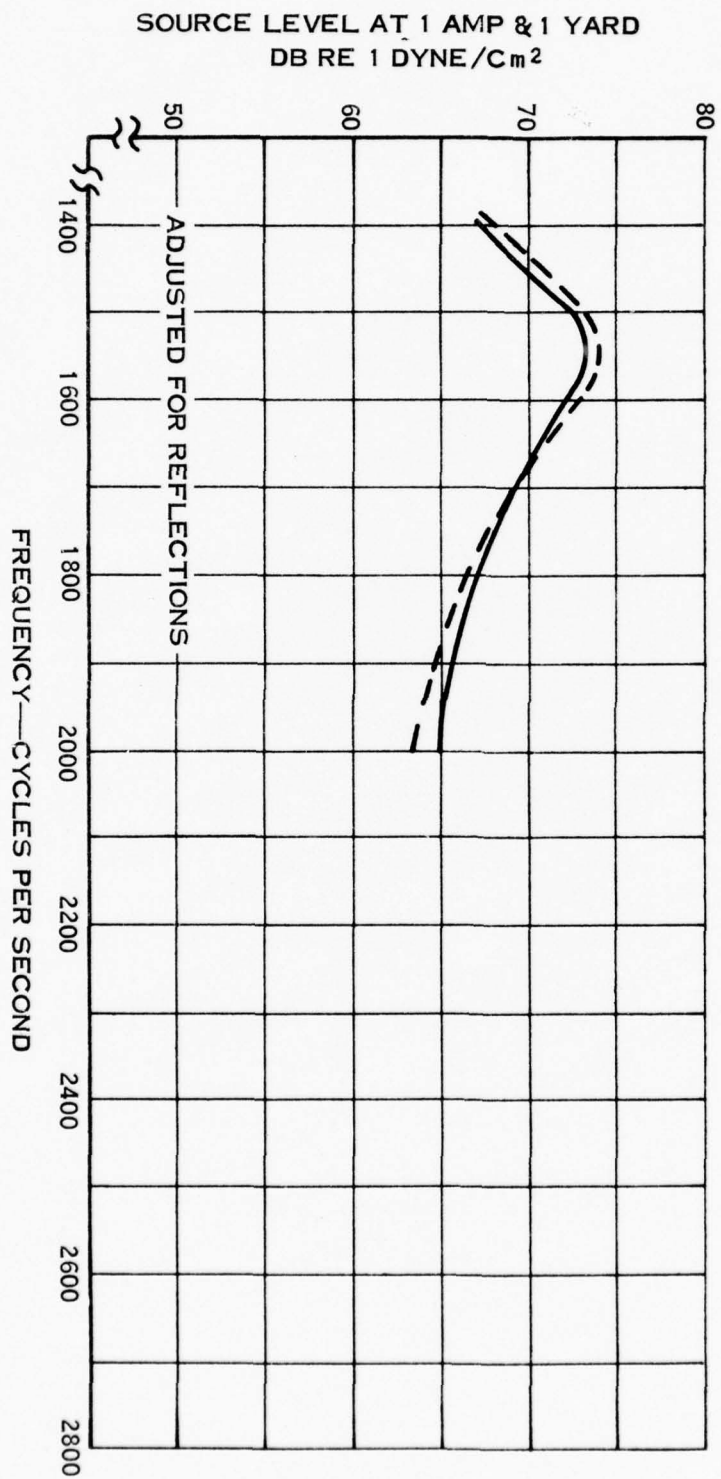
REACTIVE IMPEDANCES  
 FOR PRIMARY CONFIGURATIONS  
 FIGURE C-11



# SPEAR MODEL TESTS



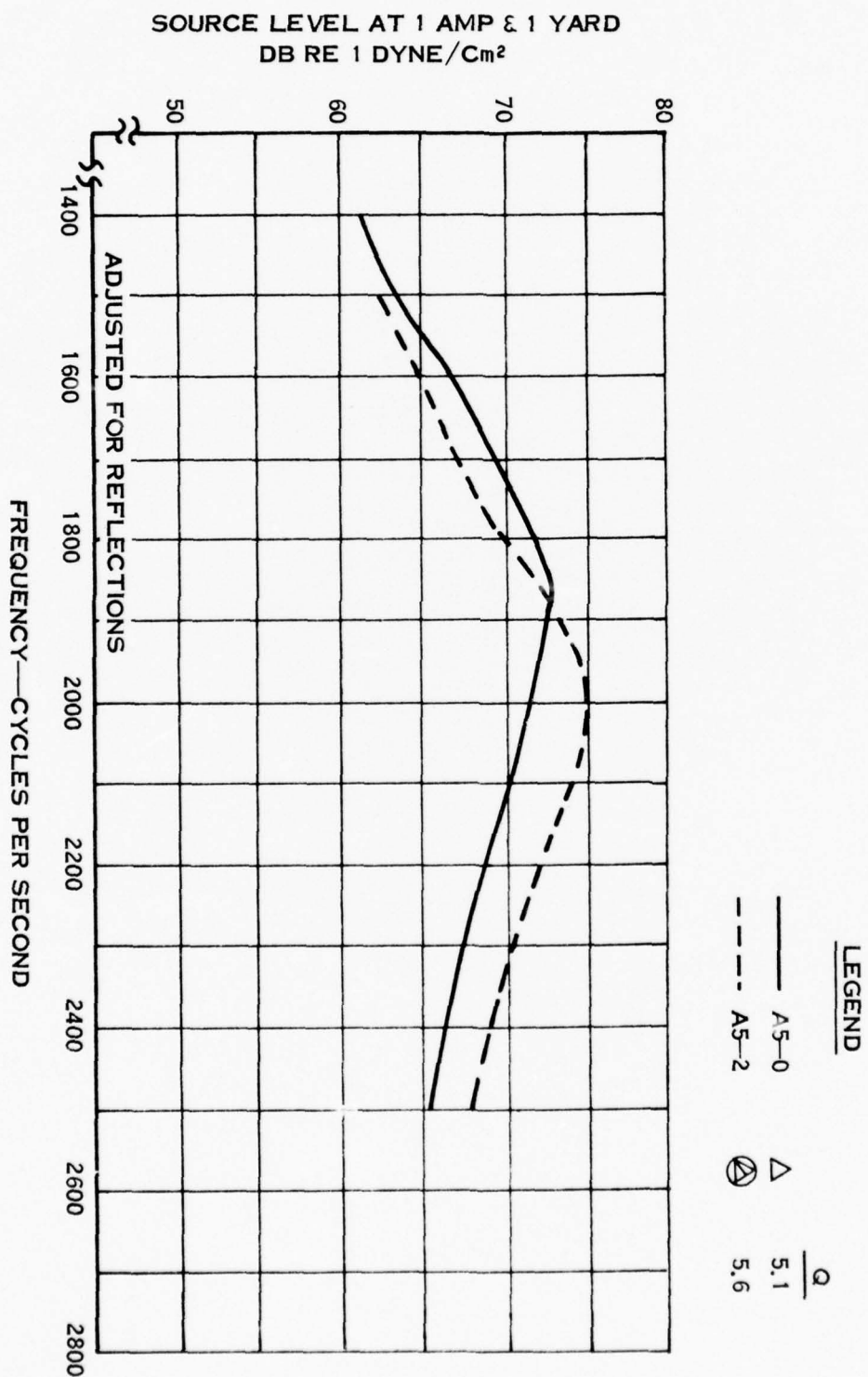
REACTIVE IMPEDANCES  
FOR SECONDARY CONFIGURATIONS  
FIGURE C-12



SPEAR MODEL TEST  
TRANSMITTING RESPONSE  
FIGURE C-13

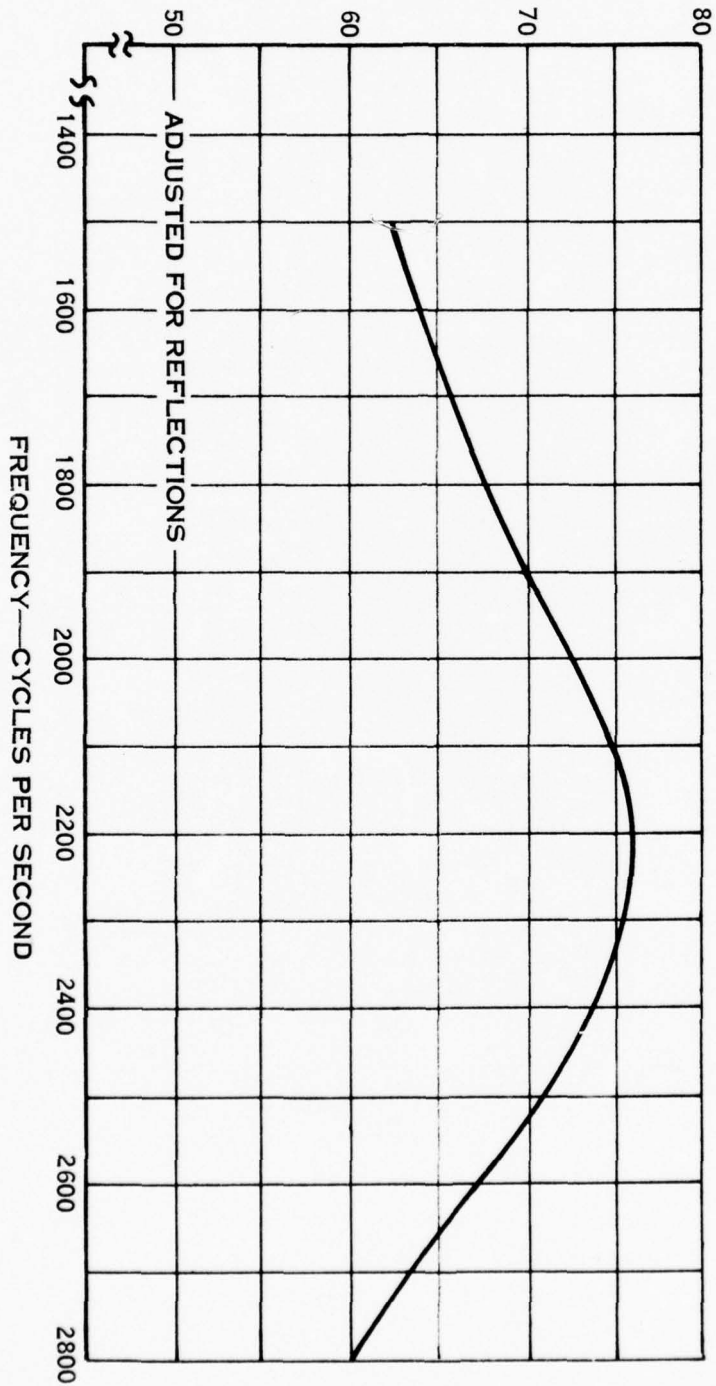
LEGEND

- |                                 |                                                                                       |
|---------------------------------|---------------------------------------------------------------------------------------|
| <p>— A4-0</p> <p>- - - A4-1</p> | <p>○</p> <p>⊙</p> <p><math>\frac{Q}{8.3}</math></p> <p><math>\frac{Q}{7.7}</math></p> |
|---------------------------------|---------------------------------------------------------------------------------------|



SPEAR MODEL TEST TRANSMITTING RESPONSE  
FIGURE C-14

SOURCE LEVEL AT 1 AMP & 1 YARD  
DB RE 1 DYNE/C<sub>m</sub><sup>2</sup>



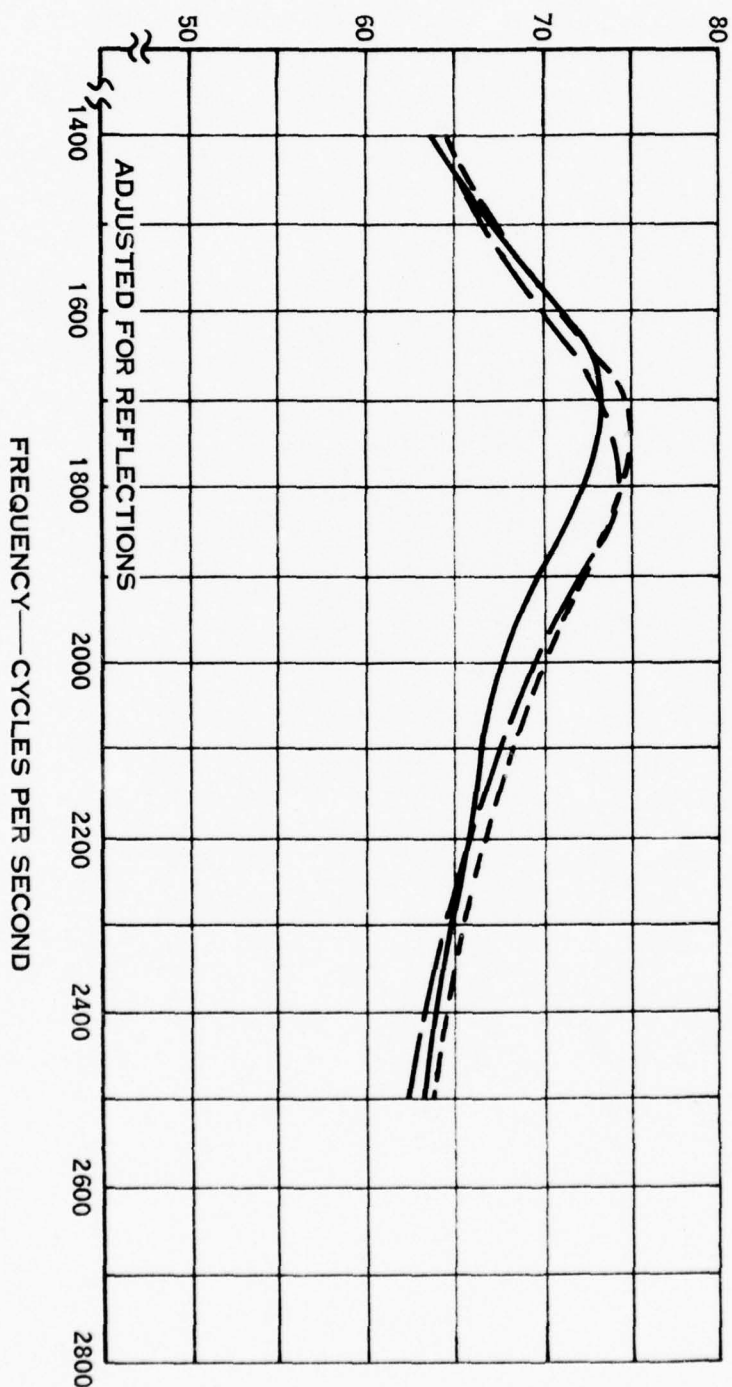
CONFIGURATION A6-4 Q = 5.4



SPEAR MODEL TEST  
TRANSMITTING RESPONSE  
FIGURE C-15



SOURCE LEVEL AT 1 AMP & 1 YARD  
DB RE 1 DYNE/Cm<sup>2</sup>

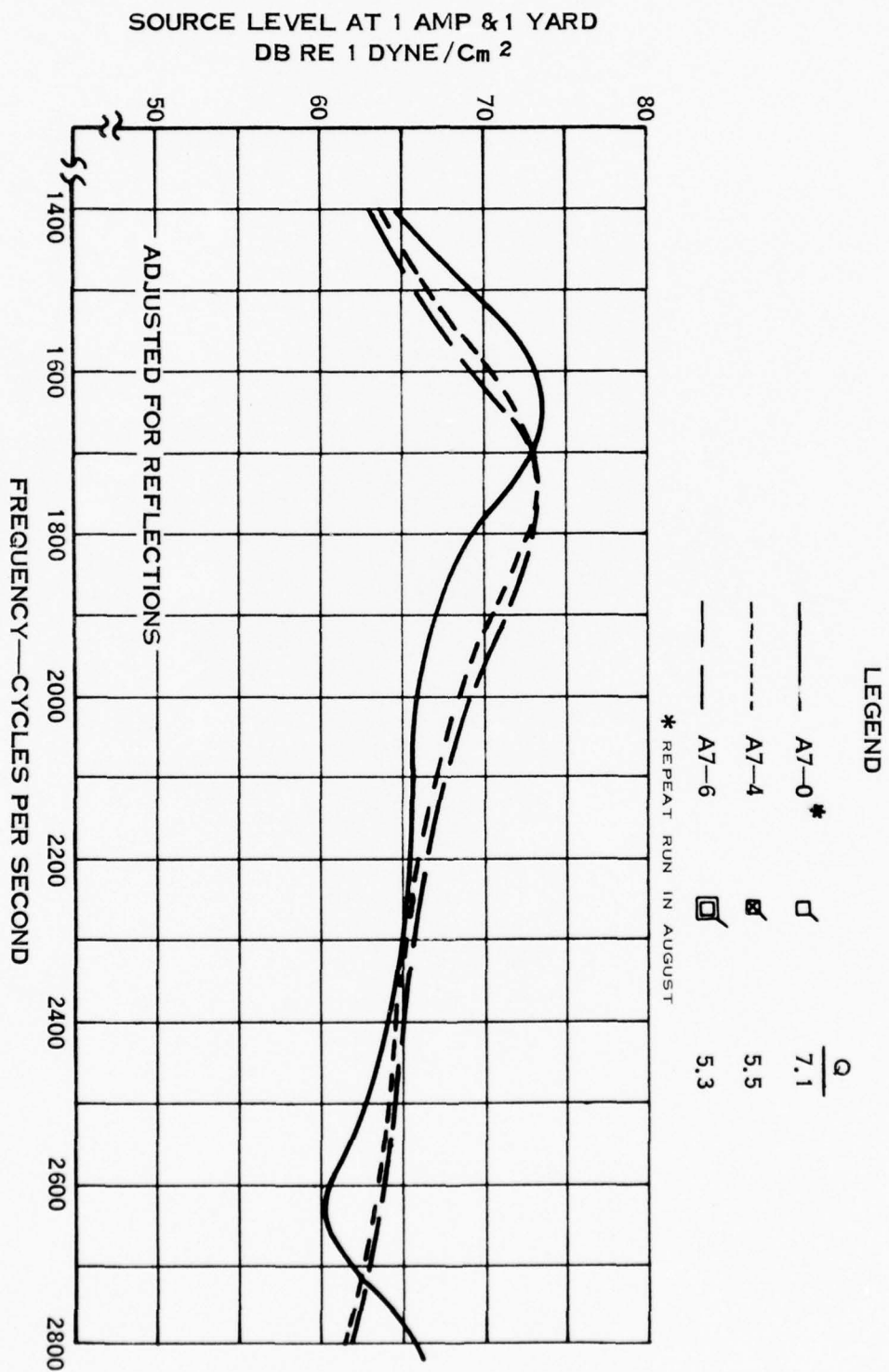


LEGEND

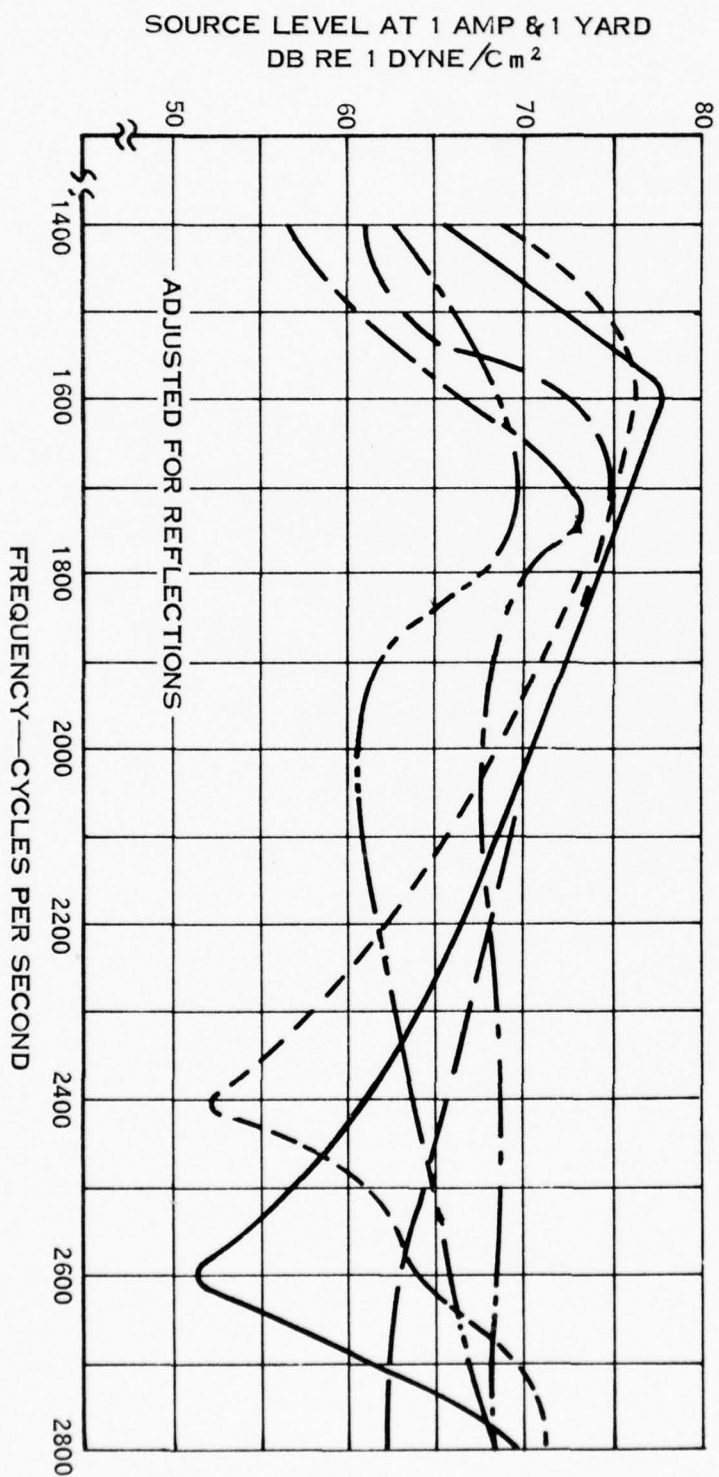
—	A7-0	□	Q
- - -	A7-2	⊗	5.6
- · -	A7-5	⊙	5.8
		⊗	6.4

SPEAR MODEL TEST TRANSMITTING RESPONSE

FIGURE C-16



SPEAR MODEL TEST  
TRANSMITTING RESPONSE  
FIGURE C-17

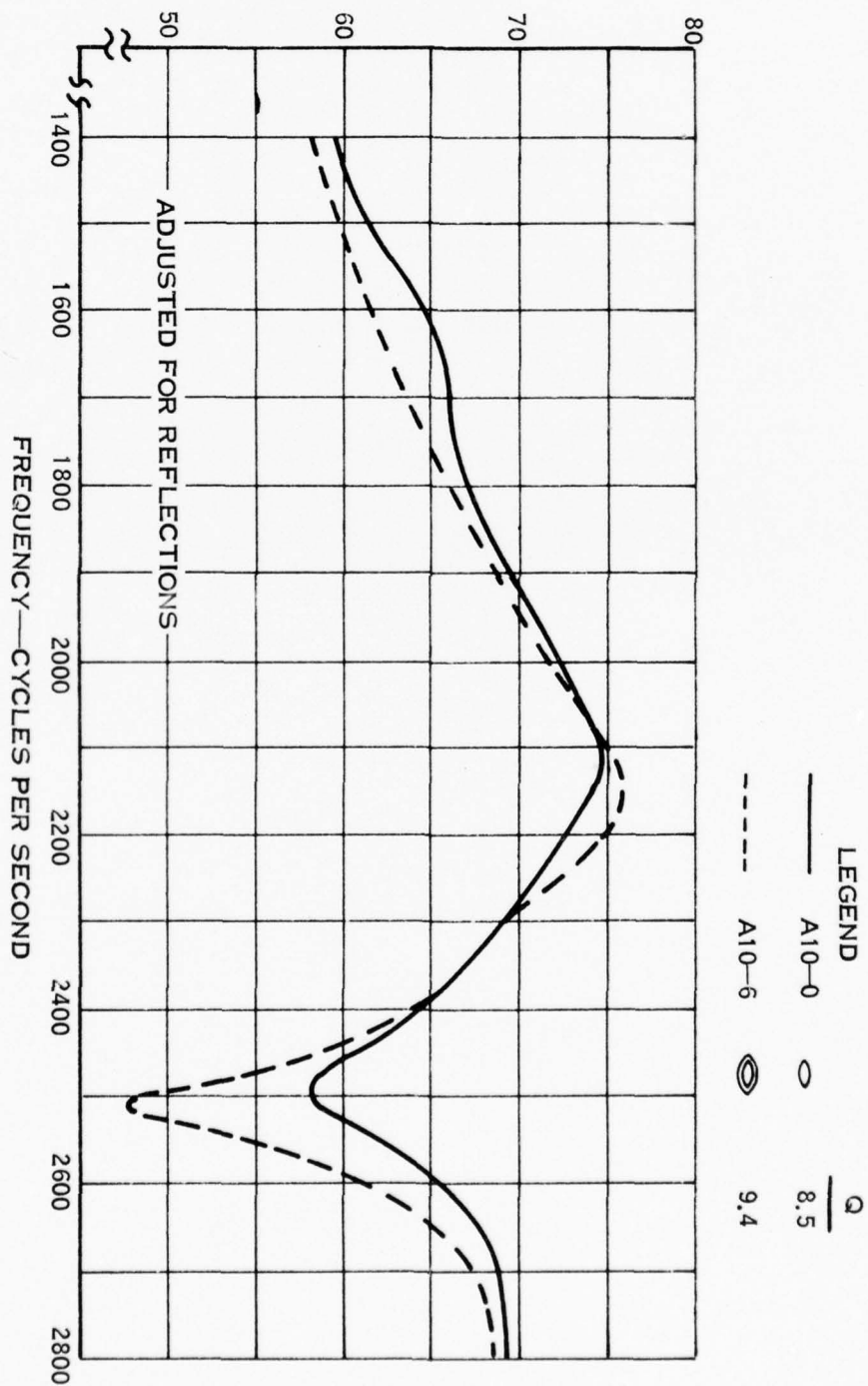


# LEGEND

CONFIGURATION A7-7	$\frac{Q}{\phi}$
----- L = 17 $\frac{1}{2}$ IN.	5.1
----- L = 15 $\frac{1}{2}$ IN.	9.6
----- L = 13 $\frac{1}{2}$ IN.	5.0
----- L = 10 $\frac{1}{8}$ IN.	11.6
----- L = 6 $\frac{7}{8}$ IN.	5.5

SPEAR MODEL TEST  
TRANSMITTING RESPONSE  
FIGURE C-18

SOURCE LEVEL AT 1 AMP & 1 YARD  
DB RE 1 DYNE/C<sub>m</sub><sup>2</sup>

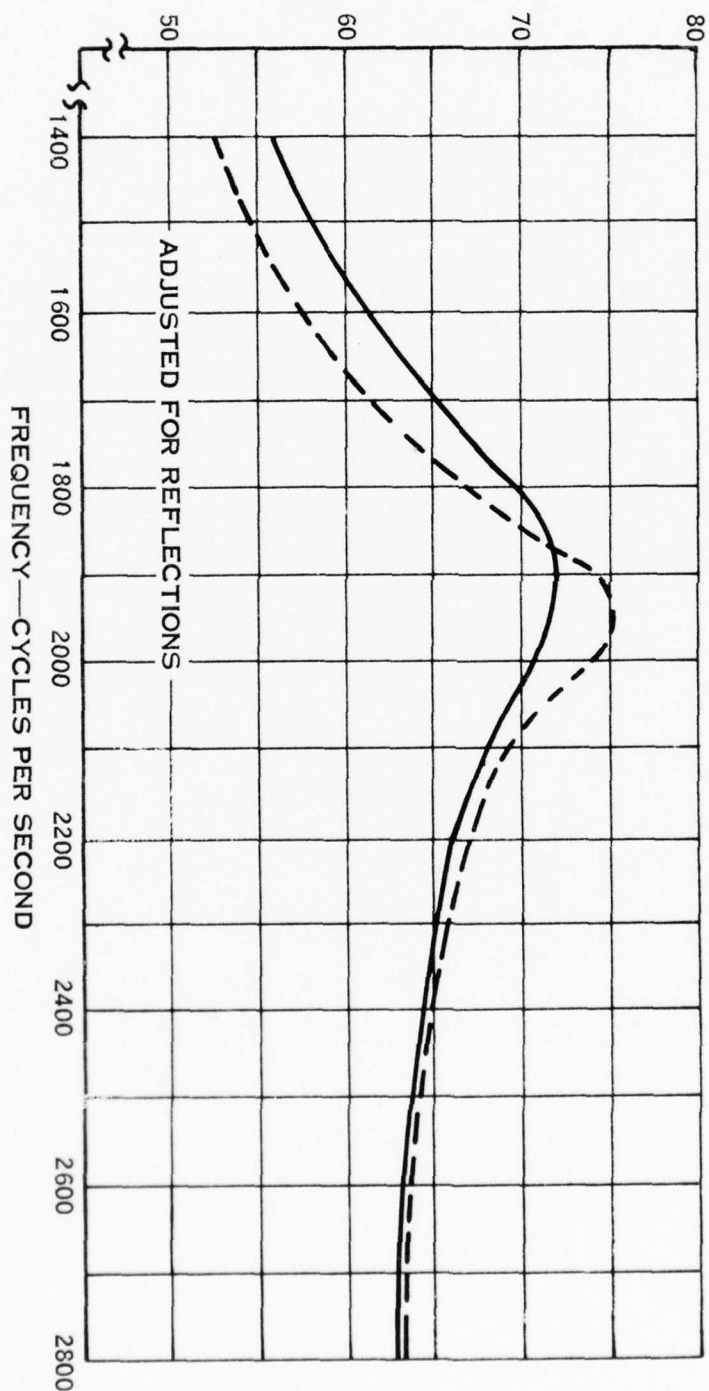


SPEAR MODEL TEST  
TRANSMITTING RESPONSE

FIGURE C-19



SOURCE LEVEL AT 1 AMP & 1 YARD  
DB RE 1 DYNE/C<sub>m</sub><sup>2</sup>



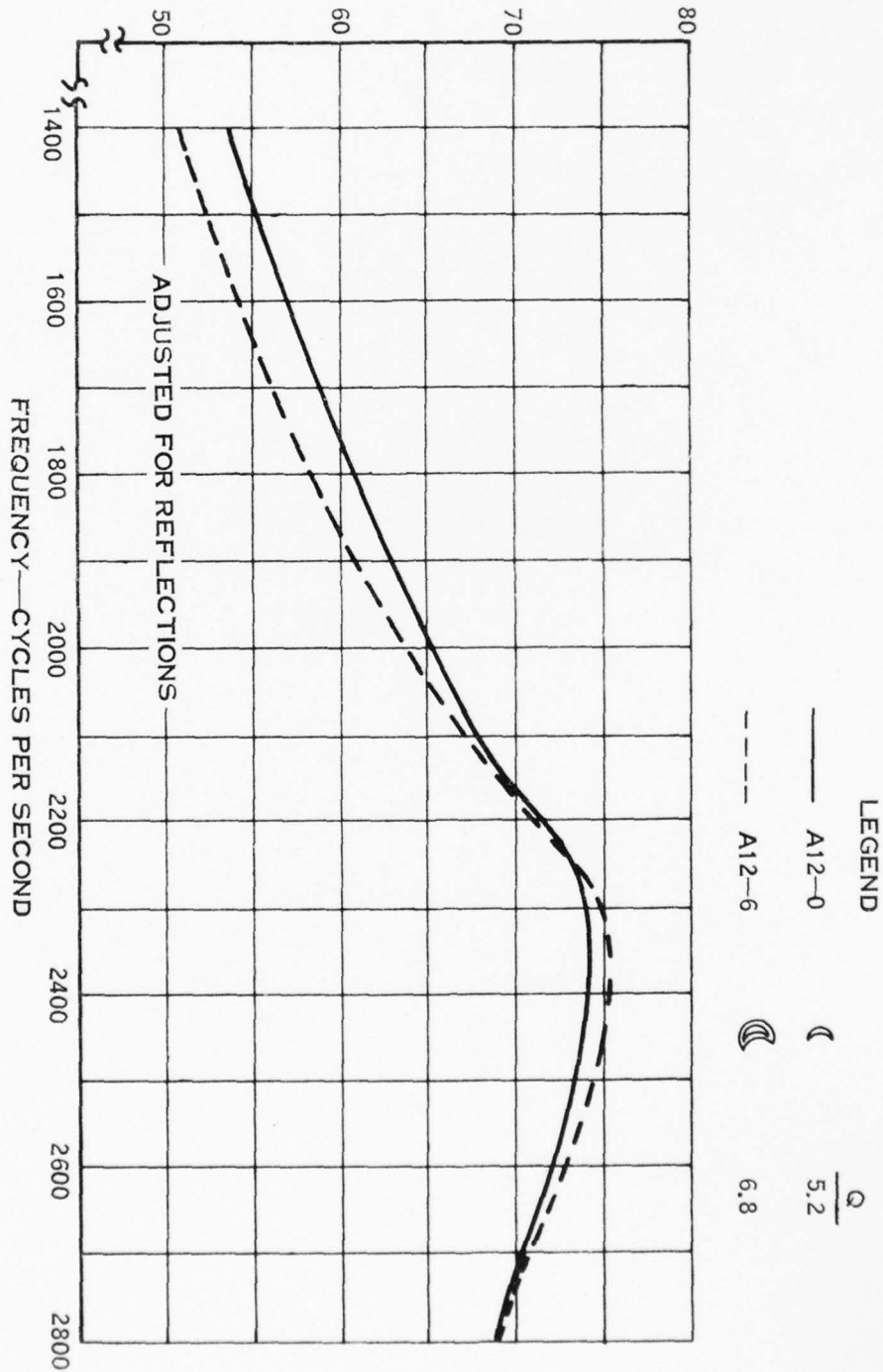
LEGEND

—— A11-0      ⊕       $\frac{Q}{7.4}$

----- A11-6      ⊗       $\frac{Q}{12.2}$

SPEAR MODEL TEST  
TRANSMITTING RESPONSE  
FIGURE C-20

SOURCE LEVEL AT 1 AMP & 1 YARD  
DB RE 1 DYNE CM<sup>2</sup>



SPEAR MODEL TEST  
TRANSMITTING RESPONSE  
FIGURE C-21

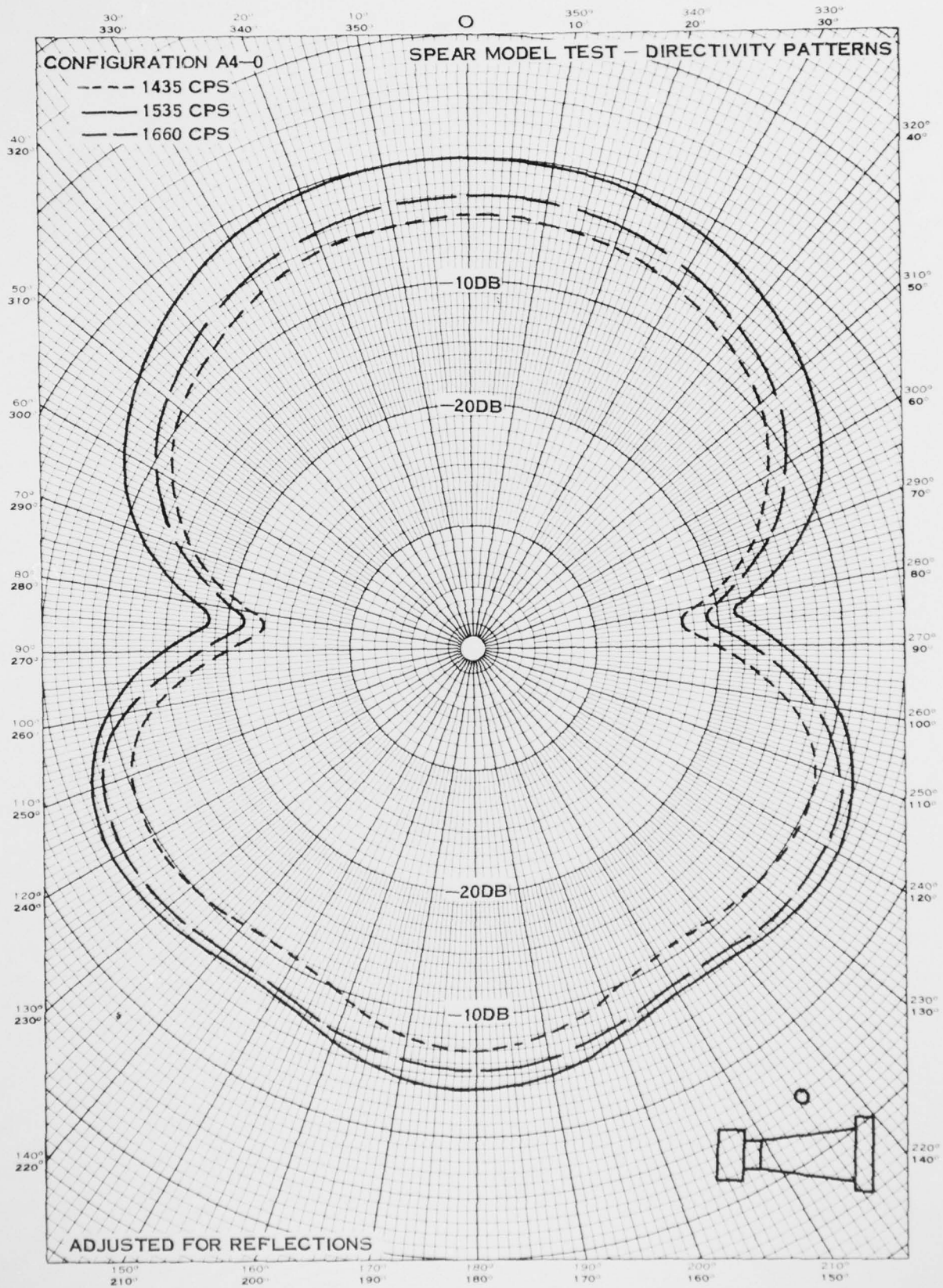


FIGURE C-22

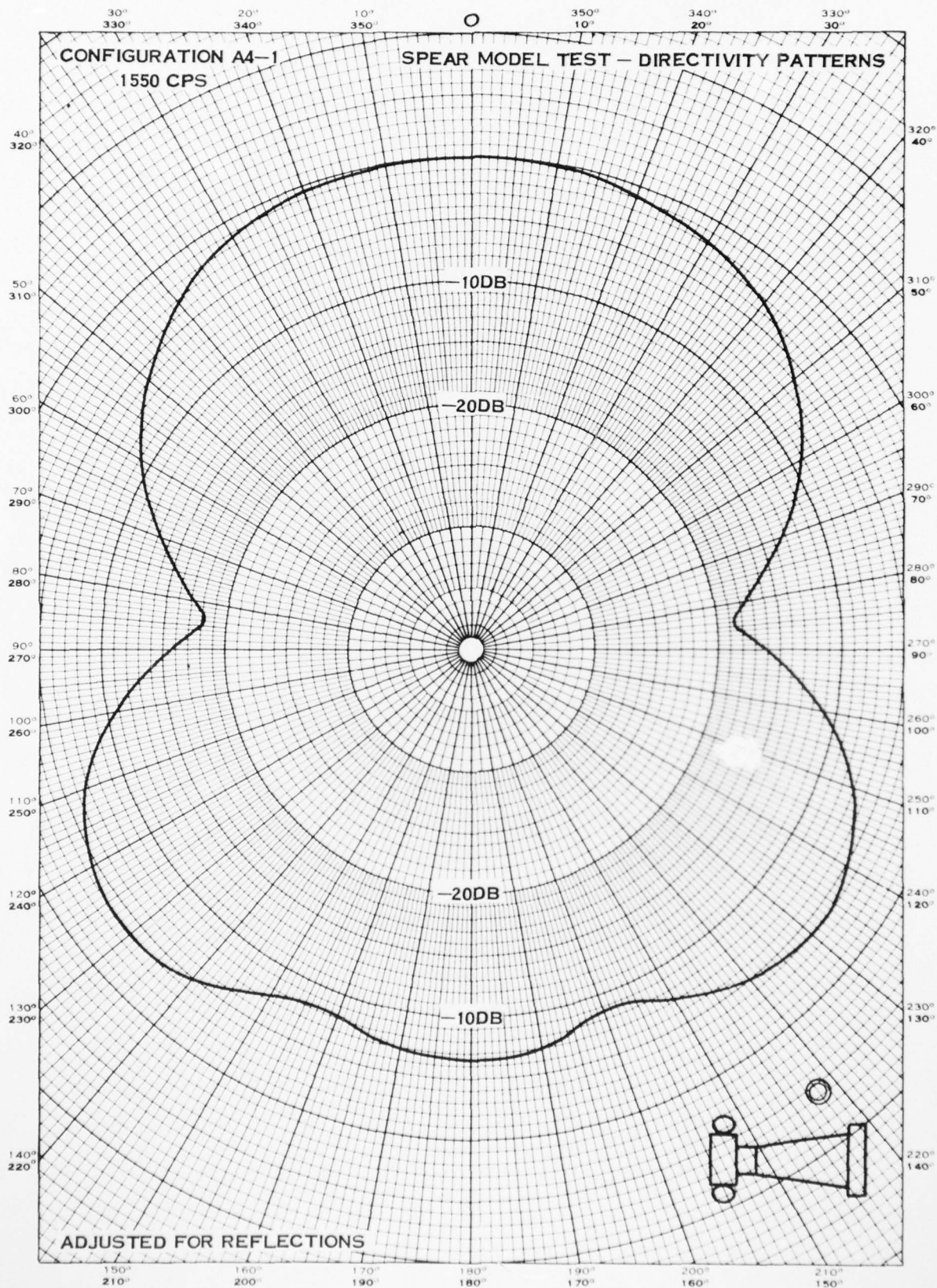


FIGURE C-23



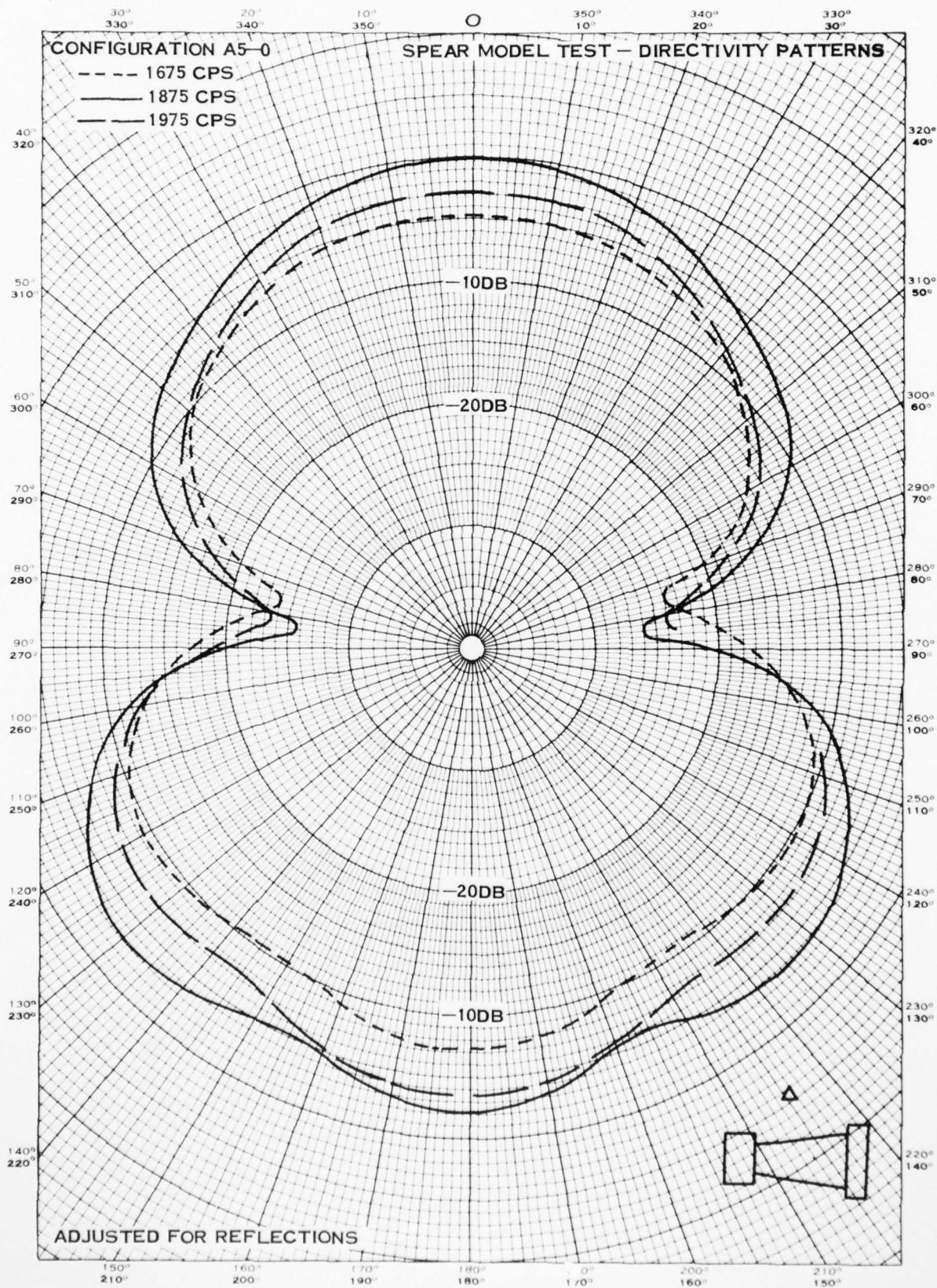


FIGURE C-24

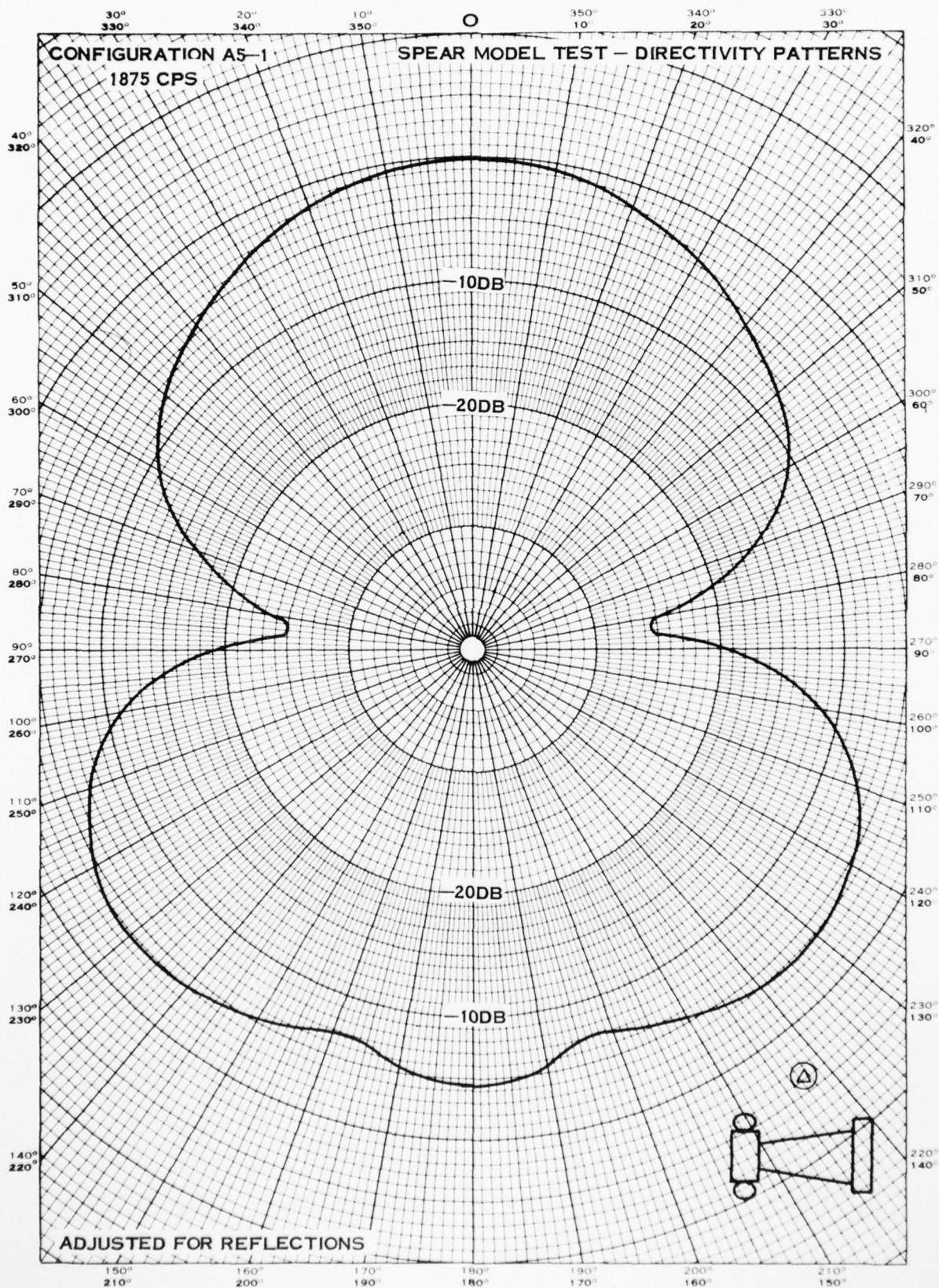


FIGURE C-25



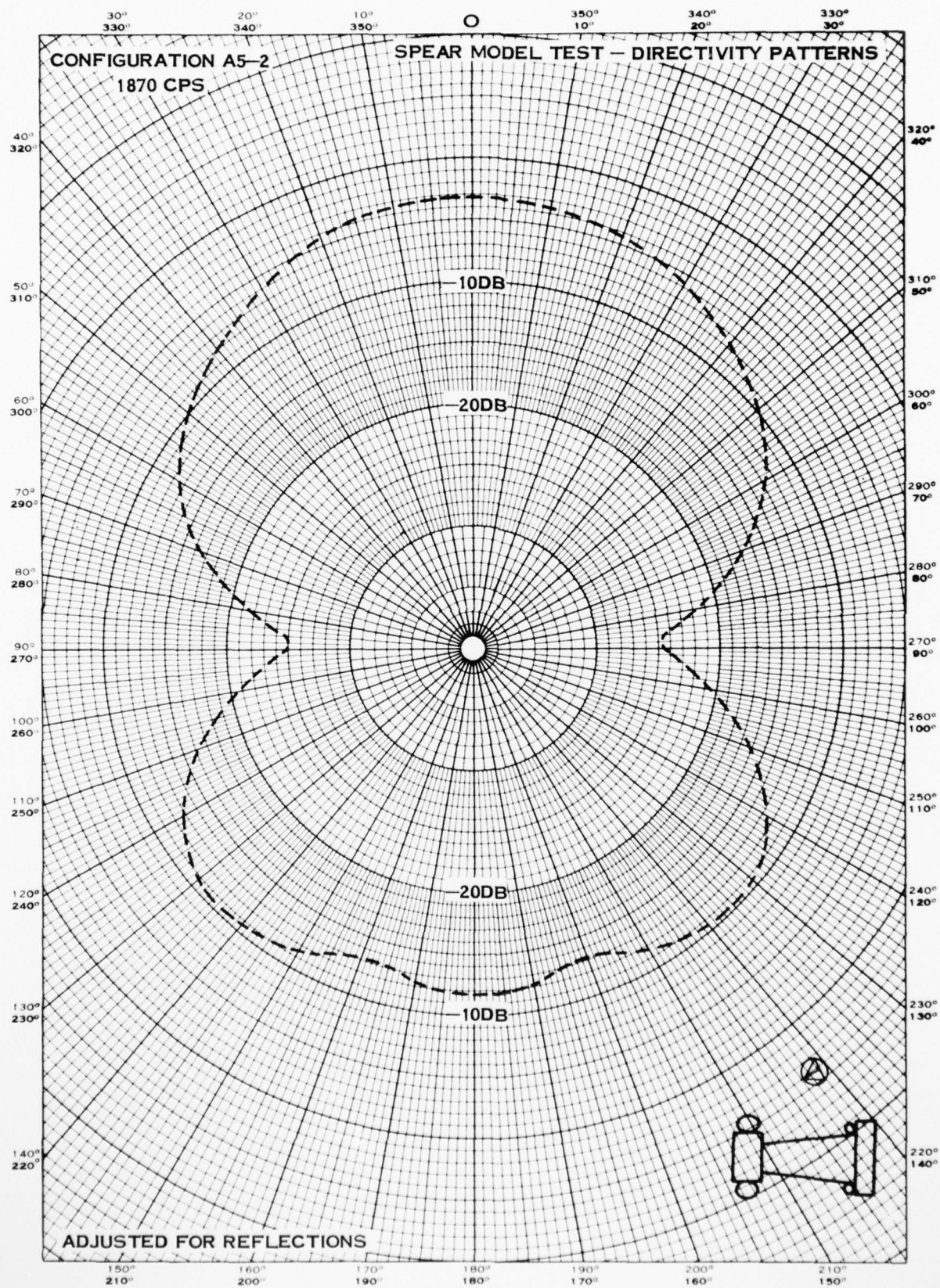


FIGURE C-26

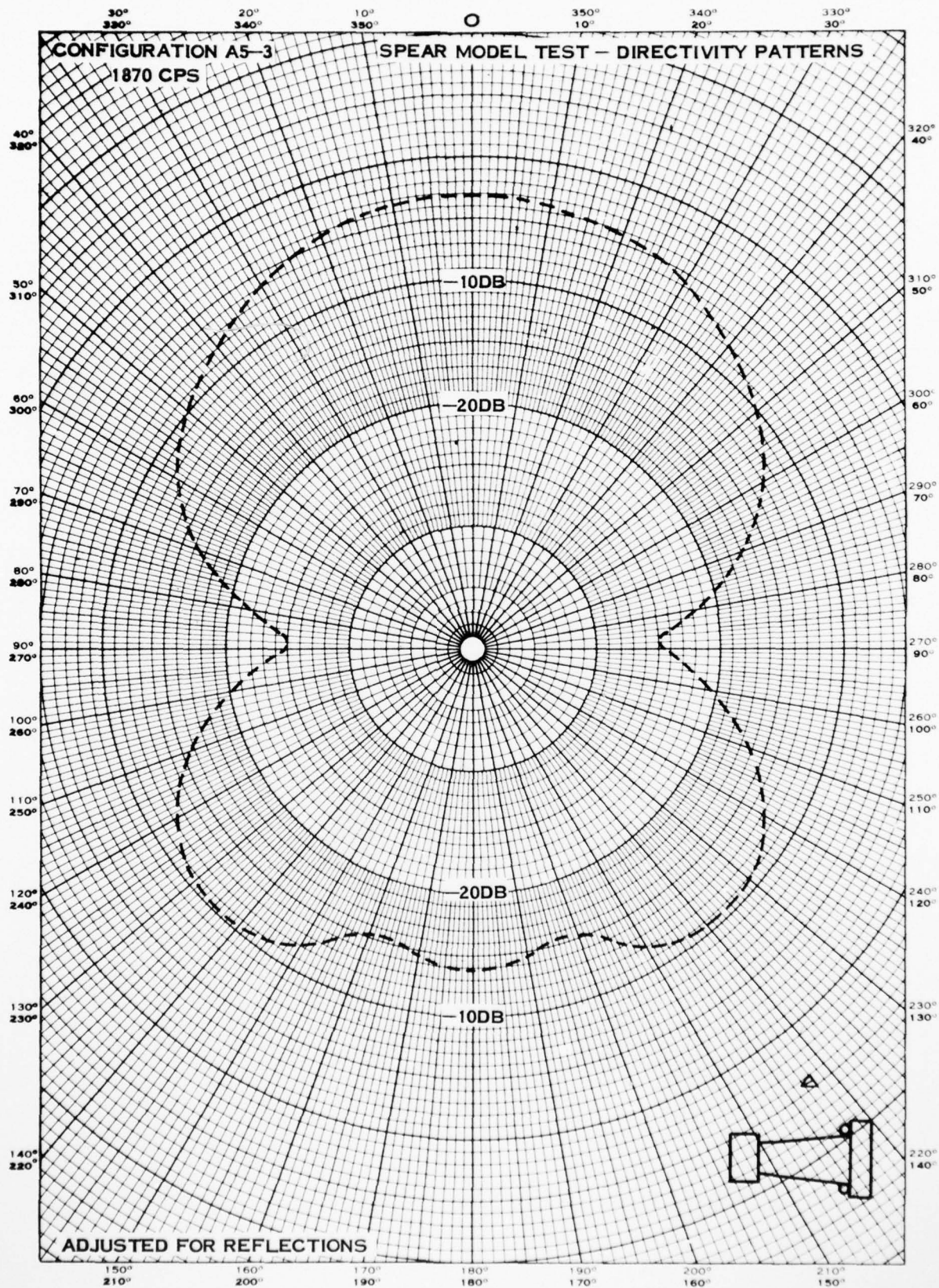


FIGURE C-27



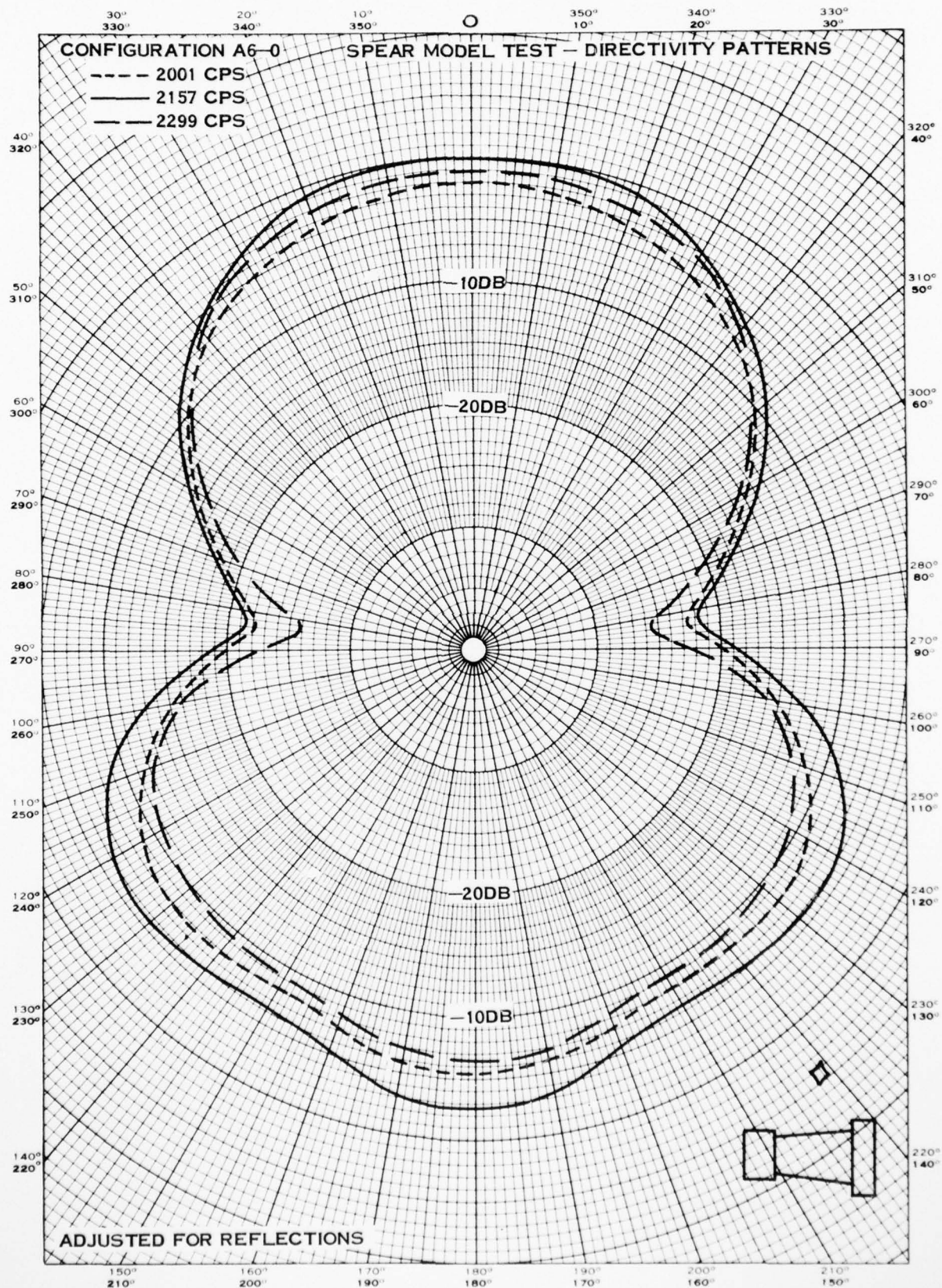


FIGURE C-28

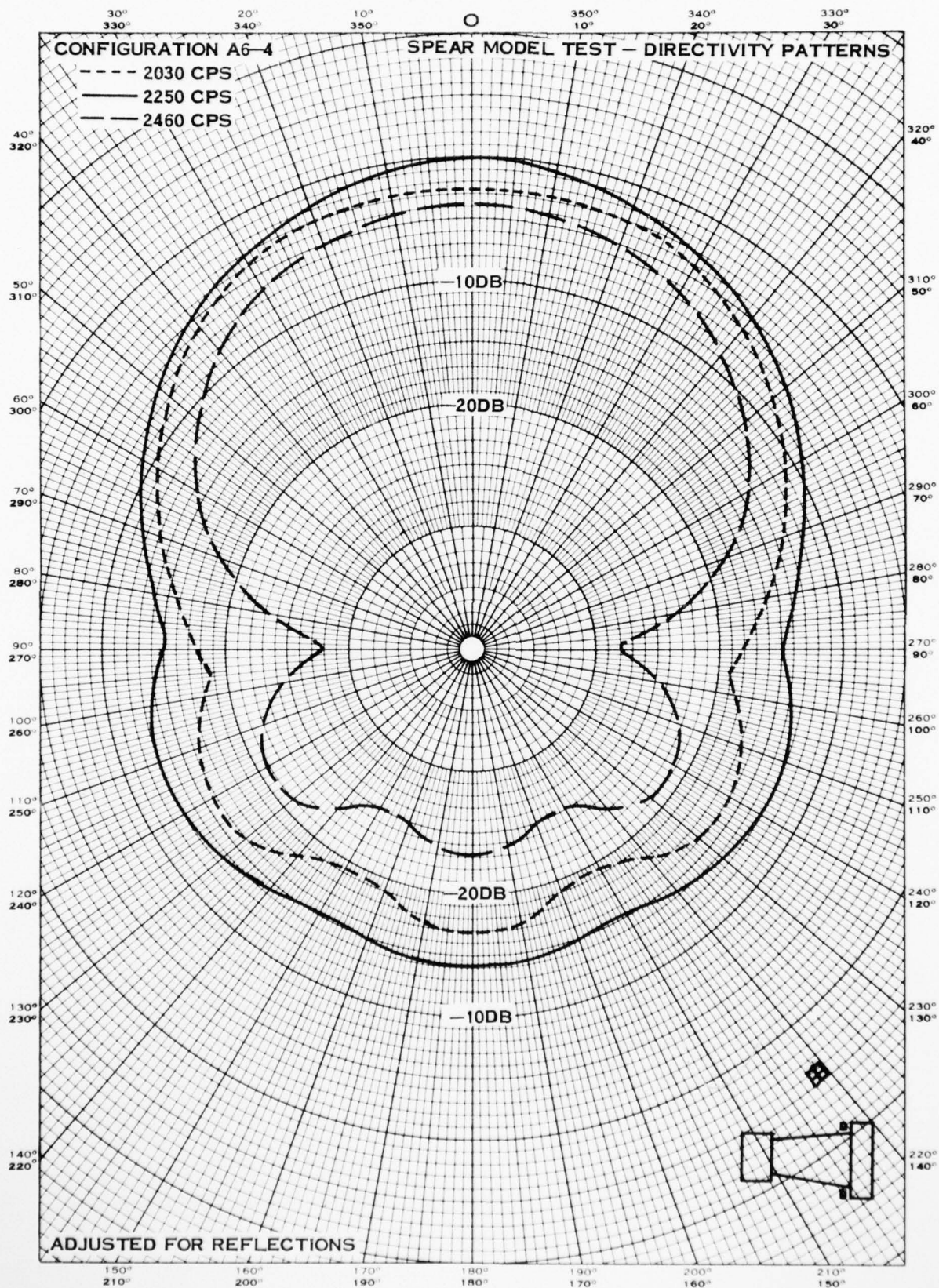


FIGURE C-29



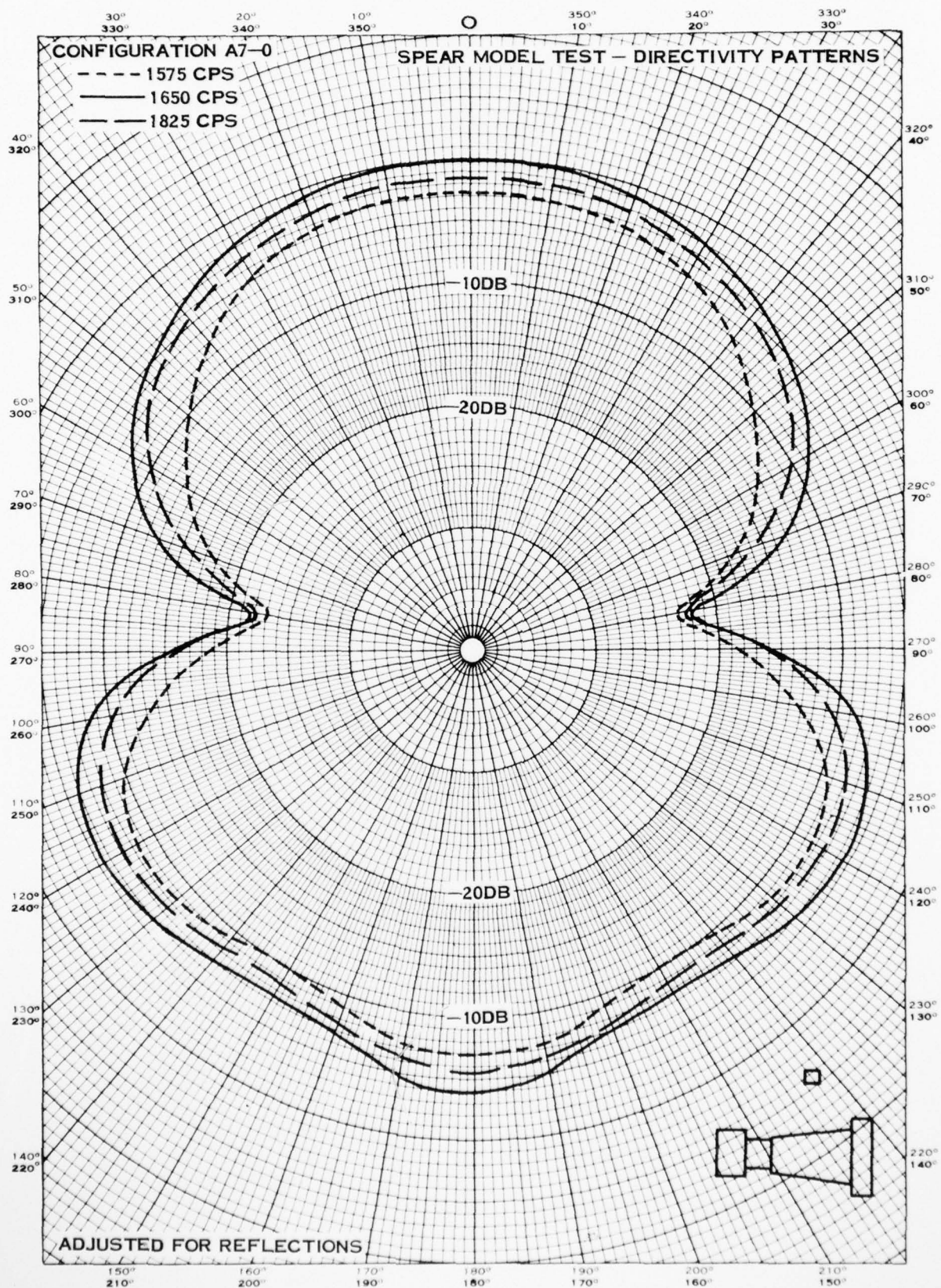


FIGURE C-30

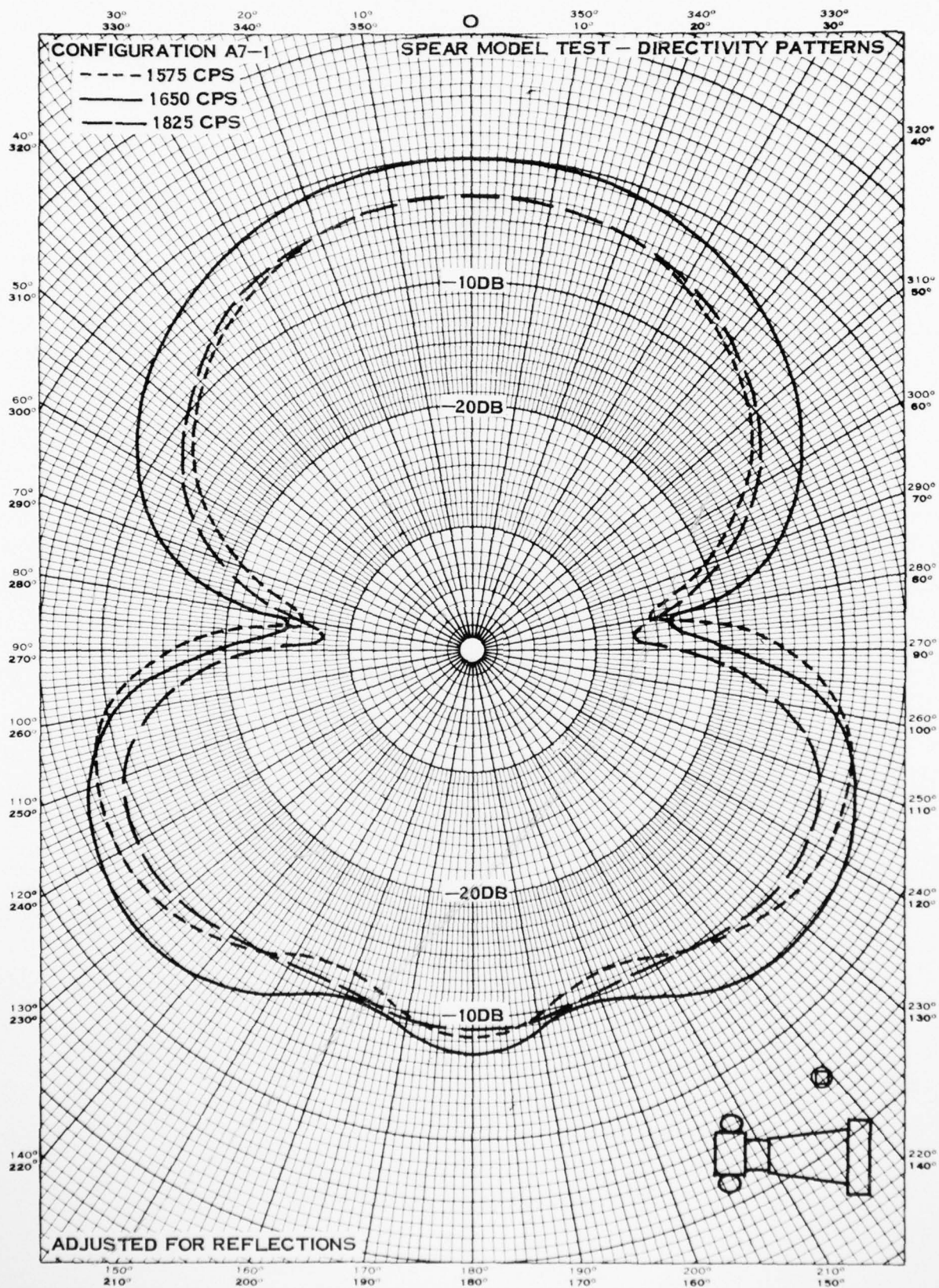


FIGURE C-31



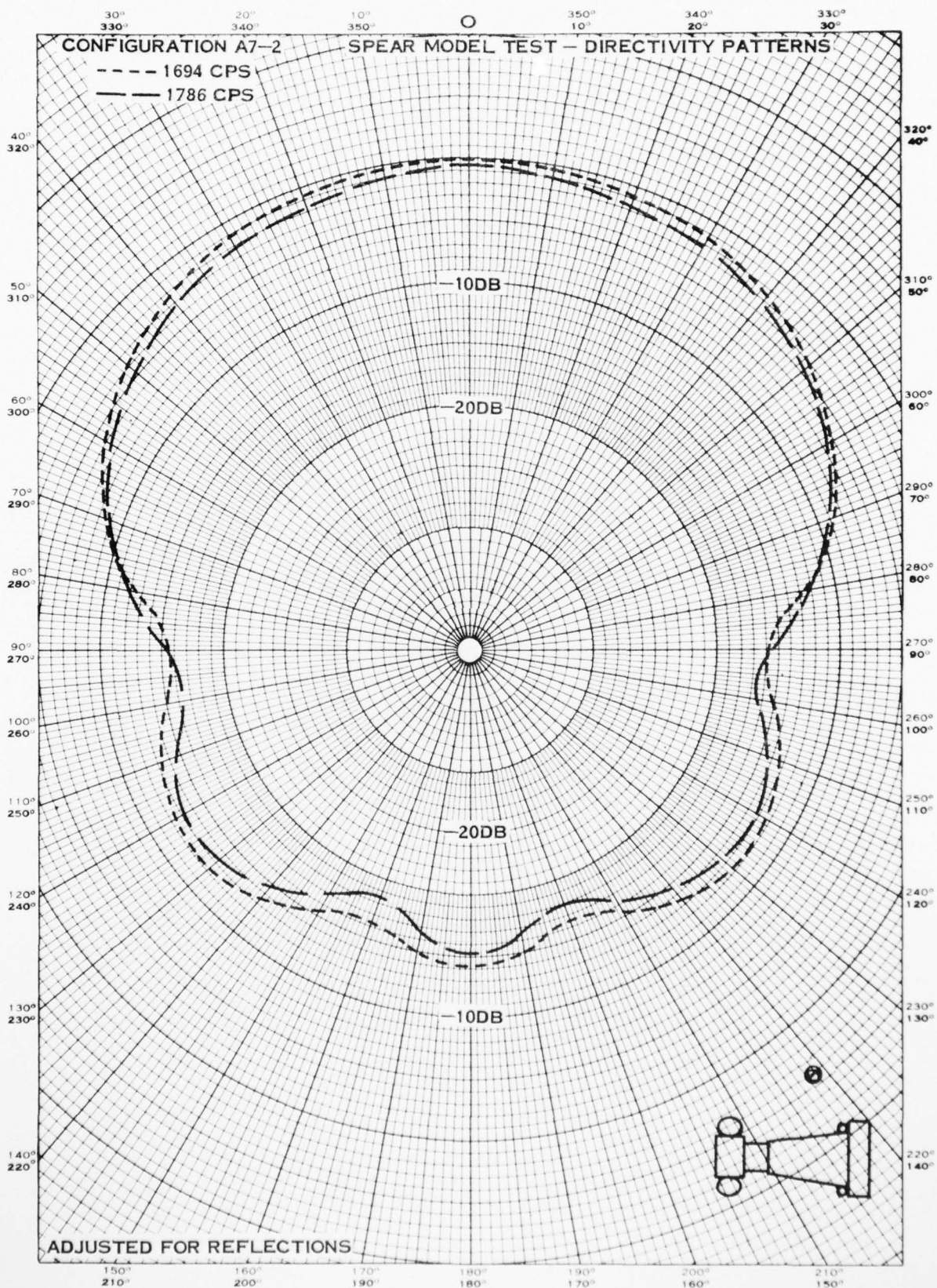


FIGURE C-32

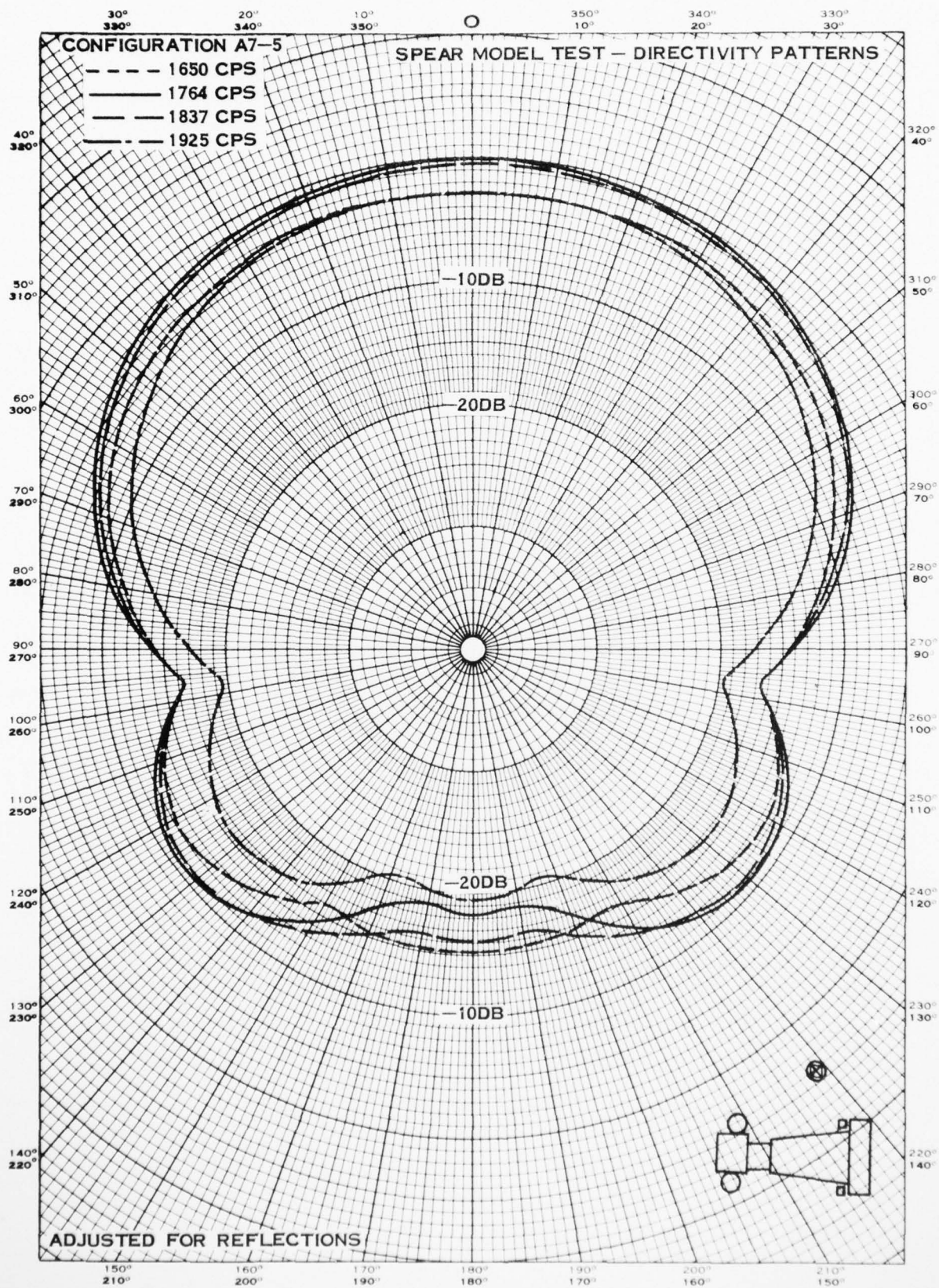


FIGURE C-33



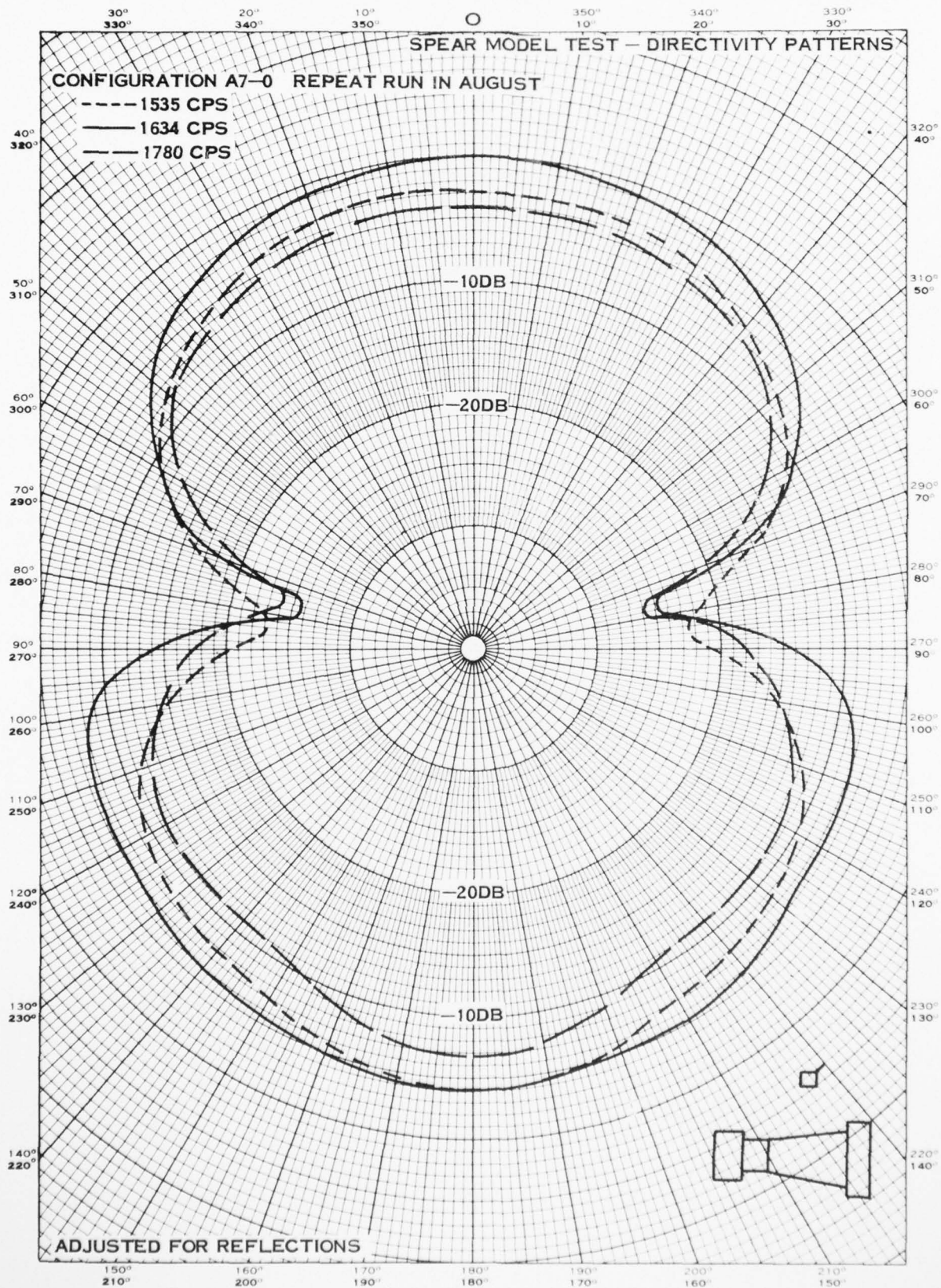


FIGURE C-34

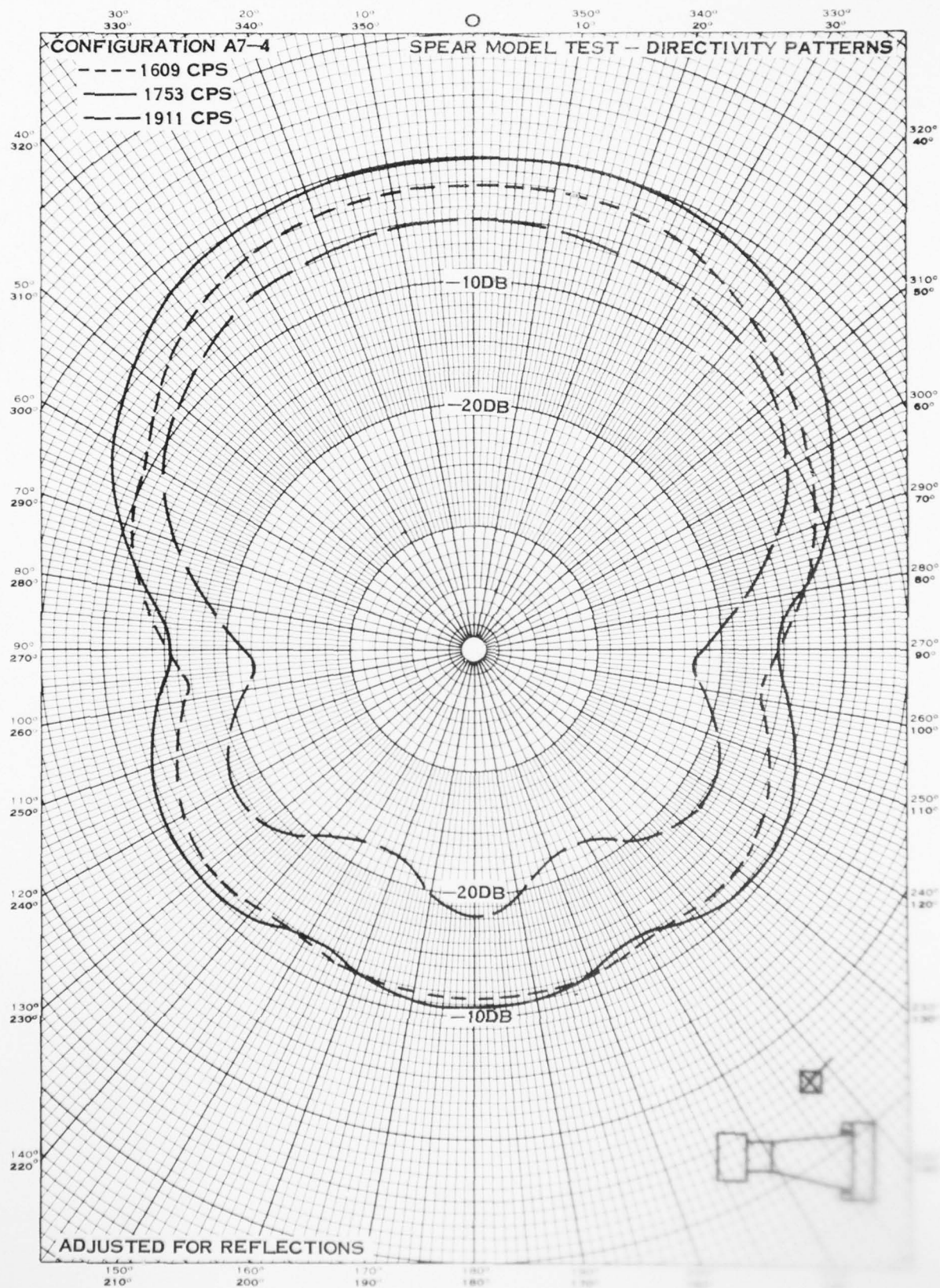


FIGURE C-35



AD-A039 617

UNITED TECHNOLOGIES CORP WINDSOR LOCKS CONN HAMILTON --ETC F/G 17/1  
SPEAR MODEL ACOUSTIC FEASIBILITY TESTS.(U)

JUN 62 L W SMITH

NONR-3350(00)

UNCLASSIFIED

HSER-2464

NL

2 of 2

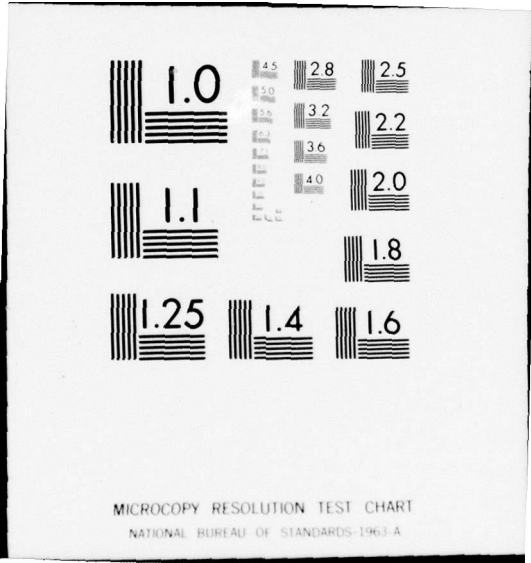
ADA039 617



END

DATE  
FILMED

6-77



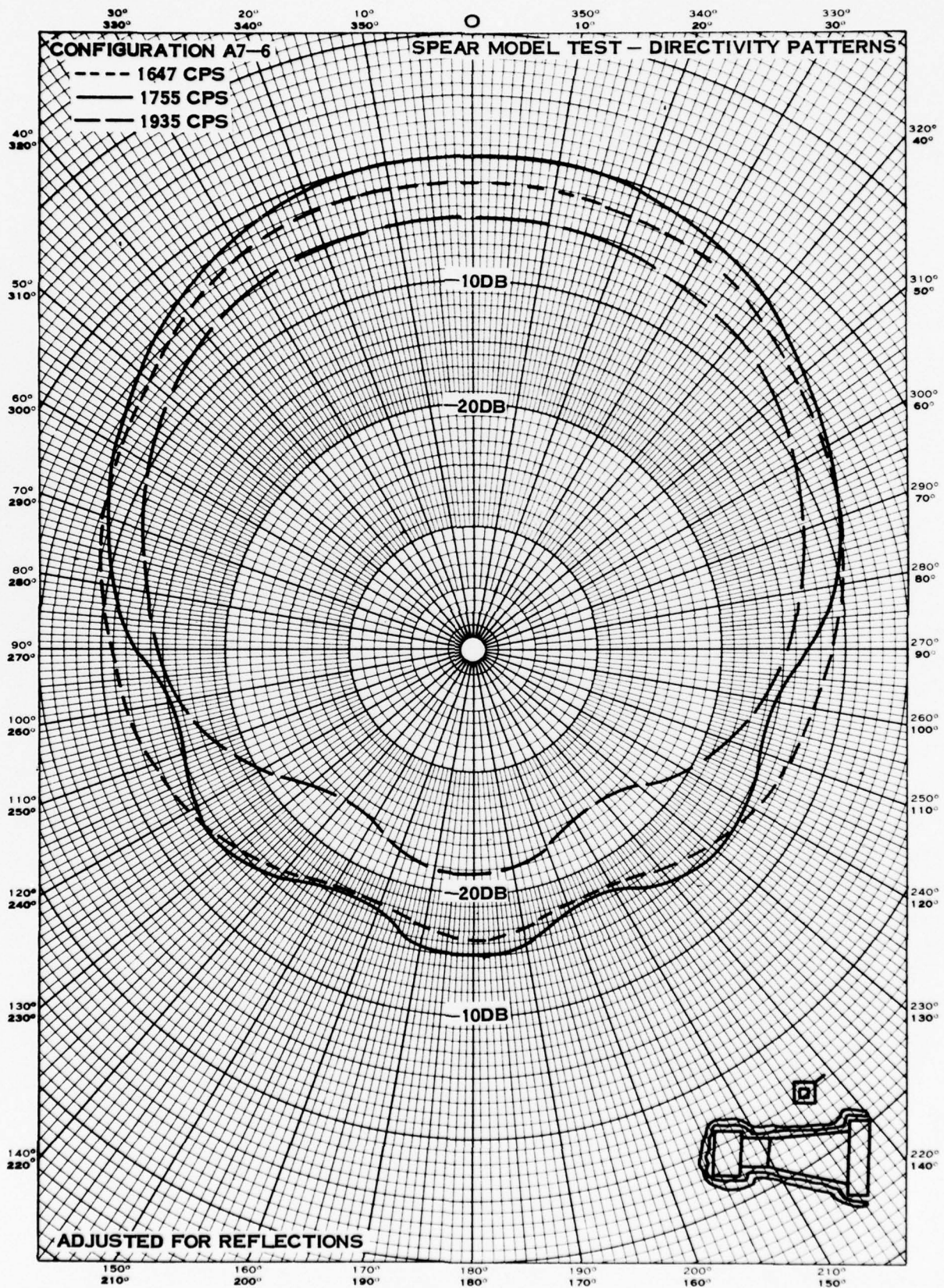


FIGURE C-36

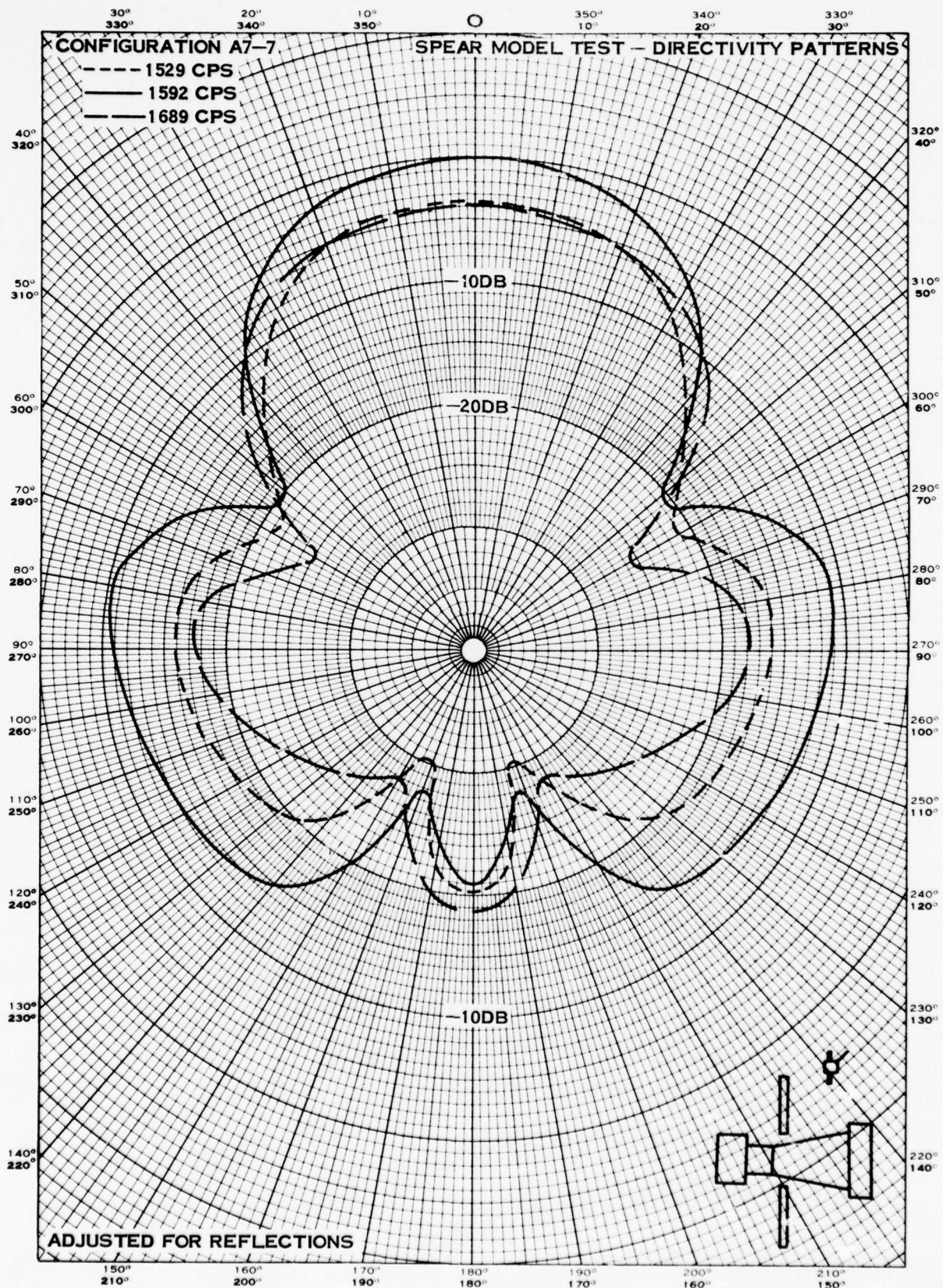


FIGURE C-37



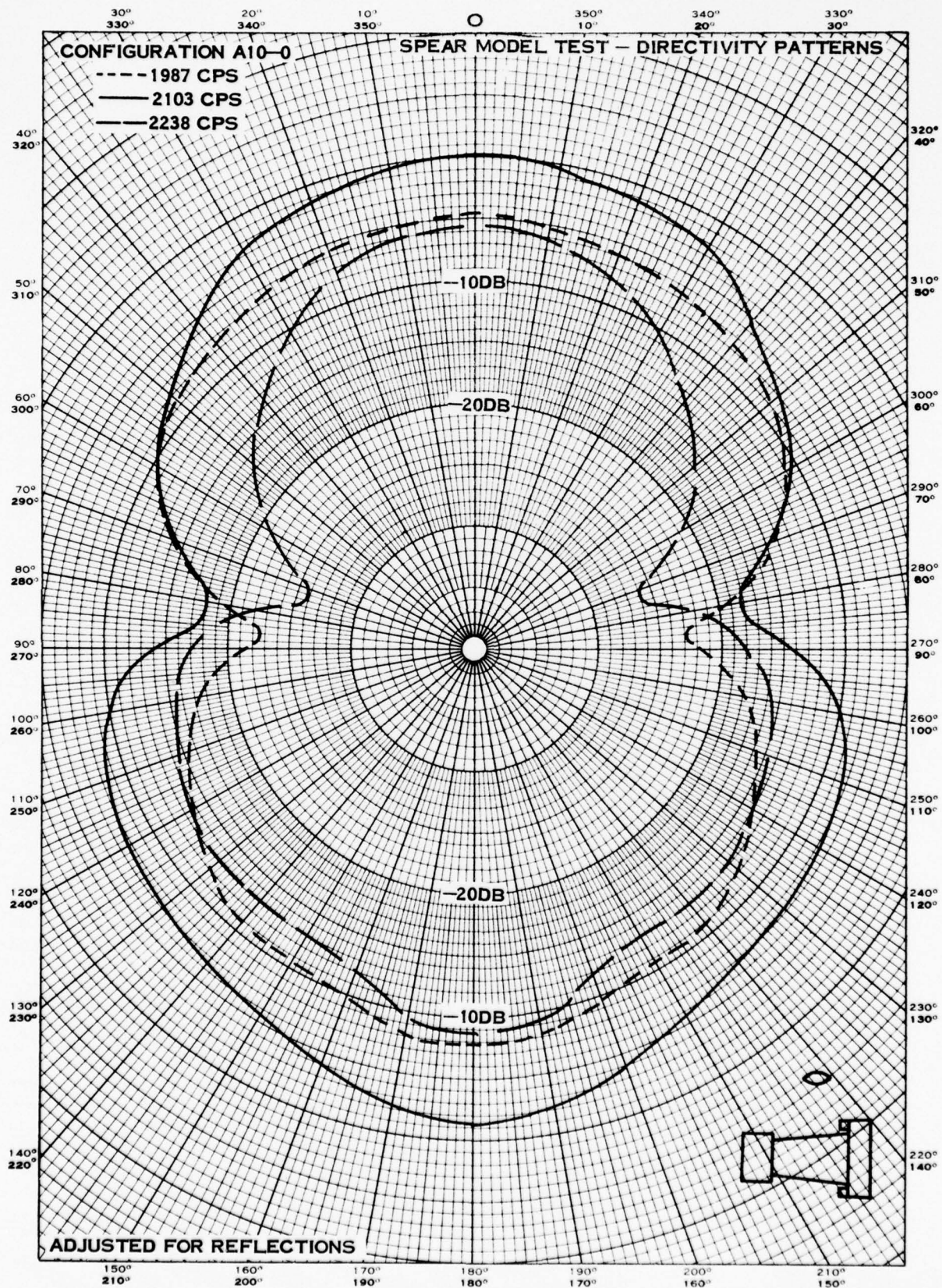


FIGURE C-38

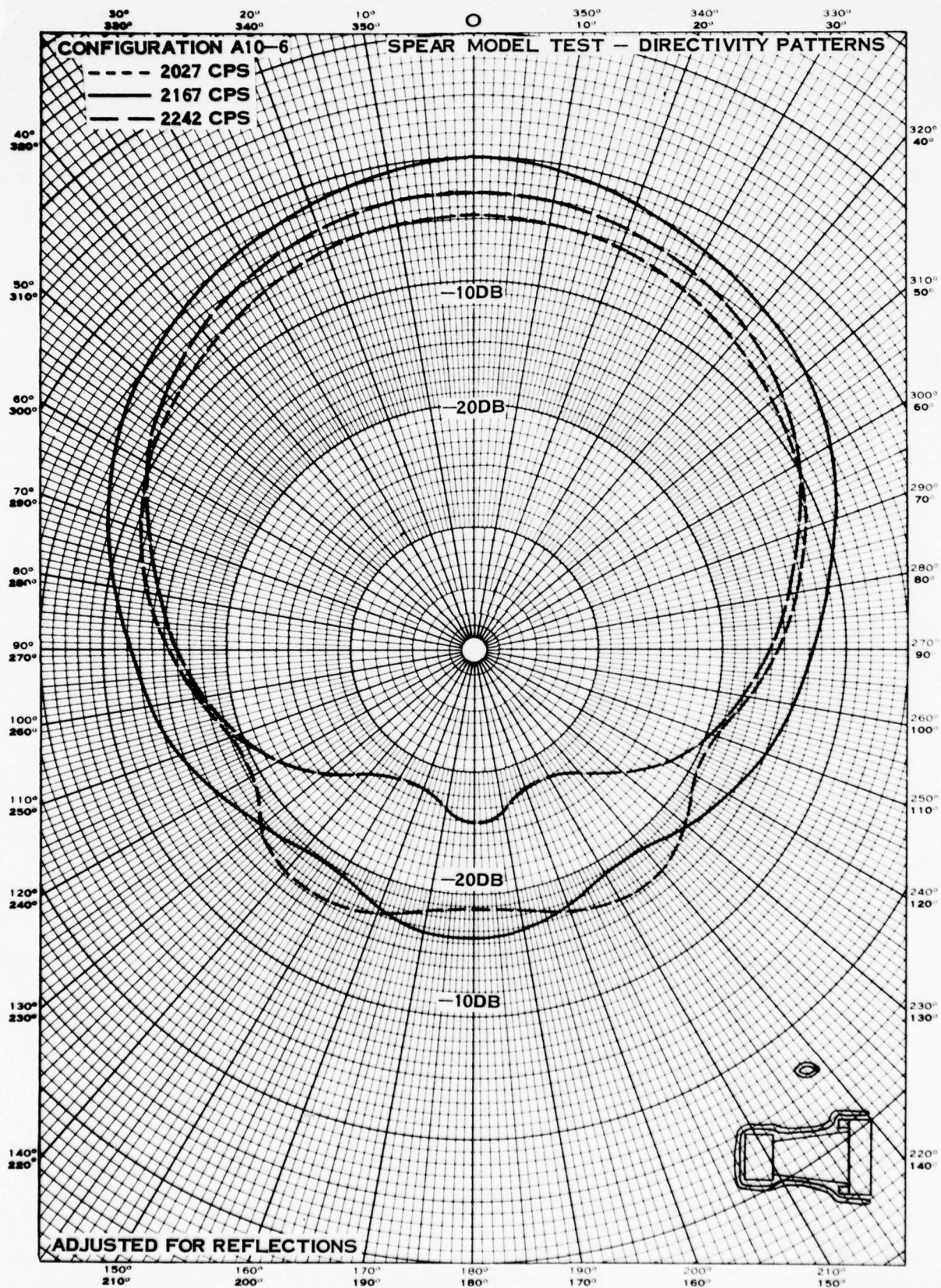
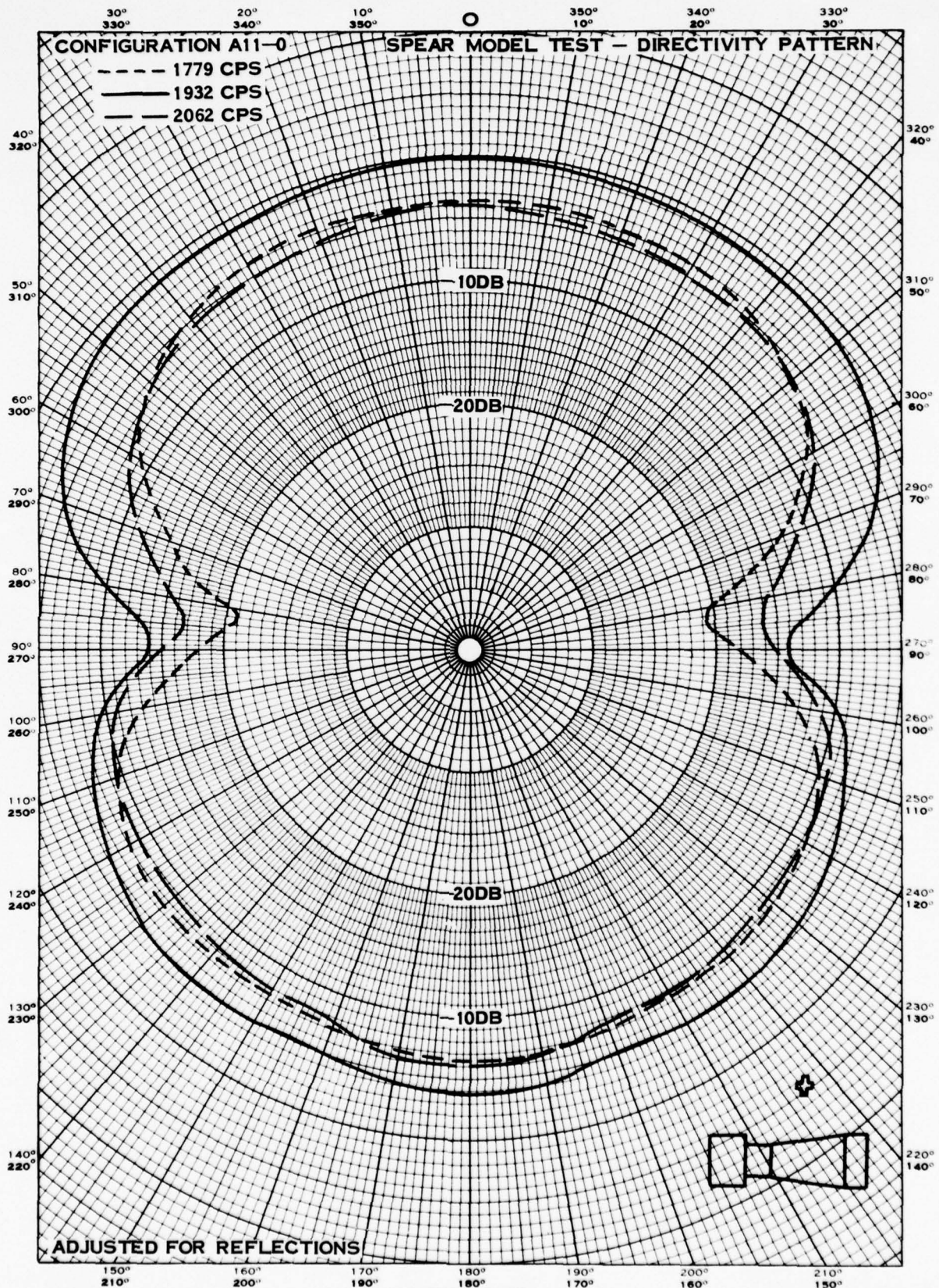


FIGURE C-39





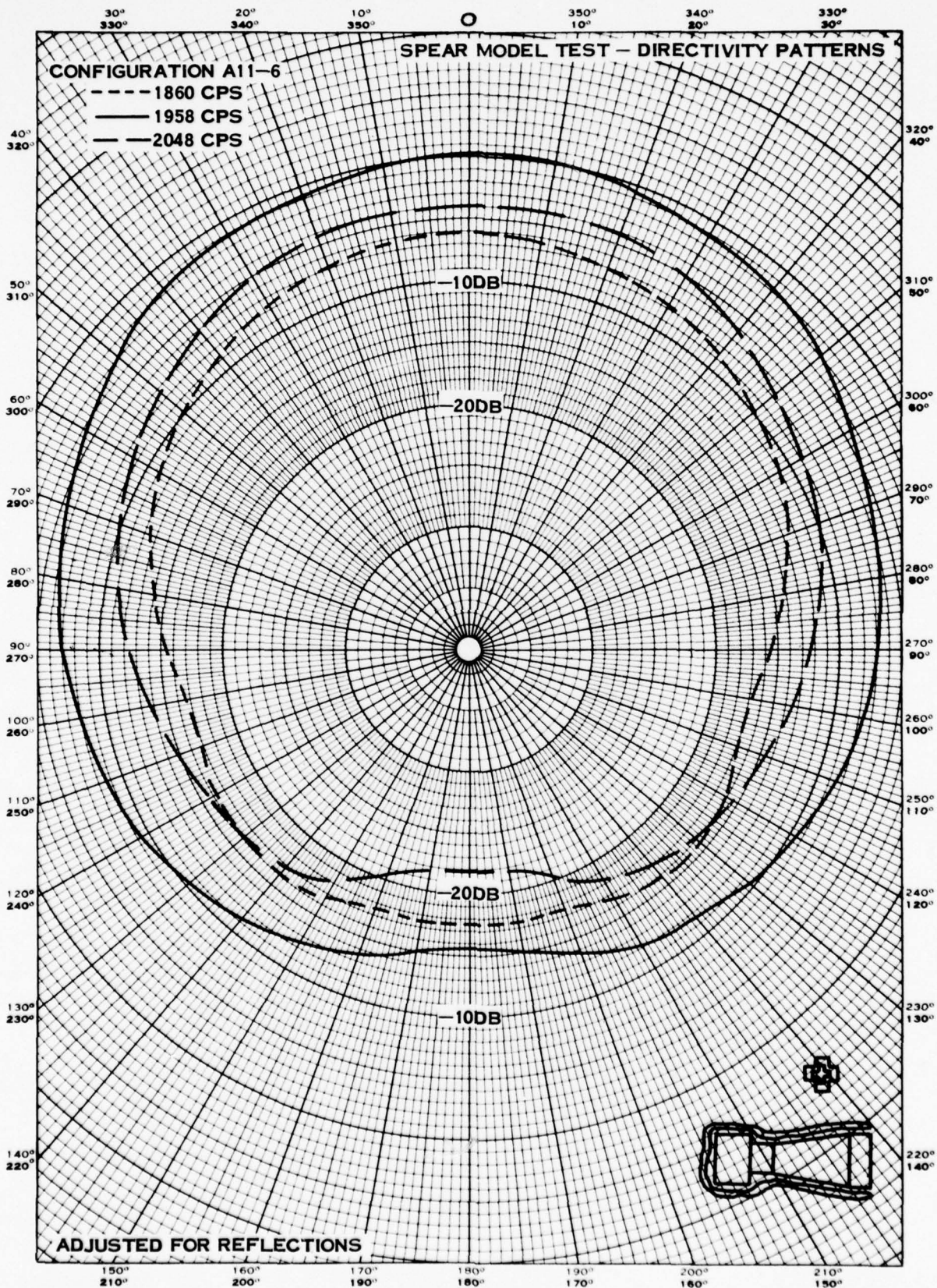
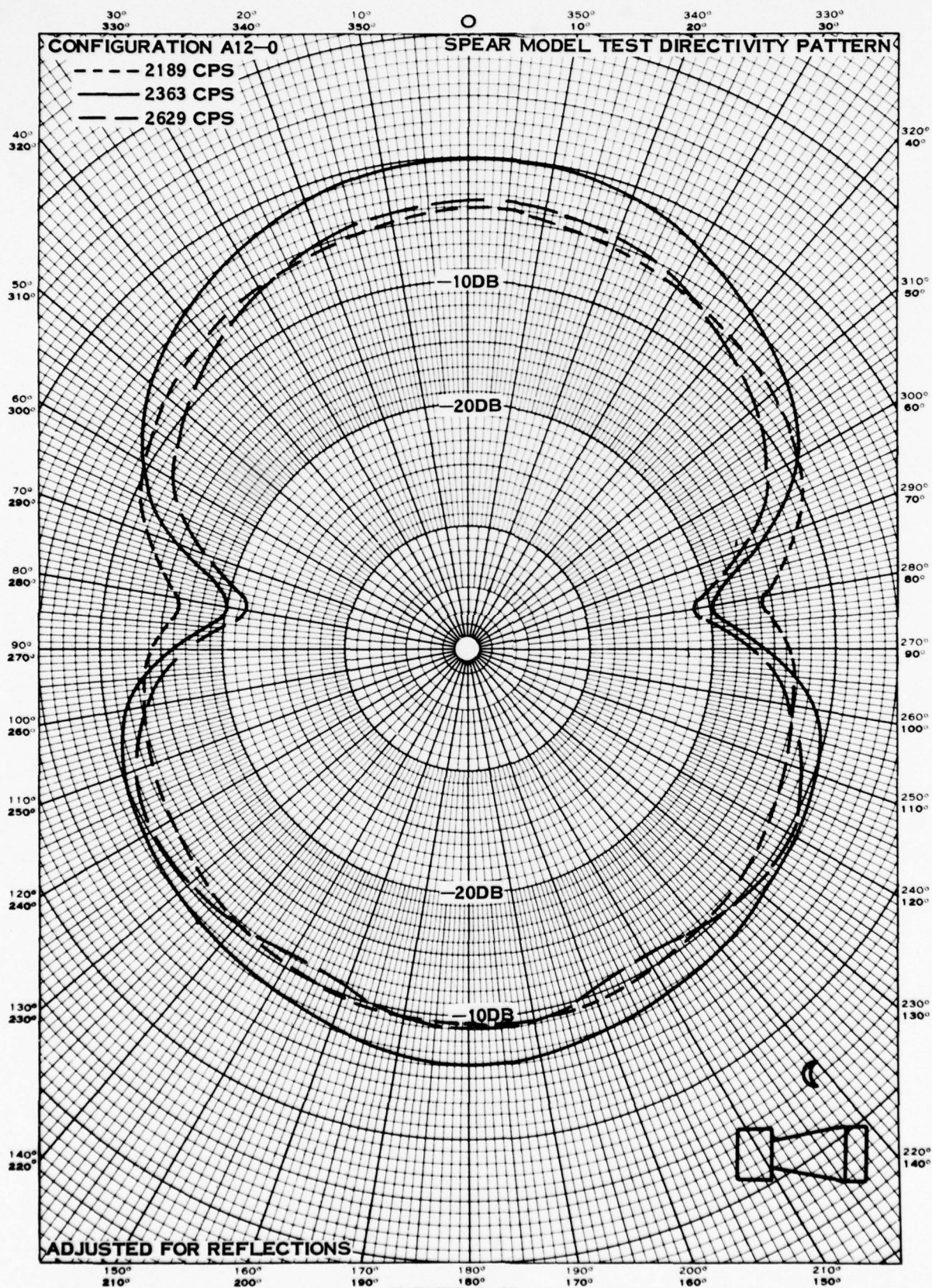


FIGURE C-41





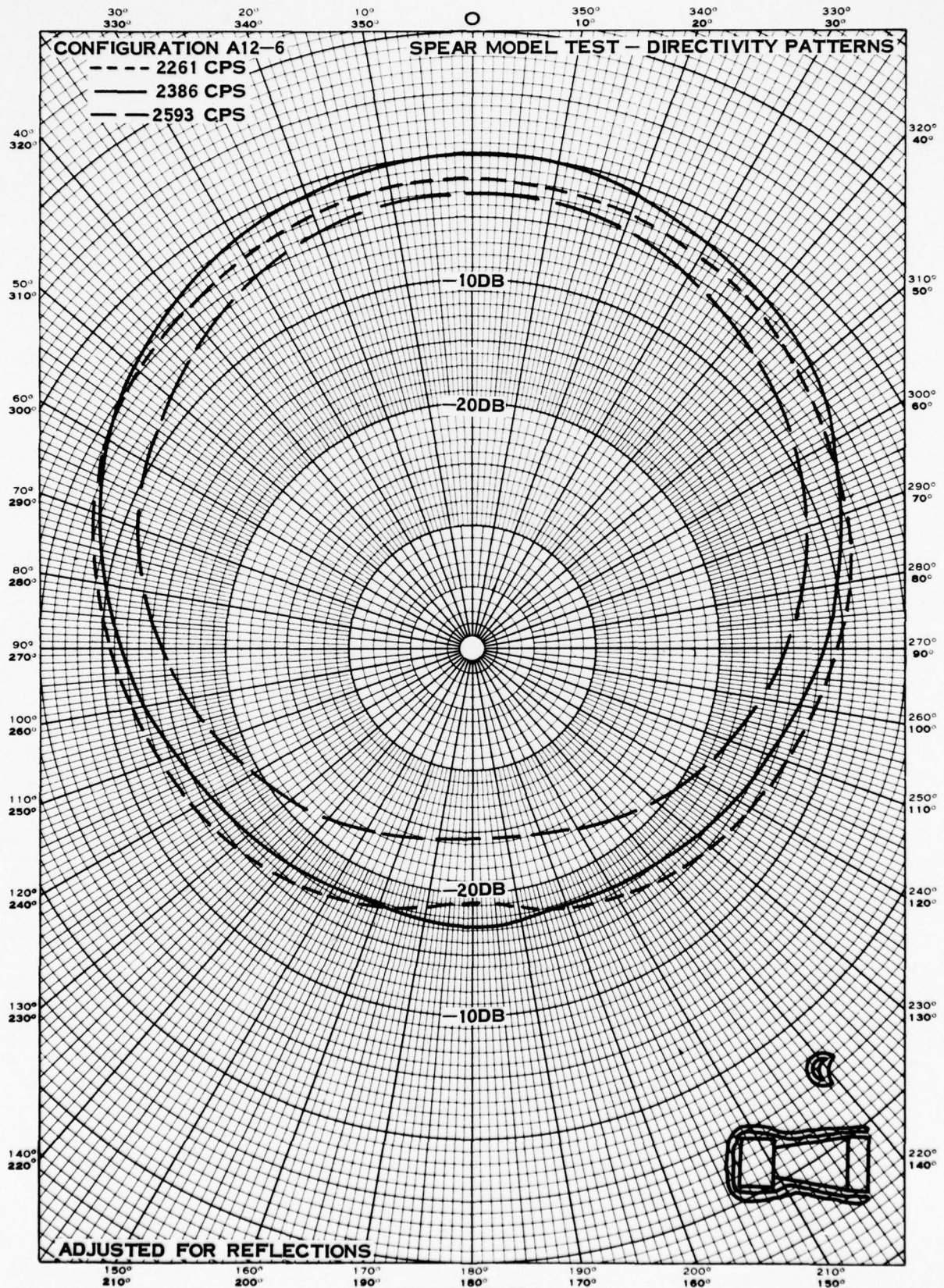


FIGURE C-43



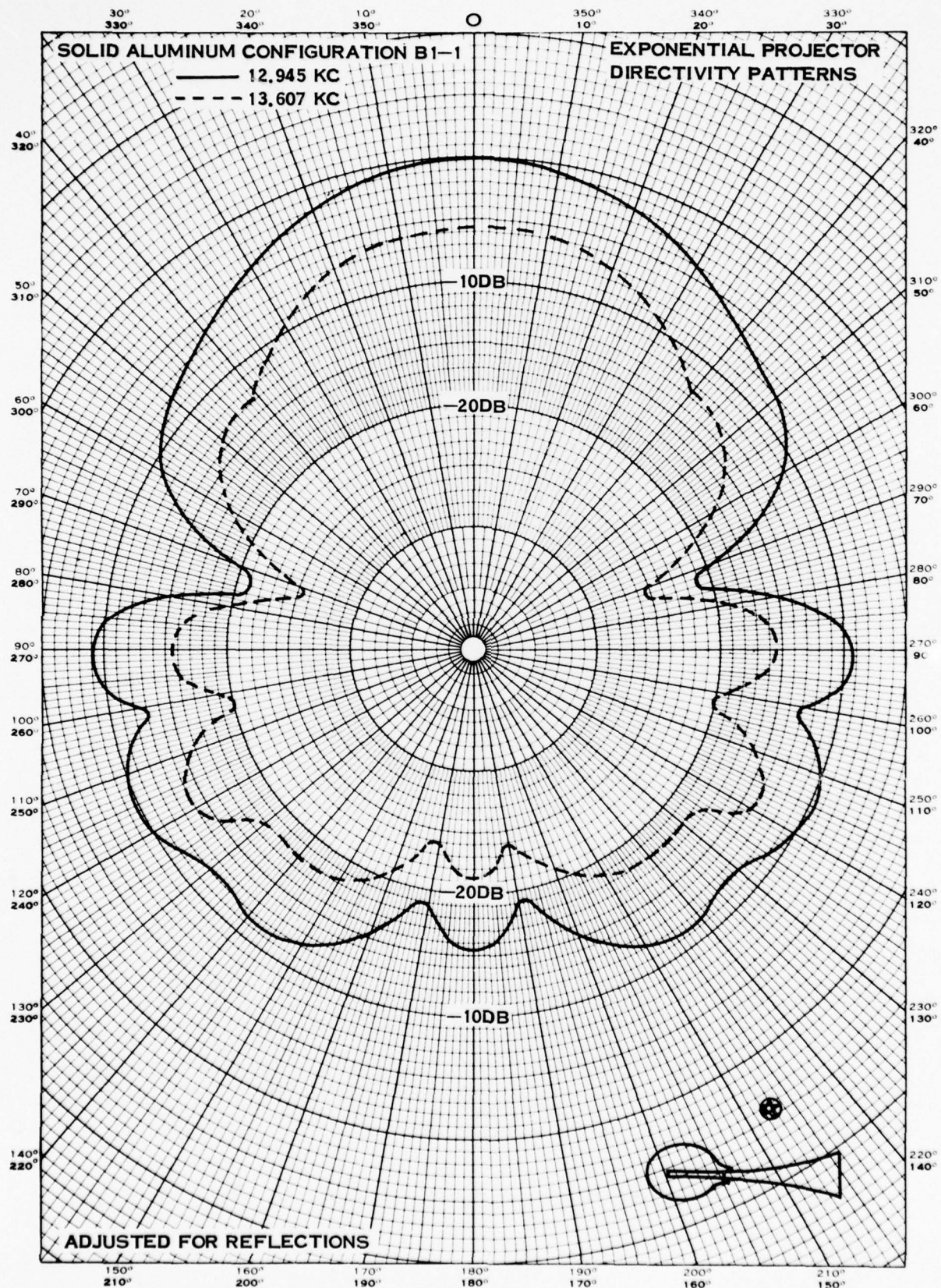
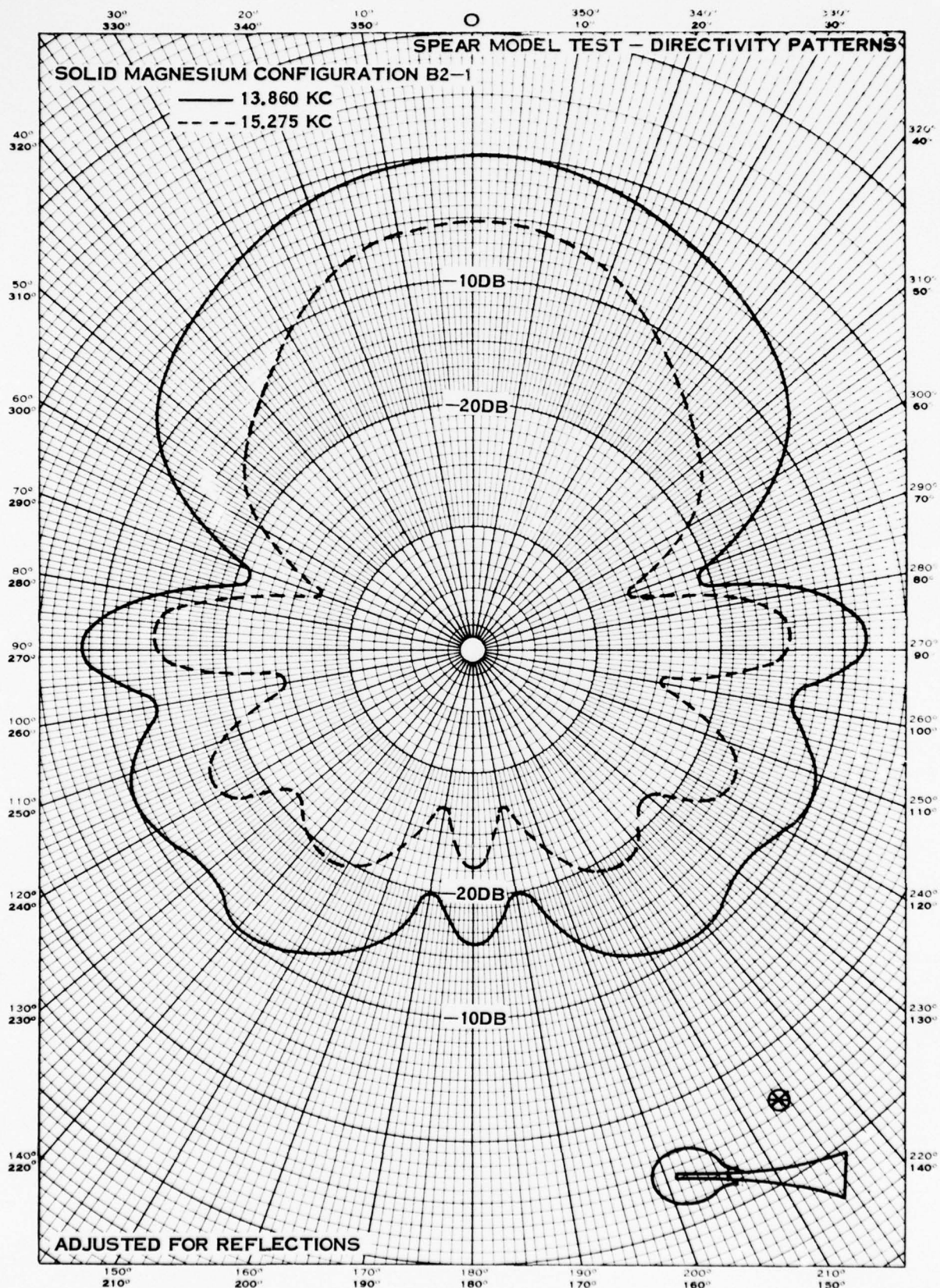


FIGURE C-44





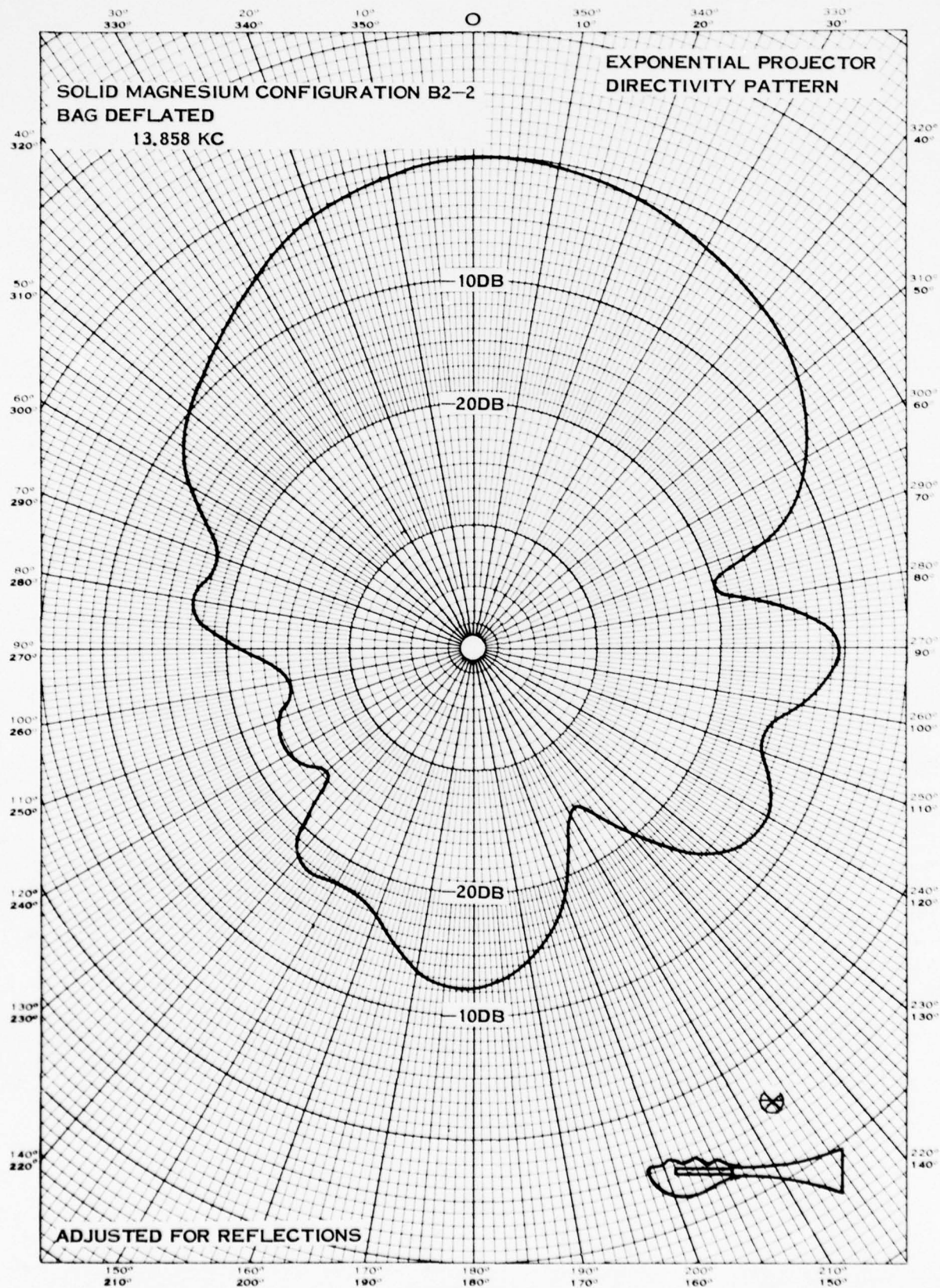
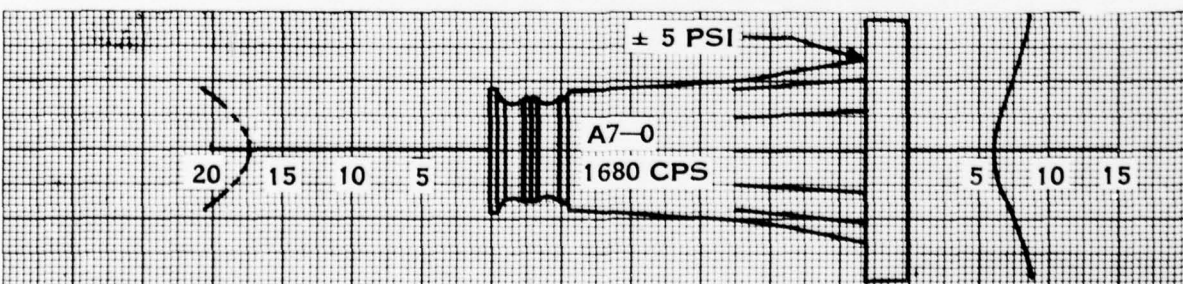
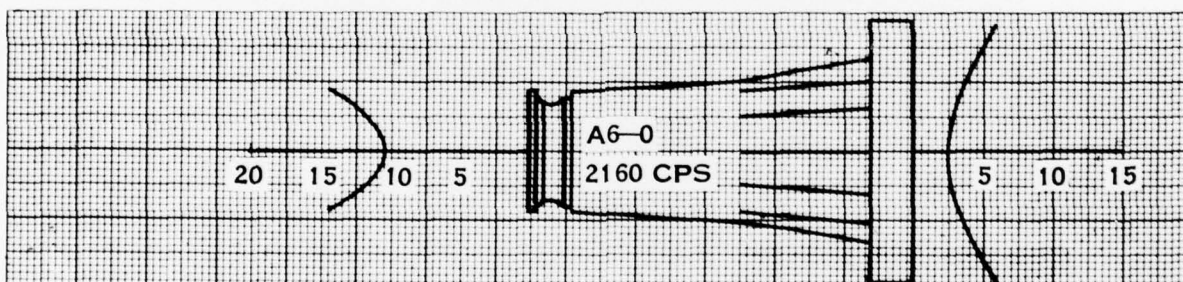
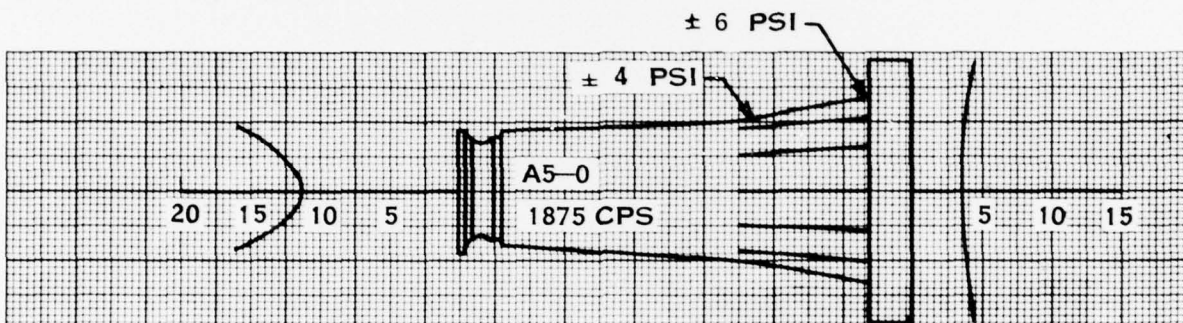
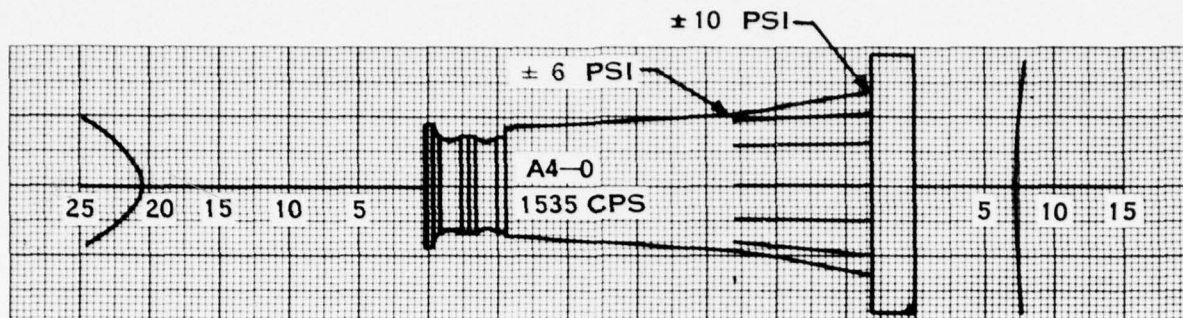


FIGURE C-46

ADAPTER DISPLACEMENT:  $\pm$  MICROINCHES



PISTON DISPLACEMENT:  $\pm$  MICROINCHES

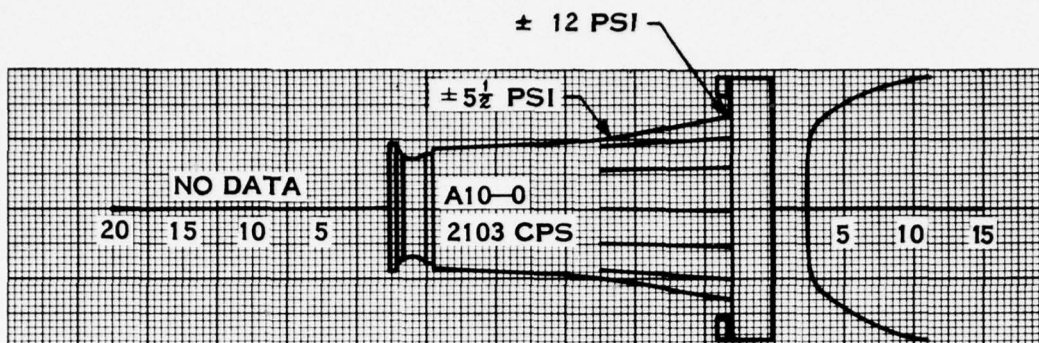
ALL DATA ARE FOR RESONANCE  
AMPLITUDES ARE REFERRED TO 1 AMPERE EXCITATION

SPEAR MODEL TEST  
DISPLACEMENTS AND STRESSES  
PRIMARY CONFIGURATIONS

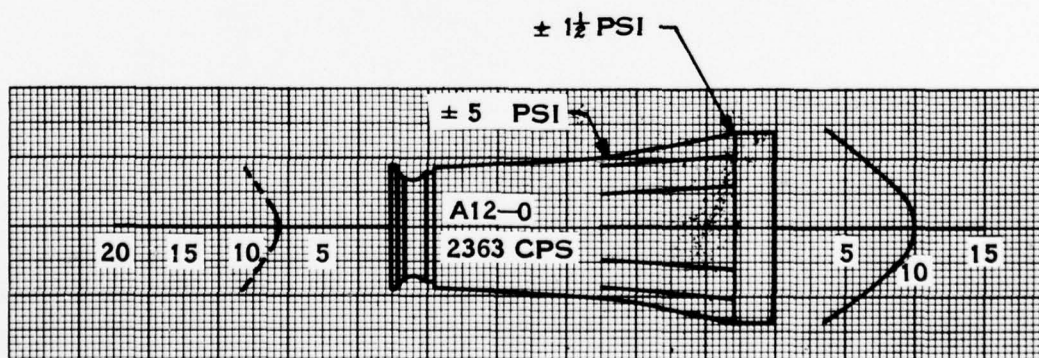
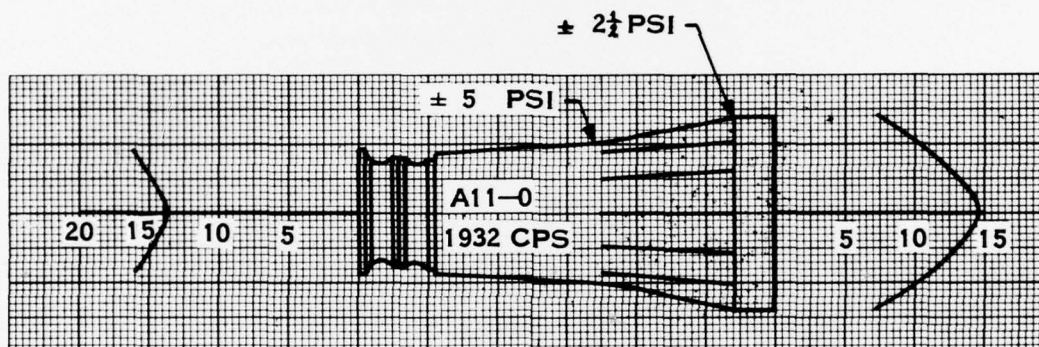
FIGURE C-47



ADAPTER DISPLACEMENT:  $\pm$  MICROINCHES



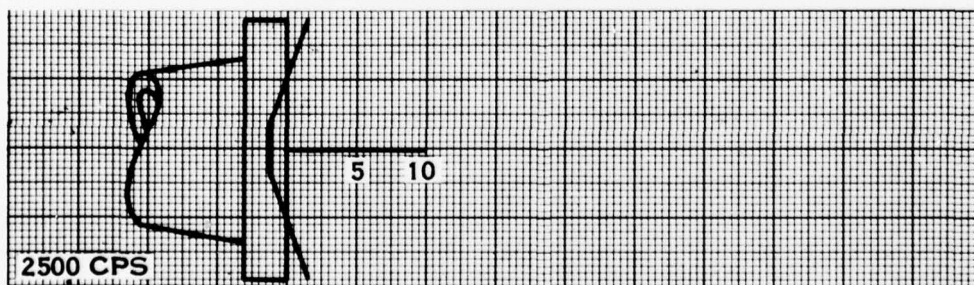
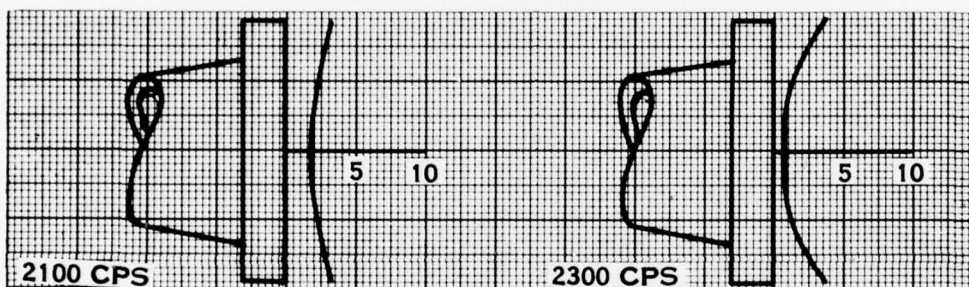
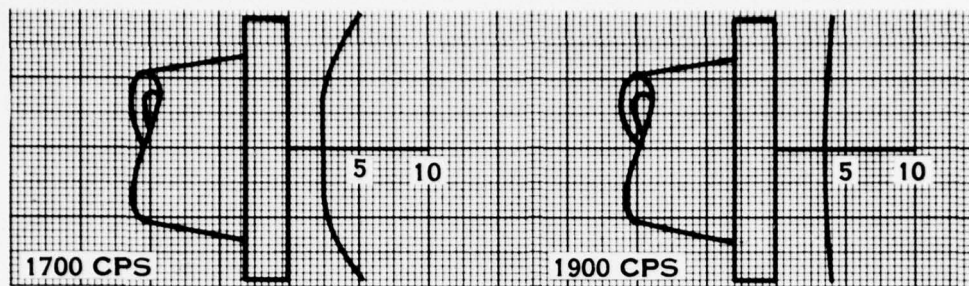
PISTON DISPLACEMENT:  $\pm$  MICROINCHES



ALL DATA ARE FOR RESONANCE  
AMPLITUDES ARE REFERRED TO 1 AMPERE EXCITATION

SPEAR MODEL TEST  
DISPLACEMENTS AND STRESSES  
SECONDARY CONFIGURATIONS

FIGURE C-48



PISTON DISPLACEMENT:  $\pm$  MICROINCHES

AMPLITUDES ARE REFERRED TO 1 AMPERE EXCITATION

SPEAR MODEL TEST  
PISTON DISPLACEMENT VS  
FREQUENCY  
CONFIGURATION A5-0 ONLY

FIGURE C-49



## APPENDIX D

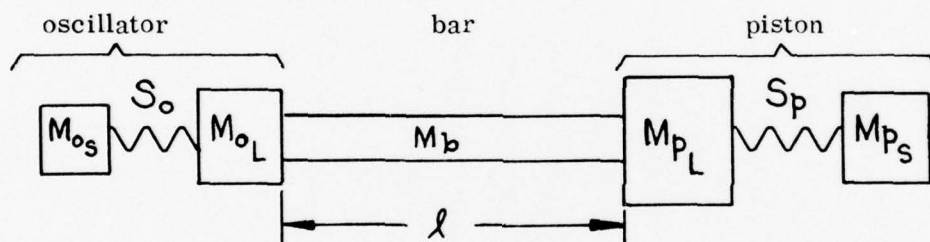
### ANALYSES

<u>Section</u>	<u>Title</u>
D-I	Natural Frequency Calculations
D-II	Reactive Impedance Calculations from Frequency Shift Upon Immersion
D-III	The Calculation of Resistive Impedance from Test Data
D-IV	Impedance of a Nonrigid Piston
D-V	Theoretical Study of the Effect of Bar Taper
D-VI	The Effect of Rear Surface Motion on the Directivity Pattern

## APPENDIX D-I

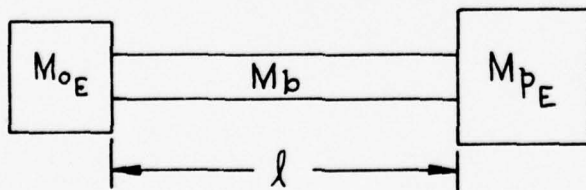
### NATURAL FREQUENCY CALCULATIONS

When it was found that frequency analyses of the SPEAR vibratory system, with the oscillator and piston considered as lumped masses, did not correlate well with observed natural frequencies, the first attempt to improve the correlation was to represent the oscillator hardware (the exciter adapter and the spacer) as axially flexible extensions of the bar. This approach was not productive, so it was felt that secondary bending actions of the oscillator and the piston were causing an increase in the effective masses of these items. The mathematical model then established to represent the system, which did produce good correlation, was the following:



Subscripts: L = attached to the bar  
 s = attached to spring S  
 o = oscillator  
 p = piston

This representation was simplified to the following configuration, in which the mass-spring systems on each end were replaced by equivalent masses:



Each of the equivalent masses had a magnitude which is a function of frequency according to the relationship

$$M_E = M_L + \frac{M_s}{1 - (f^2 M_s / S)}$$

The expression describing the natural frequency of the simplified mass-bar-mass system is

$$\tan k\ell = \frac{\frac{M_b}{k\ell} (M_{oE} + M_{pE})}{M_{oE} M_{pE} - \left(\frac{M_b}{k\ell}\right)^2} \quad \text{where } k = 2\pi f/c$$

With these basic relationships, the several configurations of oscillator and piston were broken down into attached and sprung portions for each component which were generally consistent with the geometry and were so sized as to produce the best agreement with the observed natural frequencies in air for all configurations tested. Fifteen different combinations of oscillator type, spacer, bar length, piston diameter, and piston rim weights were tested in air; the agreement of computed frequency with observed frequency was generally within 1% and at the worst about 2%.

## APPENDIX D-II

### REACTIVE IMPEDANCE CALCULATIONS FROM FREQUENCY SHIFT UPON IMMERSION

For each of the configurations tested in water, the effective mass of piston plus water required to give the observed resonant frequency was computed from the expressions given in the preceding section. Then by extracting the piston from the total effective mass, the contribution of the water was determined; this led to the reactive mass of the water, i.e., the accretion to mass of the piston in the water. This determination involved the assumption that the water mass ( $M_w$ ) was distributed in two portions, one attached to the bar, the other attached to the spring, in the same proportion as the piston mass itself.

Since the Mechanical Reactance ( $X_m$ ) is a function of water mass and frequency,

$$X_m = 2 \pi f M_w$$

and the dimensionless reactive impedance is

$$X_i = X_m / \pi a^2 \rho c$$

where  $\pi a^2$  is the piston area and  $\rho c$  is the specific impedance of the water, then  $X_i$  was computed from

$$X_i = 2 \pi f / a^2 \rho c .$$



### APPENDIX D-III

#### THE CALCULATION OF RESISTIVE IMPEDANCE FROM TEST DATA

The element of acoustic power ( $\Delta W$ ) radiated through an increment of co-latitude angle ( $\phi$ ) with an elemental area ( $\Delta A$ ), is

$$\Delta W = \frac{p_\phi^2}{\rho c} \Delta A$$

where  $p_\phi$  is the acoustic pressure and  $\rho c$  is the specific impedance. Since the pressure is a function of the Sound Pressure Level (SPL) and the reference pressure (1 dyne/cm<sup>2</sup>), then

$$p_\phi^2 = 10^{\frac{\text{SPL}_\phi}{10}}$$

and the expression for  $\Delta W$  becomes

$$\Delta W = \left( \frac{\Delta A}{\rho c} \right) 10^{\frac{\text{SPL}_\phi}{10}}$$

Then, introducing a factor  $f(\phi)$  to properly weight the element of spherical surface associated with an increment of the angle  $\phi$ ,

$$\Delta W = \frac{2\pi r^2}{\rho c} f(\phi) 10^{\frac{\text{SPL}_\phi}{10}}$$

so that the summation of total power ( $W$ ) becomes

$$W = \frac{2\pi r^2}{\rho c} \sum f(\phi) 10^{\frac{\text{SPL}_\phi}{10}}$$

Now, defining  $\text{SPL}_{\text{ref}}$  as the SPL at one yard from a point source of one watt:

$$\text{SPL}_{\text{ref}} = 10 \log \frac{\rho c}{4\pi(3\text{ft})^2} = 71.4 \text{ db}$$

and using the definitions of Directivity Index (DI) and Source Level ( $S_o$ )

$$\text{DI} = \text{SPL}_o - \text{SPL}_{\text{ave}} = S_o - \text{SPL}_{\text{ave at one yard}}$$

Then, the relationship of power to Source Level and Directivity Index is

$$\begin{aligned}
 10 \log W &= \text{SPL}_{\text{ave at one yard}} - \text{SPL}_{\text{ref}} \\
 &= S_o - 71.4 - \text{DI} \\
 W &= (10)^{\frac{S_o - 71.4 - \text{DI}}{10}}
 \end{aligned}$$

The source level of each configuration was determined directly from the transmitting response test data. Directivity Index was computed from the directivity patterns using the equations above and summing the power over discrete intervals of  $\phi$ .

The radiated power is related to the piston velocity ( $\dot{u}$ ) and the mechanical resistance ( $R_m$ ), which itself is a function of the dimensionless resistive impedance ( $R_i$ ), the specific impedance, and the piston area ( $\pi a^2$ ):

$$\begin{aligned}
 W &= 1/2 R_m \dot{u}^2 \\
 R_m &= \rho c \pi a^2 R_i
 \end{aligned}$$

Now, since the test data gave piston acceleration ( $\ddot{u}$ ) not velocity directly, and

$$\begin{aligned}
 u &= 2 \pi f \dot{u} \\
 \text{Then } W &= \frac{R_i \rho c a^2}{8 \pi} \left( \frac{\ddot{u}}{f} \right)^2 = (10)^{\frac{S_o - 71.4 - \text{DI}}{10}}
 \end{aligned}$$

$$\text{or } R_i = \frac{8 \pi}{\rho c a^2} \left( \frac{f}{\ddot{u}} \right)^2 (10)^{\frac{S_o - 71.4 - \text{DI}}{10}}$$

From this expression, using the average piston acceleration, the observed frequency and source level, and the computed Directivity Index, the dimensionless resistive impedance for each test condition was calculated.

## APPENDIX D-IV

### IMPEDANCE OF A NONRIGID PISTON

It was realized early in the SPEAR program that treatment of the piston of the projector as a perfectly rigid body in estimations of its acoustic characteristics constituted a justifiable approximation in view of the thickness of the piston disc. Whatever bending deflections the piston actually underwent were, from this point of view, spurious effects. The question presents itself, however, as to whether these inherent bending oscillations might be utilized in some manner to improve certain operating characteristics of the projector. What follows is an attempt to formulate a theoretical basis for estimating the effect of varying the piston deformation upon the Quality Factor of the projector. The theory is based upon some comments and suggestions of Dr. M. C. Junger of Cambridge Acoustical Associates. Two simple parabolic mode shapes for the deformation are assumed: a "cupping" mode for which the radiating surface of the piston is concave and a "bulging" mode for which it is convex.

Consider the "cupping" configuration. Let the total displacement of the piston surface at a distance  $r$  from its center be  $x = d + \xi$  where  $d$  is the rigid body displacement of the piston measured from its equilibrium position to the center of the disc and  $\xi$  is the deflection due to bending relative to the center. If the rigid body displacement is simple harmonic, it can be expressed as  $d = d_0 e^{i\omega t}$  where  $d_0$  is the maximum rigid displacement. For a simple harmonic deflection of parabolic shape, the bending deflection can be written  $\xi = \delta_0 (r/a)^2 e^{i(\omega t - \beta)}$  where  $\delta_0$  is the maximum bending deflection of the edge of the disc relative to its center,  $a$  is the radius of the disc and  $\beta$  is the phase angle (as yet undetermined) between the rigid body and bending motions. It will be convenient to rewrite this in terms of another arbitrary phase angle  $\phi$  defined by  $e^{-i\beta} = i e^{-i\phi}$  as  $\xi = -i \delta_0 (r/a)^2 e^{i(\omega t - \phi)}$ . (The assumption of a parabolic mode shape is suggested by the fact that this is a fairly good approximation to the actual shape of the lowest vibrational mode of an unsupported disc with a free edge.) The total displacement will be  $x = d_0 [1 + \alpha (r/a)^2] e^{i\omega t}$  where  $\alpha = -i(\delta_0/d_0) e^{-i\phi}$  is the relative bending deflection normalized to the rigid body displacement. Since the rigid body velocity is  $V_0 = i\omega d_0 e^{i\omega t}$  the total velocity  $v = v_0 [1 + \alpha (r/a)^2]$  and the maximum total displacement  $x_m = d_0 [1 + \alpha (r/a)^2]$  follow directly. If  $\alpha > 0$  the mode has a "cupping" shape, while if  $\alpha < 0$  it has a "bulging" shape.

Treating the piston as a "free disc" the effect of the water load in actually determining the bending deflections is neglected, the shape of the piston surface being prescribed. The radiation impedance can then be estimated by the usual "piston theory" procedure of considering each point of the piston face to act as a source of spherical waves (Huyghen's principle) and then integrating overall elemental source areas  $dS$  to obtain the total pressure on an element of area  $dS'$ . Integration over

$dS'$  then gives the total force on the piston due to its own radiation and division by the "volume current" (the integral over the piston surface of the product of local velocity and area) gives the radiation impedance. Thus, the force on the piston is

$$f = K e^{i\omega t} \int dS' \int v(\kappa') \frac{1}{\kappa'} e^{-ik\kappa'} dS$$

where  $K$  is a constant and  $k = \omega/c$  ( $c$  is sonic velocity).

So the impedance  $Z$  is  $Z = \frac{F_d + \alpha F_\xi}{2\pi \int_0^a v(\kappa) \kappa d\kappa}$  where

$$F_d = KV_0 e^{i\omega t} \int dS' \int e^{-ik\kappa'} \frac{dS}{\kappa'} \quad \text{and} \quad F_\xi = KV_0 \alpha e^{i\omega t} \int dS' \int \left(\frac{\kappa'}{a}\right)^2 e^{-ik\kappa'} \frac{dS}{\kappa'}$$

If the rigid displacement is much larger than the bending deflection, then  $\delta_0 \ll d_0$

so  $Z \sim (2\pi a^2 V_0)^{-1} (F_d + \alpha F_\xi)$  which can be split into real and imaginary (resistive and reactive) components as  $Z = R + iX$  where  $R = R_d + \alpha R_\xi$  and  $X = X_d + \alpha X_\xi$  in terms of  $Z_d = R_d + iX_d$  and  $Z_\xi = R_\xi + iX_\xi$ . It is clear, therefore, that both the resistance and reactance are increased if  $\alpha$  is positive and decreased if it is negative. The additional impedance due to deflection is less in the "cupping" case than in the "bulging" case because in the "cupping" case the largest deflectional motion occurs near the edge of the disc where the edge itself provides a pressure release, since the pressure increments on the front and rear surfaces are of opposite sign and cancel wherever they are in contact, while in the "bulging" case the largest deflectional motion occurs at the center where it is shielded from cancellation by the entire piston surface. Since the impedance is proportional to the force exerted by the fluid on the piston, the "bulging" case must correspond to the larger impedance.

The relationship between the "cupping" or "bulging" of the piston and the manner of driving it is rather nebulous due to the complexity of the mutual interaction between the elastic flexure of the piston and the combination of driving force and acoustic reaction acting upon it. Some idea of the general effect of this interaction can be obtained by considering the vibrating disc to be approximately represented by a one-dimensional harmonic oscillator having an "equivalent" effective mass  $m_e$ , an "effective" stiffness constant  $S$  and a damping coefficient  $R_0$ . Since the piston mode has been assumed to be parabolic, all points of the piston face move in phase in the deformation mode and so the shape of the piston at any time is determined by a quantity  $\xi_0(t)$  where  $\xi = (a^2/\delta_0 \kappa^2) \xi$ . This analytical device is usually used to estimate the resonant frequency of a vibrating membrane and certainly represents a



drastic oversimplification for thick plates. Means of obtaining  $m_e$ ,  $S$  and  $R_o$  for circular membranes of parabolic mode shape have been devised based upon estimating the maximum kinetic energy and maximum potential energy. The actual values of these quantities in the present instance are somewhat immaterial since the objective is merely to show the phase relationship between the driving force and the bending oscillations and all that is required is that the concept of "one-dimensionalizing" the system have some validity. As the force driving the bending oscillations arises from inertial mass of the piston and from the reactive (inertial) part of the radiation impedance due to the rigid body oscillations, it will be in phase with the rigid body displacement and can therefore be written  $F = F_o e^{i\omega t}$ . So the equation of motion of the "one-dimensionalized" piston is

$$m_e (d^2 \xi_o / dt^2) + R_o (d \xi_o / dt) + S \xi_o = F_o e^{i\omega t}$$

This has the steady state solution  $\xi_o = -i F_o (\omega Z)^{-1} e^{i(\omega t - \phi)}$  where

$Z$  is the bending impedance  $Z = [R_o^2 + (\omega m_e - \frac{S}{\omega})^2]^{1/2}$  and

$\phi$  is  $\phi = \arctan \frac{\omega^2 m_e - S}{\omega R_o}$  Since the resonant angular frequency  $\omega_R = (S/m_e)^{1/2}$

this is  $\phi = \arctan \frac{m_e(\omega^2 - \omega_R^2)}{\omega R_o}$  Now if  $\omega > \omega_R$  then the argument of the arctan is

positive so  $\phi > 0$ . If  $\omega < \omega_R$  the argument is negative so that  $\phi < 0$ . Since  $\alpha$  is proportional to  $\sin \phi$  it follows that for driving frequencies just below the resonant frequency  $\alpha$  will be positive and the mode will be cupping, while just above resonance  $\alpha$  will be negative and the mode will be bulging. These considerations apply specifically to the case of a piston attached at its center to a driving rod since the rigid body displacement is measured from the equilibrium position to the base of the cup. In the case of a piston attached at its edge to a hollow cylinder, the rigid body displacement would have to be measured to the plane of the edge of the bulged piston. The bending displacement would then be of the form  $\xi = \xi_o [1 - \delta_o (r/a)^2] e^{i(\omega t - \beta)}$  and due to the negative sign, the previous relationship between  $\alpha$  and  $\omega$  would be reversed:

$\alpha$  would be negative for frequencies below  $\omega_R$  and positive for frequencies above  $\omega_R$ .

Since, in a practical case, the  $Q$  of the system  $Q = R^{-1}(\omega m_e + Z)$  is  $> 1$ , the numerator of  $Q$  is larger than the denominator.  $Q$  will therefore be reduced if the same positive quantity is added to both numerator and denominator. Since  $\alpha$  is positive if the piston is driven just below its natural frequency and it has been shown by M. Junger (private letter) that for SPEAR the numerical values of  $R \xi$  and  $Z \xi$  (the coefficients multiplying  $\alpha$ ) are nearly equal, driving the piston close to but just below resonance should lower  $Q$ . But the driving frequency is usually much lower than

the resonant frequency for bending vibrations so that the effect on  $Q$  will be negligible. In order to obtain a significant decrease in  $Q$ , the piston resonance frequency must be brought closer to the driving frequency. The effective mass of the piston is the sum of its static mass  $M_s$  and an additional  $M_a$  due to its motion  $M_e = M_s + M_a$ . Lowering the natural frequency increases  $M_a$ , however, so that in order to reduce  $Q$  by lowering the natural frequency (without increasing the effective mass) the static mass of the piston must be reduced.

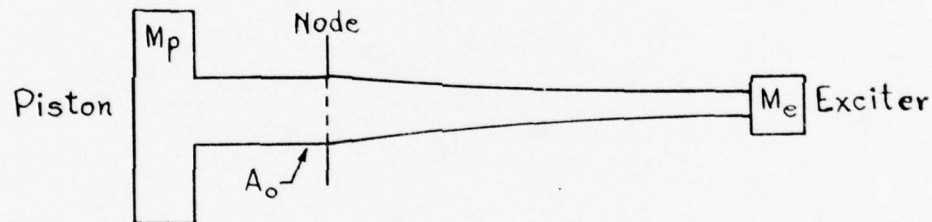
## APPENDIX D-V

### THEORETICAL STUDY OF THE EFFECT OF BAR TAPER

In connection with the design and development of the SPEAR Sonar Device, it was desired to determine whether the use of a variable area bar could enhance the operating characteristics of a SPEAR type unit. To do this, it was decided to study a device which was exactly the same as the SPEAR unit on the piston side of the node, but had a variable area bar from the node to the exciter. In order to simplify the mathematics involved and still be able to study considerable shape variation, an exponential type area variation was selected. The three parameters which were considered pertinent to the quality of a SPEAR device were exciter amplitude, weight and quality factor.

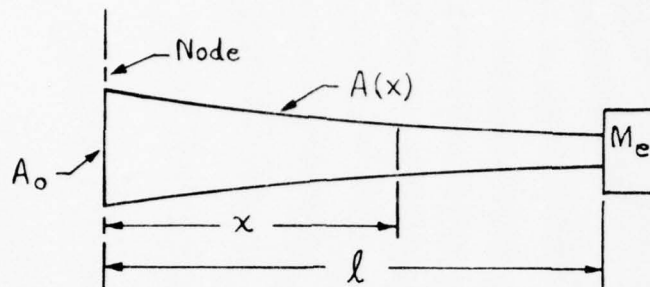
#### I. General Analysis

The system to be analyzed is schematically shown below.



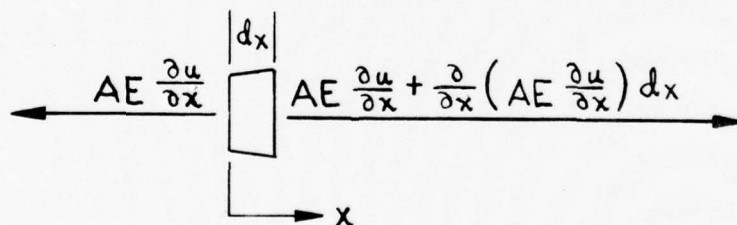
No attempt has been made to show the actual configuration details such as whether or not the bar is hollow, since this will not affect the basic analysis. The system consists of a rigid piston of mass  $M_p$  connected to a bar of constant area  $A_0$  which extends to the node, from which an exponential bar extends to a rigid exciter mass  $M_e$ . For this analysis, the system will be assumed to be conservative, i.e., no internal or external damping, since it has been shown in the past that a non-conservative analysis adds very little to the accuracy of the results and is extremely complicated.

For analysis purposes, the total system can be reduced to components similar to that shown below, where an exponential bar extends from a node to a rigid mass  $M_e$ .



Having a general analysis for this system, the system which exists from the node to the piston is a degenerate case where the bar has a constant area and the rigid end mass is the piston.

From the forces acting on an element of a variable area bar as shown below and Hookes law,



the resulting differential equation of motion is:

$$\frac{\partial}{\partial x} \left( AE \frac{\partial u}{\partial x} \right) = \rho A(x) \frac{\partial^2 u}{\partial t^2} \quad (1)$$

where  $x$  is the coordinate along the bar,  $A(x)$  is the cross sectional area as a function of  $x$ ,  $E$  is the material modulus of elasticity,  $\rho$  the material mass density and  $u$  the displacement of the bar at  $x$  in the  $x$  direction. Assuming a solution for  $u$  of

$$u = X \sin \omega t \quad (2)$$



where  $X$  is an unknown function of  $x$  only and  $\omega$  is the circular natural frequency of the system, and substituting into the differential equation of motion, the governing equation for  $X$  is:

$$\frac{d^2 X}{dx^2} + \frac{1}{A} \frac{dA}{dx} \frac{dX}{dx} + \left(\frac{\rho}{c}\right)^2 X = 0 \quad (3)$$

where

$$c = \sqrt{\frac{E}{\rho}}$$

It should be noted here that  $c$  is the customary value for the speed of sound in a thin elastic bar. Letting

$$A = A_0 e^{2\alpha x} \quad (4)$$

the governing equation for  $X$  becomes

$$\frac{d^2 X}{dx^2} + 2\alpha \frac{dX}{dx} + \left(\frac{\rho}{c}\right)^2 X = 0 \quad (5)$$

The solution of this equation is

$$X = e^{-\alpha x} \left[ C_1 \sin \sqrt{1-\psi^2} \frac{\omega x}{c} + C_2 \cos \sqrt{1-\psi^2} \frac{\omega x}{c} \right], \quad \psi^2 < 1 \quad (6)$$

where

$$\psi = \frac{\alpha c}{\omega} \quad (7)$$

$C_1$  and  $C_2$  are arbitrary constants to be determined from the boundary conditions and  $\psi^2$  is less than one. This limitation on  $\psi^2$  will be discussed later in the text. Thus Equation 2 for  $u$  becomes,

$$u = e^{-\alpha x} \left[ C_1 \sin \sqrt{1-\psi^2} \frac{\omega x}{c} + C_2 \cos \sqrt{1-\psi^2} \frac{\omega x}{c} \right] \sin \omega t \quad (8)$$

The appropriate boundary conditions for the bar being considered are:

$$\begin{aligned} \text{For all values of } t, \text{ at } x = 0, \quad (u)_{x=0} &= 0 \\ \text{For all values of } t, \text{ at } x = l, \quad \left(\frac{\partial u}{\partial x}\right)_{x=l} &= \frac{-Me}{(A)_l E} \left(\frac{\partial^2 u}{\partial t^2}\right)_l \end{aligned} \quad (9)$$

Substituting the first of these conditions into Equation 8 yields

$$C_2 = 0 \quad (10)$$

Thus,

$$u = C_1 e^{-\alpha x} \sin \sqrt{1-\psi^2} \frac{\omega x}{c} \sin \omega t \quad (11)$$

Substituting the second boundary condition and Equation 4 into Equation 11 and rearranging yields

$$\frac{\psi}{\sqrt{1-\psi^2}} \left[ 1 + \frac{\omega^2 M_e e^{-2\alpha l}}{\alpha A_0 E} \right] \tan \sqrt{1-\psi^2} \frac{\omega l}{c} = 1 \quad (12)$$

This is the frequency equation for the system. It should be noted that the equation is transcendental in  $\omega$ .

For purposes of comparison, the three design parameters, exciter amplitude, weight and quality factor were considered for both a tapered and constant area bar system operating at the same frequency and nodal force level. The constant area bar system parameters are found by letting  $\psi$  equal zero. Thus from Equation 11 the ratio of exciter amplitudes is

$$\left( \frac{u_T}{u_o} \right)_{x=l} = \frac{C_{1T} e^{-\alpha l_T} \sin \sqrt{1-\psi^2} \frac{\omega l_T}{c}}{C_{1o} \sin \frac{\omega l_o}{c}} \quad (13)$$

where the subscripts T and o indicate a tapered and uniform area bar system, respectively. The unknown ratio of the constants  $C_{1T}$  and  $C_{1o}$  is found by considering the stress at the node in the two systems. Since both systems are operating at the same frequency and nodal force level, the stress and hence the strain at the node for both systems must be equal. Therefore from Equation 11

$$\left( \frac{\partial u_T}{\partial x} \right)_{x=0} = \left( \frac{\partial u_o}{\partial x} \right)_{x=0} \quad \text{or} \quad \frac{\omega \sqrt{1-\psi^2}}{c} C_{1T} = \frac{\omega}{c} C_{1o}$$

Thus

$$\frac{C_{1T}}{C_{1o}} = \frac{1}{\sqrt{1-\psi^2}} \quad (14)$$

and

$$\left( \frac{u_T}{u_o} \right)_{x=l} = \frac{e^{-\alpha l_T} \sin \sqrt{1-\psi^2} \frac{\omega l_T}{c}}{\sqrt{1-\psi^2} \sin \frac{\omega l_o}{c}} \quad (15)$$

The weight ratio for the system on the exciter side of the node is from Equation 4.

$$\left(\frac{W_T}{W_O}\right)_{\text{exciter}} = \frac{\rho A_o \int_0^{l_T} e^{2\alpha x} dx + M_e}{\rho A_o l_o + M_e} = \frac{\frac{\rho A_o}{2\alpha} (e^{2\alpha l_T} - 1) + M_e}{\rho A_o l_o + M_e} \quad (16)$$

Combining this with the fixed weight on the piston side of the node, the weight ratio for the total system is

$$\left(\frac{W_T}{W_O}\right)_{\text{total}} = \frac{W_{\text{piston}} + W_o \left(\frac{W_T}{W_O}\right)_{\text{exciter}}}{W_{\text{piston}} + (W_o)_{\text{exciter}}} \quad (17)$$

The quality factor for a system is defined as the product of the frequency and peak potential energy divided by the power dissipated. Since we are considering two systems operating at the same frequency and nodal force level, only the peak potential energy needs to be compared. The potential energy  $V$  in the elastic bar is

$$V = \int_0^l \frac{AE}{2} \left(\frac{\partial u}{\partial x}\right)^2 dx \quad (18)$$

Substituting in Equations 4 and 11 and performing the indicated operations, the peak potential energy for a taper bar is

$$V = \frac{C_1^2 A_o E_p}{4C} \left[ \frac{\omega l}{c} + \frac{(1-2\psi^2)}{\sqrt{1-\psi^2}} \sin \sqrt{1-\psi^2} \frac{\omega l}{c} \cos \sqrt{1-\psi^2} \frac{\omega l}{c} - 2\psi \sin^2 \sqrt{1-\psi^2} \frac{\omega l}{c} \right] \quad (19)$$

Thus, using Equation (14) and letting  $\psi$  equal zero for a uniform area bar, the ratio of potential energy, and thus quality factor  $Q$  for tapered to uniform bars is

$$\left(\frac{Q_T}{Q_O}\right)_{\text{exciter}} = \frac{\frac{1}{(1-\psi^2)} \left[ \frac{\omega l_T}{c} + \frac{(1-2\psi^2)}{\sqrt{1-\psi^2}} \sin \sqrt{1-\psi^2} \frac{\omega l_T}{c} \cos \sqrt{1-\psi^2} \frac{\omega l_T}{c} - 2\psi \sin^2 \sqrt{1-\psi^2} \frac{\omega l_T}{c} \right]}{\left[ \frac{\omega l_o}{c} + \sin \frac{\omega l_o}{c} \cos \frac{\omega l_o}{c} \right]} \quad (20)$$

Combining this with the fixed  $Q$  on the piston side of the node, the  $Q$  ratio for the total system is

$$\left(\frac{Q_T}{Q_O}\right)_{\text{total}} = \frac{Q_{\text{piston}} + Q_o \left(\frac{Q_T}{Q_O}\right)_{\text{exciter}}}{Q_{\text{piston}} + (Q_o)_{\text{exciter}}} \quad (21)$$

## II. Limitations of Analysis

Earlier in this text, the limitation was put on the analysis that  $\psi^2$  be less than unity. In order to see physical significance of this limit, consider the area ratio of the bar. From Equations 4 and 7

$$\frac{A_l}{A_o} = e^{2\alpha l} = e^{2\psi \frac{\omega l}{c}} \quad (22)$$

Knowing that  $\omega$  is the circular frequency and  $c$  the velocity sound, then

$$\frac{A_l}{A_o} = e^{\frac{4\pi\psi l}{\lambda}} \quad (23)$$

where  $\lambda$  is the wave length of sound at frequency  $\omega$ . The length  $l$  from the node to exciter for a bar operating at its first natural frequency with a relatively small exciter mass will be of the order of one quarter of the wave length. Thus, for the two limiting values of  $\psi$

$$\begin{aligned} \frac{A_l}{A_o} &\cong e^{\pi\psi} \quad \text{or} \quad \psi = 1, \quad \frac{A_l}{A_o} \cong 23 \\ \psi &= 1, \quad \frac{A_l}{A_o} \cong \frac{1}{23} \end{aligned} \quad (24)$$

Thus, the limitation imposed upon this analysis by the condition  $\psi^2 < 1$  is that the area ratio for the bar be less than the order of 23 to one. If  $\psi^2$  is greater than unity, then the shape function  $X$  is exponential in form instead of exponential and trigonometric. This form of the solution was not investigated as it is only applicable for large area ratios for which, as will be shown, the assumption of plane stress used in deriving the governing differential equation is not valid.

In formulating the governing differential equation of motion for a taper bar, it was assumed that the stress and thus the strain was uniform across the cross section of the bar. In order to evaluate the seriousness of this assumption, the order of magnitude of deviation of the stress from the assumed uniform value is considered. Timoshenko and Goodier (1) show that the deviation of stress at the edge from the stress at the center of an axially loaded wedge is

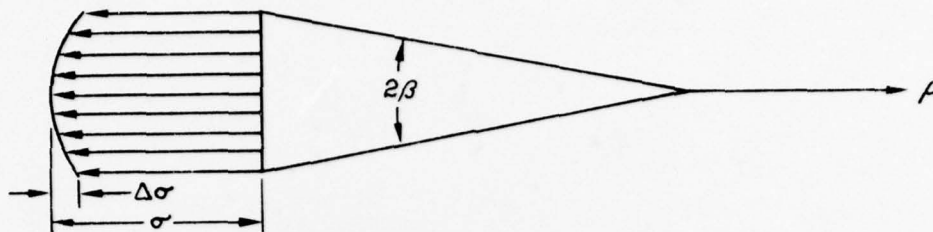
$$\Delta = 1 - \cos^4 \beta \quad (25)$$

where  $\Delta$  is the ratio of the deviation to the maximum stress at the center and  $\beta$  is the half wedge angle as shown below.

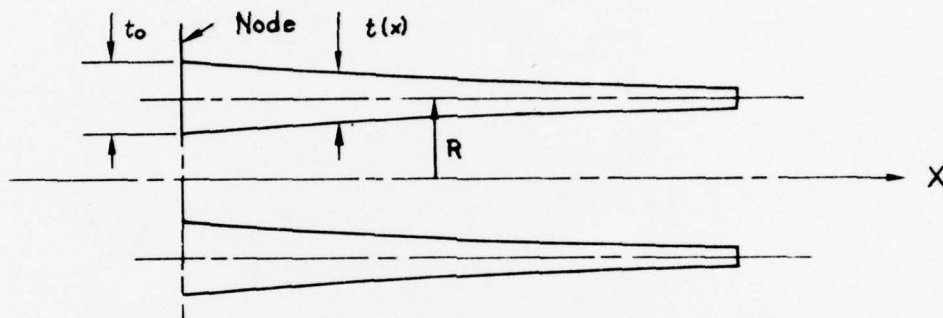
---

1. Theory of Elasticity, S. Timoshenko and J. N. Goodier, McGraw-Hill, 1951, pp. 96-99





Considering a tapered bar with geometry similar to that used in the SPEAR unit as shown below



the area from Equation 4 is

$$A = A_0 e^{2\alpha x} = 2\pi R t_0 e^{2\alpha x} = 2\pi R t(x) \quad (26)$$

therefore

$$\begin{aligned} t(x) &= t_0 e^{2\alpha x} \\ \frac{dt}{dx} &= 2\alpha t_0 e^{2\alpha x} \end{aligned} \quad (27)$$

Substituting into Equation 25 and considering small angles ( $\cos\beta = 1 - \beta^2/2$ ) the deviation is

$$\Delta = (2\alpha t_0)^2 e^{4\alpha x} \quad (28)$$

Once again substituting in Equation (7) and using the frequency, velocity, wavelength relationship, the deviation is

$$\Delta = \left(4\pi\psi \frac{t_0}{\lambda}\right)^2 e^{4\pi\psi \frac{x}{\lambda}} \quad (29)$$

Inspection of Equation 29 indicates that the maximum deviation is at the node for a converging bar ( $\psi < 0$ ) and at the free end for a diverging bar ( $\psi > 0$ ), and in both instances increases with the absolute value of  $\psi$  and thus area ratio. Considering a SPEAR type unit with a typical thickness to wavelength ratio ( $t_0/\lambda$ ) of 1/40, the stress deviation in the higher stressed nodal region is about 10% when  $\psi$  is equal to plus or minus unity. Thus for values of  $\psi$  greater than  $\pm 1$  the assumption of plane stress is not valid.

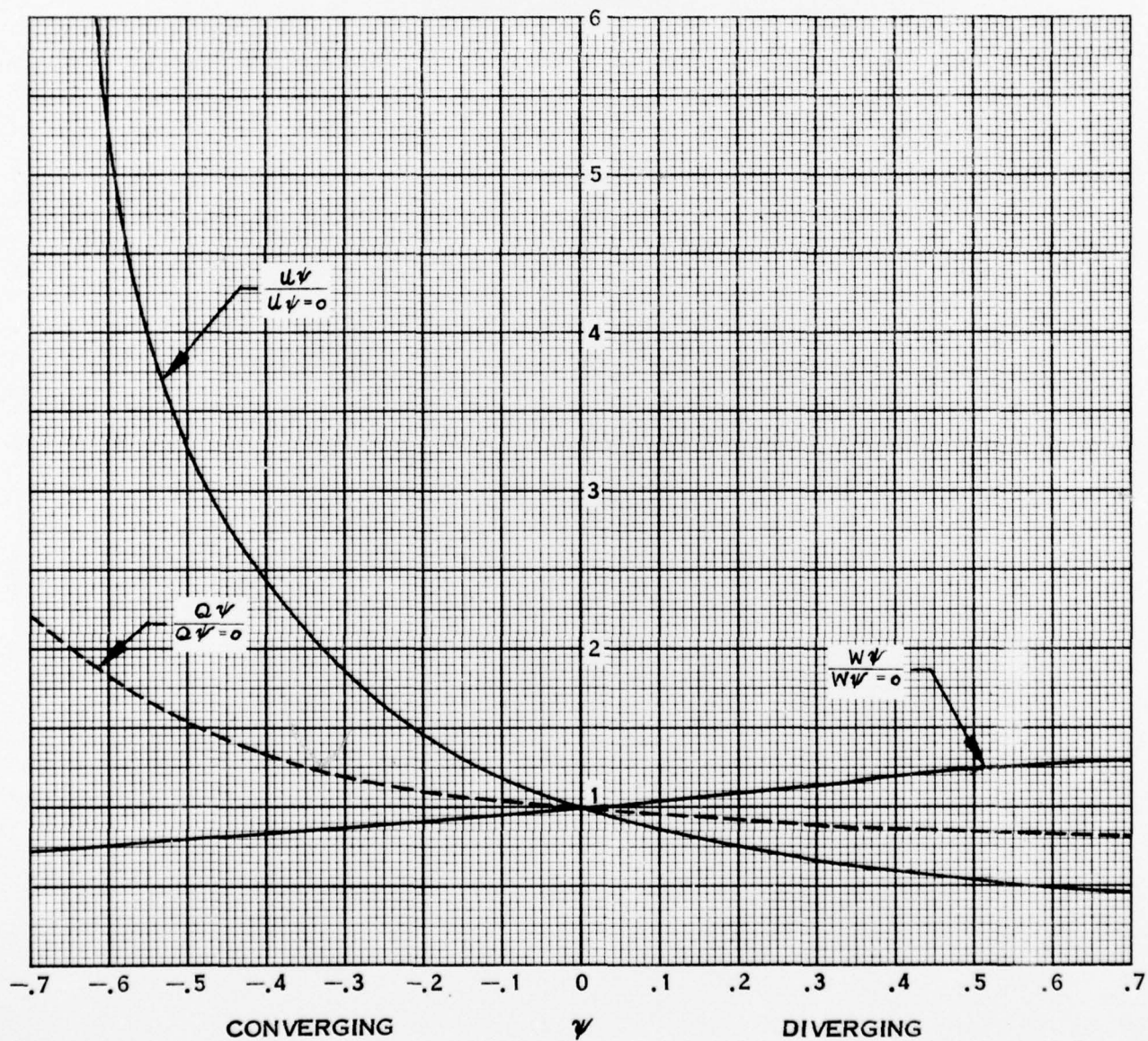
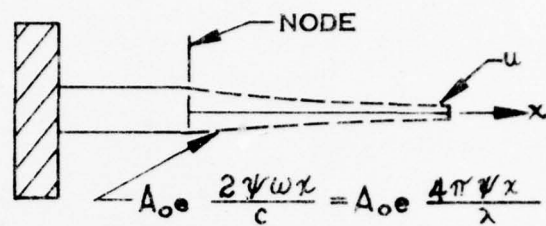
### III. Application of Analysis to SPEAR

To study the effects of a variable-area bar on a SPEAR type unit, the above analysis was applied to a unit which was similar to the HSD SPEAR model. In order to simplify the numerical effort, the exciter mass was neglected. The following is a list of the parameters used. The results obtained would apply as well to a geometrically similar full-scale design.

Piston Mass	142 lbs.
Area of Bar Where Constant	45 in. <sup>2</sup>
Material	Aluminum
Material Specific Weight	.097 lbs/in <sup>3</sup>
Modulus of Elasticity	10.3 x 10 <sup>6</sup> psi
Distance from Piston to Node	7.2 in.
Operating Frequency	2000 cps.

The following figure presents the variations of exciter amplitude, total weight and quality factor with degree of taper. Since the absolute value of rate of taper parameter,  $\psi$ , was kept below unity, the stress deviation at the high stress nodal area will be less than 10%.

The results, in general, show that exciter amplitude and quality factor both increase with a converging taper and decrease with a diverging taper. The weight varies conversely and to a smaller degree. Thus, a desirable lower Q can be achieved with a sacrifice of exciter amplitude (and consequent increase in required force) and vice versa. Therefore, the ultimate desirability of a variable-area SPEAR type system depends on the relative importance of the three performance parameters.



QUALITY FACTOR, EXCITER AMPLITUDE AND TOTAL WEIGHT VS DEGREE OF TAPER FOR EXPONENTIAL BAR SPEAR TYPE SONAR DEVICE

## APPENDIX D-VI

### THE EFFECT OF REAR SURFACE MOTION ON THE DIRECTIVITY PATTERN

Because of the desire to obtain a better Front-to-Back Ratio without the use of pressure release material, it was desired to gain a better understanding of the radiation due to structural action of the bar and piston rear face. The purpose of this appendix is to analyze the structural displacements of the bar surface, to develop equations for determining the radiation patterns due to the side wall and piston motions, and to determine the effect of these radiations on the directivity of the device.

#### A. Displacement of the Outside Surface of Bar

From Appendix D-IV, Equation (8), the axial displacement of an exponential bar is given as

$$u = e^{-\alpha x} \left[ C_1 \sin \sqrt{1-\psi^2} \frac{\omega x}{c} + C_2 \cos \sqrt{1-\psi^2} \frac{\omega x}{c} \right] \sin \omega t \quad (1)$$

where the bar area is given as  $A = A_0 e^{2\alpha x}$ ,  $\psi = \frac{\alpha c}{\omega}$ ,  $c$  is the sonic velocity in the bar, and  $\omega$  is the circular frequency. The boundary conditions are

$$\begin{aligned} \text{at } x=0, \left( \frac{\partial u}{\partial x} \right)_0 &= \frac{M_p}{A_0 E} \left( \frac{\partial^2 u}{\partial t^2} \right)_0 \\ \text{at } x=l, \left( \frac{\partial u}{\partial x} \right)_l &= -\frac{M_e}{A_l E} \left( \frac{\partial^2 u}{\partial t^2} \right)_l \end{aligned} \quad (2)$$

where  $M_p$  and  $M_e$  are the effective masses of the piston and exciter respectively. Substituting the first boundary condition into Equation (1), we find

$$R = \frac{C_1}{C_2} = - \left( \frac{\omega^2 M_p}{A_0 E} + \alpha \right) / \frac{\omega}{c} \sqrt{1-\psi^2} \quad (3)$$

Substituting this into Equation (1), we arrive at

$$u = u_0 e^{-\alpha x} \left[ R \sin \sqrt{1-\psi^2} \frac{\omega x}{c} + \cos \sqrt{1-\psi^2} \frac{\omega x}{c} \right] \quad (4)$$

where  $u_0$  is the maximum amplitude of the piston motion. From Equation (3), the value of  $R$  and, therefore, the mode shape given by Equation 4 can be obtained if the effective mass of the piston and the frequency are known. Applying



the second boundary condition, we find

$$\begin{aligned} R \sin \sqrt{1-\psi^2} \frac{\omega l}{c} + \cos \sqrt{1-\psi^2} \frac{\omega l}{c} + \frac{\omega^2 M_e}{\alpha A l E} \left( R \sin \sqrt{1-\psi^2} \frac{\omega l}{c} + \cos \sqrt{1-\psi^2} \frac{\omega l}{c} \right) \\ = \frac{\sqrt{1-\psi^2}}{\psi} \left( R \cos \sqrt{1-\psi^2} \frac{\omega l}{c} - \sin \sqrt{1-\psi^2} \frac{\omega l}{c} \right) \end{aligned} \quad (5)$$

If the effective masses of both the piston and exciter are known, the frequency and  $R$  can be obtained from Equations (3) and (5). If the frequency and effective exciter mass are known, Equation (5) can be used to determine constant

$R$  and thus the mode shape using Equation (4).

Knowing the axial deflection distribution, the radial displacement can be obtained as follows: For axisymmetric stress distribution

$$\begin{aligned} \sigma_x &= E \frac{\partial u}{\partial x} \\ \epsilon_\theta &= \frac{1}{E} (\sigma_\theta - \mu [\sigma_x + \sigma_r]) \\ w &= R_o \epsilon_\theta = \frac{R_o}{E} (\sigma_\theta - \mu [\sigma_x + \sigma_r]) \end{aligned} \quad (6)$$

where  $w$  is the radial displacement of the outside surface of the bar,  $\mu$  is Poisson's ratio, and  $R_o$  is the outside radius of the cylinder. Assuming that the axial stress,  $\sigma_x$ , is uniform over the cross-section and the radiation pressure is negligible,  $\sigma_r = \sigma_\theta = 0$ . In this case, the radial displacement becomes

$$w = -\mu R_o \frac{\partial u}{\partial x} \quad (7)$$

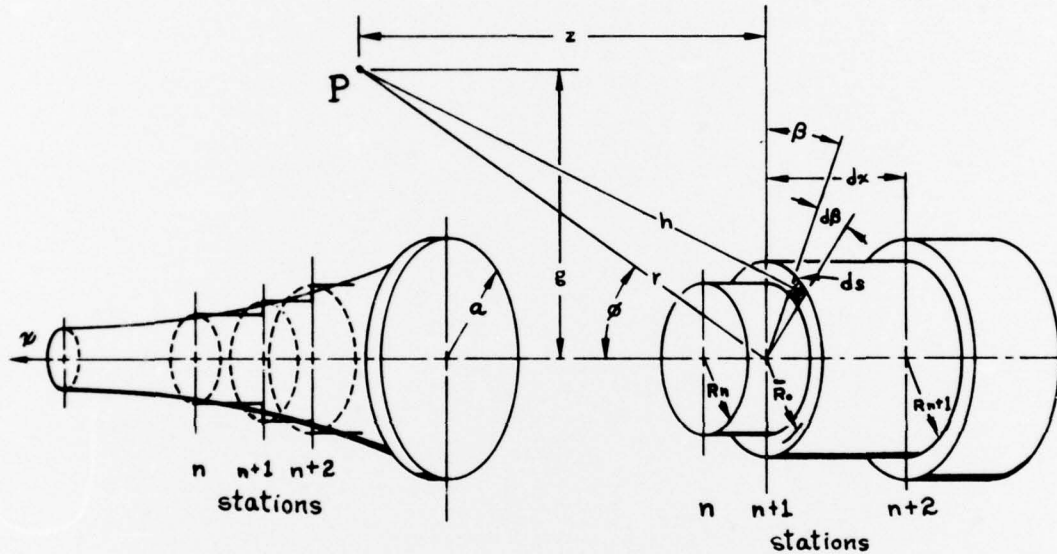
#### B. Radiation Due to Structural Action of Bar and Piston Motion

The next step in the analysis is to determine the radiation pressure which results from the displacements given by Equations (4) and (7). After obtaining the pressure components from the separate motions, they can be added to give the resultant pressure pattern due to axial and radial motion of the bar and piston rear face. The third radiation pattern to be considered is that due to the front surface of the piston. Analyses of the radiations due to each of these motions are given below.

### 1. Radiation due to axial motion of bar and piston rear face

The radiation pressure,  $dp$ , at point  $P$  due to axial motion of the surface element  $ds$  is given by the expression\*

$$dp \simeq -i \frac{2\pi\rho f^2 u ds}{h} e^{ik(h-ct)} \quad (8)$$



where  $\rho$  is the medium mass density,  $f$  is the frequency in cps,  $u$  is the amplitude of motion,  $k = 2\pi f/c$ , and  $c$  is the velocity of sound in the surrounding medium. From geometry  $h^2 = r^2 + \bar{R}_0^2 - 2r\bar{R}_0 \sin \phi \cos \beta$  where  $\bar{R}_0 = \frac{1}{2}(R_n + R_{n+1})$ ,  $n$  is the station,  $r = \sqrt{z^2 + g^2}$ , and  $\sin \phi = g/\sqrt{z^2 + g^2}$ . Now for  $\bar{R}_0^2/r^2 \ll 1$  this equation reduces to  $h = r - \bar{R}_0 \sin \phi \cos \beta$ . Also, if  $\bar{R}_0/r \ll 1$ ,  $\frac{1}{h} \simeq \frac{1}{r}$ . Substituting these expressions into Equation (8) and recognizing that the elemental surface area,  $ds = \bar{R}_0 dR_0 d\beta$ , we arrive at

$$dp \simeq -2\pi i \rho f^2 \frac{u \bar{R}_0}{r} e^{ik(r-ct)} e^{-ik\bar{R}_0 \sin \phi \cos \beta} dR_0 d\beta \quad (9)$$

Using Huygens' Principle, the total pressure at  $P$  is the sum of the contributions from all the elements, i.e.,

\*See Vibration and Sound - pg. 327, by P. M. Morse, McGraw-Hill

$$p \approx -2\pi i \rho f^2 \int_{R_1}^{R_2} \int_{\beta=0}^{2\pi} \frac{u \bar{R}_0}{r} e^{ik(r-ct)} e^{-ik \bar{R}_0 \sin \phi \cos \beta} dR_0 d\beta$$

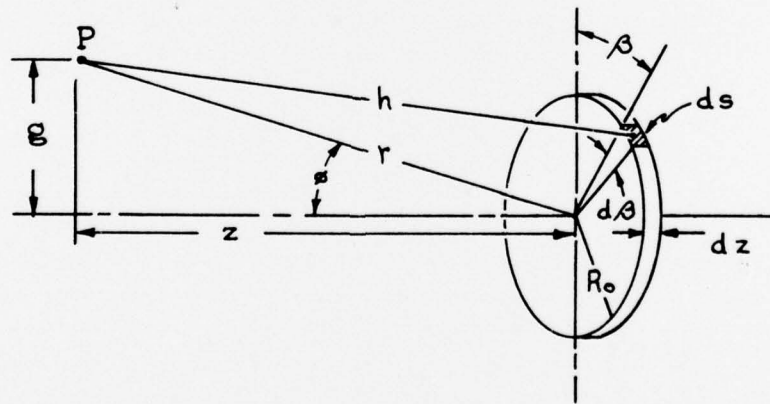
$$p \approx -2\pi \rho f^2 \int_{R_1}^{R_2} \frac{u \bar{R}_0}{\sqrt{z^2 + g^2}} J_0\left(\frac{k \bar{R}_0 g}{\sqrt{z^2 + g^2}}\right) \left( i \cos[k\sqrt{z^2 + g^2}] - \sin[k\sqrt{z^2 + g^2}] \right) e^{-ikct} dR_0$$

(10)

where  $J_0(x)$  is the Bessel Function of the first kind, order zero. With  $u$  and  $R_0$  functions of  $z$ , this equation cannot be integrated analytically except in special cases, so that the evaluation of the real and imaginary components of pressure was accomplished by numerical integration on a digital computer.

## 2. Radiation resulting from radial motion of the bar

The radiation pressure  $dp$ , at point  $P$  due to the surface element  $ds$  in harmonic radial motion is given by the expression



$$dp \approx -i \frac{2\pi \rho f^2 w ds}{h} e^{ik(h-ct)}$$

(11)

where the parameters are as described in Section 1. Integrating the pressure effect as before

$$p \simeq -2\pi\rho f^2 \int_{z_1}^{z_2} \frac{w R_o}{\sqrt{z^2 + g^2}} J_0\left(\frac{k R_o g}{\sqrt{z^2 + g^2}}\right) \left( i \cos\left[k\sqrt{z^2 + g^2}\right] - \sin\left[k\sqrt{z^2 + g^2}\right] \right) e^{-ikct} \quad (12)$$

Again with  $w$  and  $R_o$  functions of  $z$ , this equation cannot be analytically integrated except in special cases. Therefore, Equation (12) was integrated numerically on a digital computer to give the real and imaginary components of the pressure.

### 3. Radiation due to motion of the piston

The analysis which most accurately describes the radiation pattern due to a piston of radius  $a$  in the end of a long tube is given by Levine and Schwinger\*. This analysis is applied to the case at hand for the radiation due to the piston, by use of the power gain function  $G(\phi)$

$$G(\phi) = \frac{4}{\pi \sin^2 \phi} \frac{J_1[ka \sin \phi]}{\left\{ (J_1[ka \sin \phi])^2 + (N_1[ka \sin \phi])^2 \right\}^{1/2}} \times \frac{|R|}{1 - |R|^2} e^{\frac{2ka \cos \phi}{\pi} P} \quad (13)$$

$$\text{where } P = \text{principal value of } \int_0^{ka} \frac{x \tan^{-1}[-J_1(x)/N_1(x)] dx}{[x^2 - (ka \sin \phi)^2] [x^2 + (ka)^2]^{1/2}} \quad (14)$$

$$\text{and } |R| = e^{\left\{ -\frac{2ka}{\pi} \int_0^{ka} \frac{\tan^{-1}(-J_1(x)/N_1(x))}{x [(ka)^2 - x^2]^{1/2}} dx \right\}} \quad (15)$$

\*On the Radiation of Sound From an Unflanged Circular Pipe  
by H. Levine and J. Schwinger, Physical Review, Feb. 15, 1948



$|R|$  being the magnitude of the reflection coefficient for the pipe, and the Bessel functions,  $J_1$  and  $N_1$ , are defined in the reference. The power gain function gives the intensity of radiation relative to an isotropically radiating point source. Now the total power radiated from a piston in a long tube is

$$W = \frac{1}{2} \pi a^2 \rho c V_o^2 \theta_o \quad (16)$$

where  $\theta_o$  is the resistive impedance of the piston and  $V_o$  is the maximum piston velocity, i.e.,  $V_o = 2\pi f u_o$ . The value of  $\theta_o$  is given by L. Beranek as a function of  $ka$ . \* Substituting for  $V_o$  we get

$$W = 2 \pi^3 a^2 \rho c f^2 u_o^2 \theta_o \quad (17)$$

The average intensity due to this source is therefore

$$I_{av} = \frac{W}{A} = \frac{\pi^2 a^2 \rho c f^2 u_o^2 \theta_o}{2 r^2}$$

and the intensity at any angle  $\phi$  is

$$I(\phi) = \frac{\pi^2 a^2 \rho c f^2 u_o^2 \theta_o G(\phi)}{2 r^2} \quad (18)$$

where  $\phi$  is measured from the axis normal to the piston. Now at large distance from the piston,  $I(\phi) = p^2 / \rho c$ , so that

$$p(\phi) = \frac{\pi}{\sqrt{2}} \frac{a \rho c f u_o}{r} \sqrt{\theta_o G(\phi)} \quad (19)$$

#### 4. Combination of derived pressure patterns

The pressure patterns due to the structural action of the bar and piston rear face in axial and radial motion can be combined to produce a single analytical pattern. This is done by adding the real and imaginary components of Equation (10) and (12) separately and taking the square root of the sum of the squares of these components. The phase of the pressure distribution due to the piston diffraction radiation is not defined in the paper by Levine and Schwinger.

\* Acoustics - pg. 119, by L. F. Beranek

Therefore, it is not possible, without extension of this paper, to combine the piston pattern directly with that due to the bar and piston rear face. However, the limits of the total radiation pattern could be obtained by assuming that the rear surface radiation is  $0^\circ$  and  $180^\circ$  from that due to the piston front face. After adding the pressures due to the various sources, Equations (10), (12), and (19), the directivity pattern is computed by taking  $20 \log_{10} \left( \frac{p(\phi)}{p(\phi)} \right)$ .

### C. Application to Model Tests

In applying the foregoing analysis, configurations A4-0, A11-0, and B1-1 were chosen. These were chosen because A4-0 represents the standard design, A11-0 is an example of the reduced diameter piston, and B1-1 represents the exponentially tapered configuration and has a higher  $ka$  than A4-0 and A11-0. For these configurations the radiation pressure was calculated, and directivity patterns referenced to the Levine and Schwinger solution of the radiation from an unflanged circular pipe have been plotted in Figures 1, 2 and 3 for the piston near face alone, for the bar surfaces alone, for the combination of bar surfaces and piston near face, and for the front piston face alone. Also normalized to the same reference is the experimental pattern which is given to allow comparison of analytical and test results. In analyzing these configurations, the following details were involved.

**Configurations A4-0 and A11-0:** For these configurations the mode shapes were determined by using Equations (3) and (4) where the measured frequency was used as well as the effective mass required to produce the measured ratio of exciter to piston axial amplitude. Equation (7) was then applied to find the corresponding radial displacement. Equations (10) and (12) were applied, the radiation due to axial motion being calculated with and without the piston rear face. In order to obtain the pressure at  $\phi = 0$ , Equation (19) was used. We therefore have the data required to plot Figures 1 and 2.

**Configuration B1-1:** In this case, the exciter mass is negligible because an antinode exists near the end of the bar. Therefore, by using Equation (5) with  $M_e = 0$  and the known operating frequency in water, we can determine the value of  $R$  and thus the mode shape from Equation (4). The plot of the resulting radiation is shown in Figure 3. In all cases, the bar was divided into twenty sections for the numerical integrations, providing element lengths of about  $1/20$ th of a wave length and giving adequate accuracy.

### Discussion:

To check the general correlation between the analysis and test results, the absolute pressure at  $\phi = 0^\circ$  for configuration A4-0 was calculated from the analysis. Using the previously derived equations and the measured piston motion, the Source

Level was calculated to be about 71.4 db compared to the measured value of 73.3 db. It is believed that this is adequate correlation considering the nature of the work.

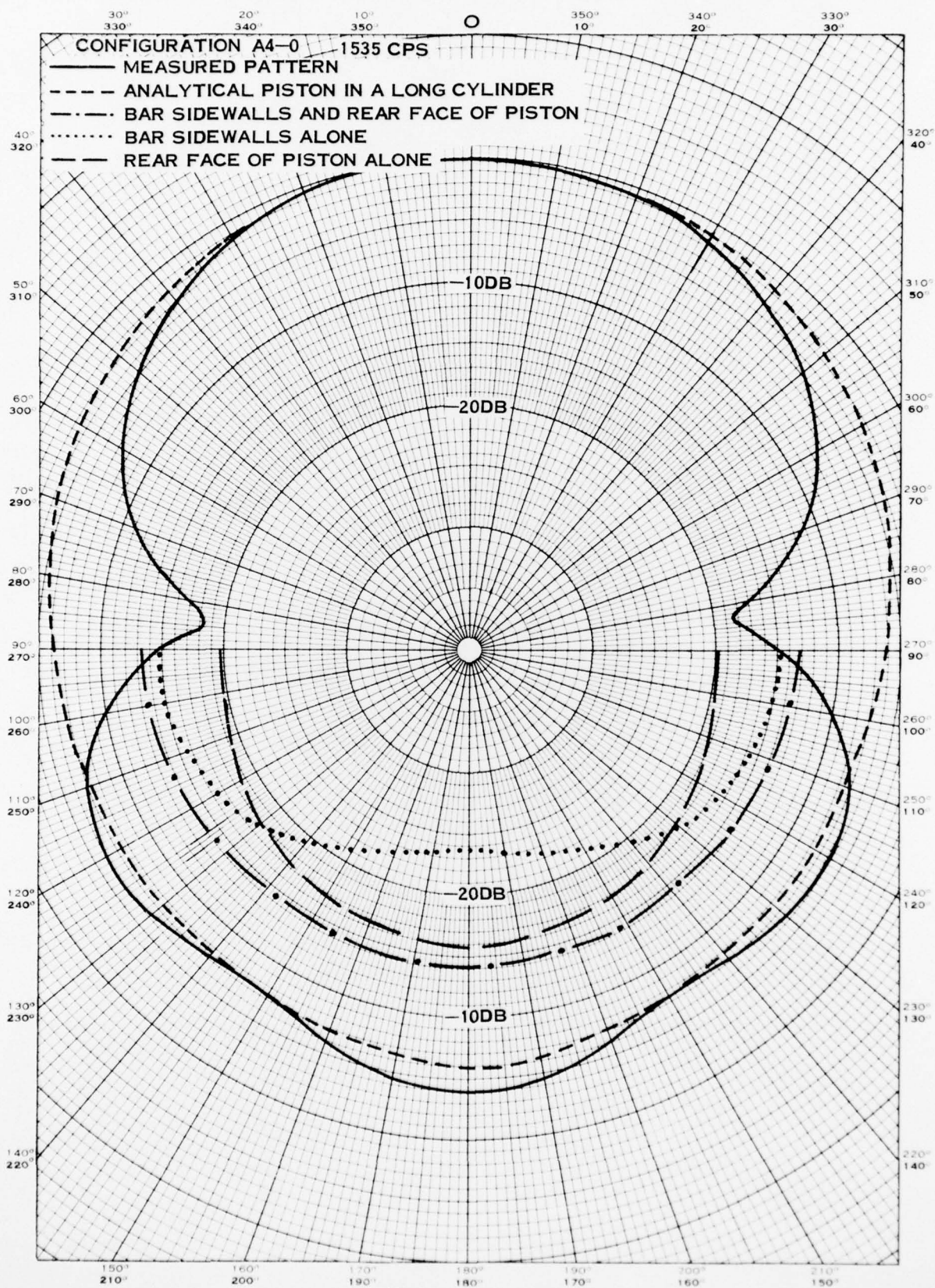
Figures 1 and 2 show the directivity patterns due to motion of the piston rear face alone, the bar surface alone, the bar surface and piston rear face, and the Levine and Schwinger solution as well as the test results. These figures show that the piston rear face and bar surface are both important as concerned Front-to-Back ratio. At 180° the piston rear face radiation is about 16 db down for configuration A4-0 and about 21 db down for configuration A11-0, whereas the radiation at

$\phi = 90^\circ$  due to the bar surface is down 14.5 db for A4-0 and down 20 db for A11-0. The differences in directivity between these configurations are indicative of their relative geometry. The bar in A4-0 is 18% longer and has a piston overhang of 3.5 inches vs. 1.5 inch for A11-0. The shorter length in combination with a different mode shape explains why the radiation due to the bar is smaller for A11-0. The much smaller piston overhang for A11-0 in part explains why the rear piston face radiation is less than that for A4-0.

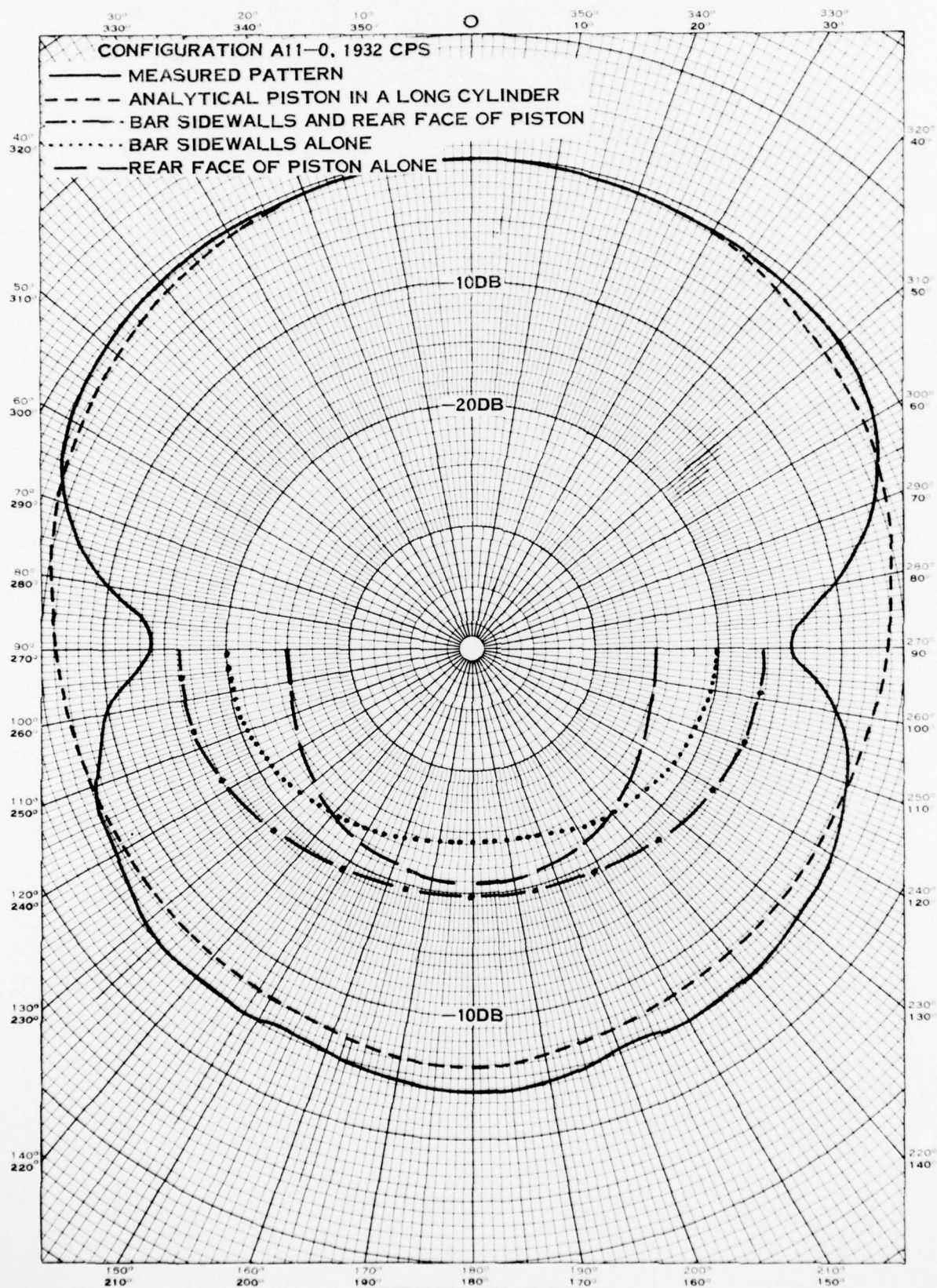
As mentioned previously, the radiation pressure due to the front of the piston was not combined analytically with that due to the rear surface motion because the relative phase was not known. However, we can obtain limits by assuming that they are at 0° phase and 180° phase. If this is done, the limits of the analytical results bracket the experimental results in all but a few small areas. In general, the results of the analysis show that the Levine and Schwinger solution will be modified within the limits +4 db and -7 db by radiation due to the bar surfaces and piston rear face.

The analysis shows that changes in the geometry of the bar, nodal position and size of the piston overhang can appreciably affect the magnitude of the rear radiation pressure due to the surfaces other than the front of the piston. However, until the relative phase of the diffracted pressure pattern from the piston front is known, the bar and piston rear face radiation cannot be combined with that from the front to give a total radiation pattern for the device. An extension of this analysis would give total patterns and permit the examination of design variables affecting Front-to-Back ratio.

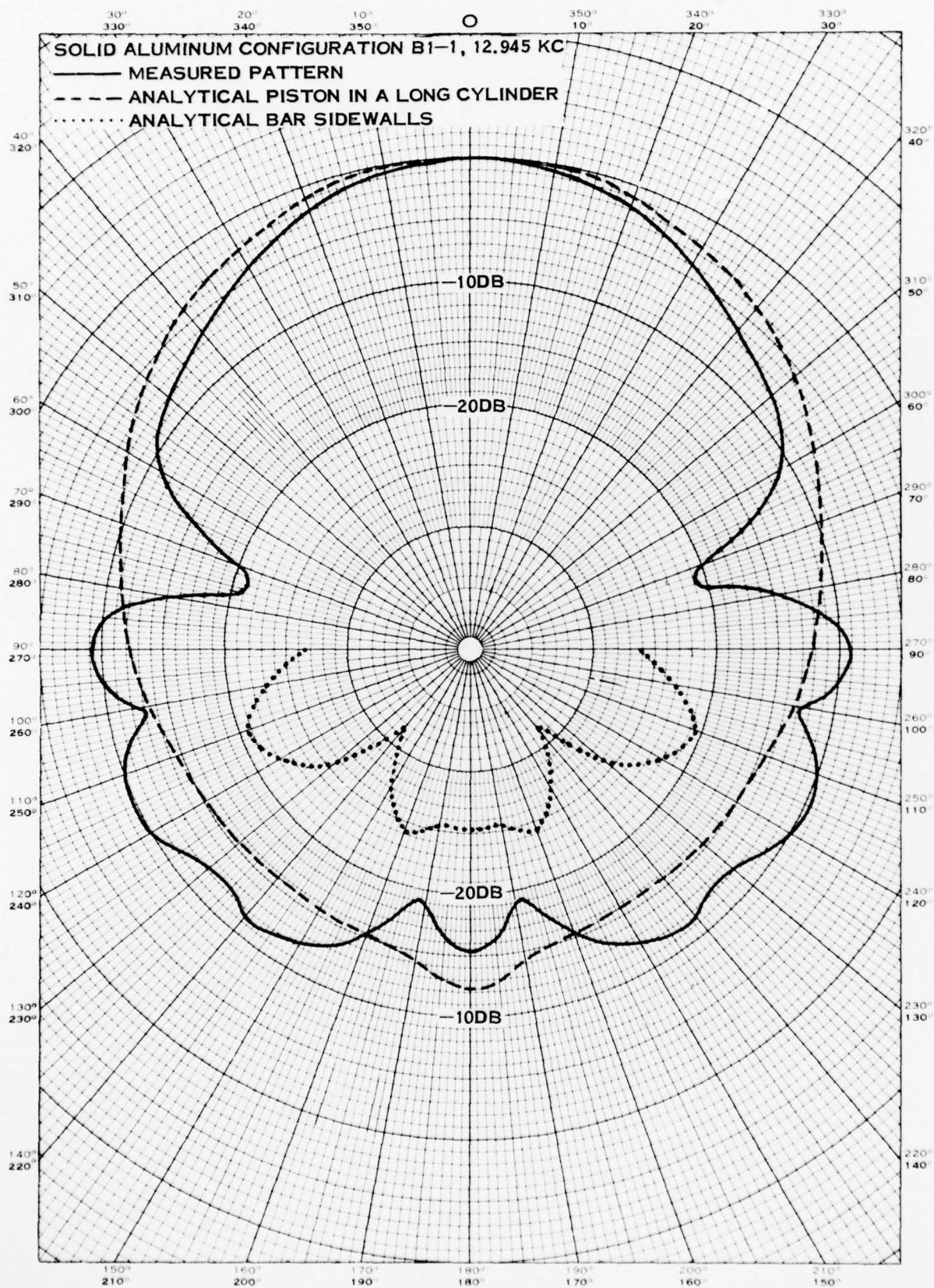








APPENDIX D-VI, FIGURE 2



APPENDIX D-VI, FIGURE 3